[AMERICAN JOURNAL OF SCIENCE, VOL. 274, DECEMBER, 1974, P. 1199-1261]

THEORETICAL PREDICTION OF THE THERMODYNAMIC BEHAVIOR OF AQUEOUS ELECTROLYTES AT HIGH PRESSURES AND TEMPERATURES: II. DEBYE-HÜCKEL PARAMETERS FOR ACTIVITY COEFFICIENTS AND RELATIVE PARTIAL MOLAL PROPERTIES

HAROLD C. HELGESON and DAVID H. KIRKHAM

Department of Geology and Geophysics, University of California, Berkeley, California 94720

ABSTRACT. Electrostatic parameters in the Debye-Hückel equations for activity coefficients and the relative partial molal enthalpies, internal energies, isochoric and isobaric heat capacities, volumes, compressibilities, and expansibilities of aqueous electrolytes have been computed for pressures and temperatures from 1 bar to 5 kb and 0° to 600°C. The calculations are based on the equation of state for H_2O derived by Keenan and others (1969) for pressures $\leq$ a kilobar together with power functions of temperature and density (or pressure) obtained by regression analysis (Helgeson and Kirkham, 1974a) of dielectric constant data (Oshry, ms; Owen and others, 1961; Heger, ms) and finite difference coefficients of isobaric thermal expansion and isothermal compressibility generated (Helgeson and Kirkham, 1974a) from densities (Burnham, Holloway, and Davis, 1969) of H_2O at pressures $>$ a kilobar. The Debye-Hückel parameters are sensitive quasi-asymptotic functions of pressure and temperature, which may be monotonic or exhibit extrema, depending on the property. Changes in the dielectric constant and the Debye-Hückel parameters with increasing temperature and/or decreasing pressure favor increasing mineral solubilities and extension of the applicability of Debye-Hückel theory to electrolytes with progressively higher concentrations. In the supercritical region, the absolute values of the limiting law parameters for the relative partial molal properties of electrolytes are of the order of 5 to $>$ 1000 times larger than they are at 25°C and 1 bar.

INTRODUCTION

Calculation of the partial molal properties of aqueous electrolyte solutions as well as controlled extrapolation to infinite dilution of apparent molal properties computed from experimental data requires values for the electrostatic parameters in the Debye-Hückel theory (Debye and Hückel, 1923) of electrolytes. The purpose of this communication is to present a comprehensive summary of these parameters for temperatures and pressures from 0° to 600°C and 1 bar to 5 kb. The results of the calculations are presented in diagrams as well as tables to facilitate analysis of the nature and extent to which the parameters change and the role they play in high pressure-temperature solution chemistry.

Despite the fact that aqueous electrolytes become associated at high temperatures and pressures, the Debye-Hückel formulation is applicable if the "true" ionic strength of the solution can be computed. Ionic strength calculations can be carried out with the aid of high pressure-temperature conductance measurements such as those reported by Hensel and Franck (1964) and Quist and Marshall (1966; 1968a, b, c, and d; 1969), which make it possible to compute the degrees of formation of complexes in electrolyte solutions as a function of pressure and temperature. Although considerable discussion in the literature has been devoted to the applicability of the dielectric constant of pure H_2O to represent

the electrostatic environment of solute species in dilute aqueous solutions, the success of continuum theory (Sen and Cobble, 1974) and the solvated ion model adopted by Robinson and Stokes (1959) afford reasonable justification for doing so.

With few exceptions, previously reported values of Debye-Hückel parameters (for example, Robinson and Stokes, 1959; Harned and Owen, 1958; Lewis and Randall, 1961; Marshall and Slusher, 1968; Bromley, 1968; Bromley and others, 1970; Gardner, Mitchell, and Cobble, 1969; Redlich and Meyer, 1964; Hamer, 1968; Hamer and Wu, 1972; Lietzke and Stoughton, 1962; Helgeson, 1967b) are limited to pressures and temperatures along the saturation curve for water. Many of these are inconsistent with one another owing to use of different experimental data and/or power functions to represent the dielectric constant, density, and their partial derivatives as functions of temperature and pressure. In contrast, the calculations reported below are based on an internally consistent set of values for the thermodynamic/electrostatic properties of H_2O.

UNITS, CONVENTIONS, AND UNCERTAINTIES

Except where confusion might arise (as, for example, in the use of E to represent internal energy as well as expansibility), the definitions, symbols, and notation employed below conform (or are analogous) to those used by Lewis and Randall (1961). In certain cases arbitrary sign conventions (given below) were adopted for convenience. Energy is expressed in thermochemical calories (4.184 cal = 1 joule) or kcal $mole^{-1}$ and heat capacity in cal $mole^{-1}$ $(°K)^{-1}$. All temperatures are on the thermodynamic (celsius) scale, expressed in degrees kelvin (°K) or degrees centigrade (°C). The values of the gas constant employed in the calculations are 1.98719 cal $mole^{-1}$ $(°K)^{-1}$ or 83.14241 cm^3 bar $mole^{-1}$ $(°K)^{-1}$.

Although volumetric concentration units are specified in Debye-Hückel theory, molality units of concentration are generally more convenient for calculations in which pressure and temperature are variables. Despite recent arguments to the contrary (Quist and Marshall, 1968a), no concentration scale is intrinsically more correct than another. In contrast to molarity, molality is independent of temperature and pressure, which facilitates calculation and comparison of activity coefficients and the relative partial molal properties of aqueous electrolytes at different concentrations, pressures, and temperatures. For this reason, all properties given below are expressed in molality units, which can be converted to the molarity scale by dividing the values of the parameters by the square root of the density of H_2O. The standard state adopted in this study is the conventional one of unit activity of the solute in a hypothetical one (mean) molal solution. At infinite dilution, activity coefficients are taken to be unity at all pressures and temperatures. The labels *sat* and *saturation* in the tables and diagrams refer to steam-saturated liquid H_2O.

The density and dielectric constant of H_2O together with their partial derivatives have been computed as functions of pressure and temperature from 0.001 to 5 kb and 25° to 600°C (Helgeson and Kirkham, 1974a). The results of these calculations were used in the present study to calculate the Debye-Hückel parameters shown in the following tables and diagrams.

Because the temperature and pressure dependence of many of the Debye-Hückel parameters is controlled by the relative size of the partial derivatives of ln ε and ln V with respect to temperature or pressure, these two variables are plotted against each other in figure 1, where it can be seen that ln ε decreases as ln V increases, either at constant pressure or constant temperature. Note that in the latter case the two variables are almost linearly related with a slope close to unity. This relation not only has an important effect on the behavior of the Debye-Hückel parameters for relative partial molal volumes and compressibilities as functions of pressure and temperature (discussed below), but it also minimizes the effect of absolute uncertainties in calculated values of the partial derivatives of ln V and ln ε on derived values of Debye-Hückel parameters. The latter variables are affected to a much greater extent by the *relative* uncertainties in the computed values of the derivatives, which are smaller than their absolute counterparts.

Uncertainties in the calculated Debye-Hückel parameters reported in the following pages are difficult to assess, but they are of the order of 1 to 5 percent or less, except for 450° $\lesssim$ t $\leq$ 550°C and 1000 $<$ P $\lesssim$ 1500

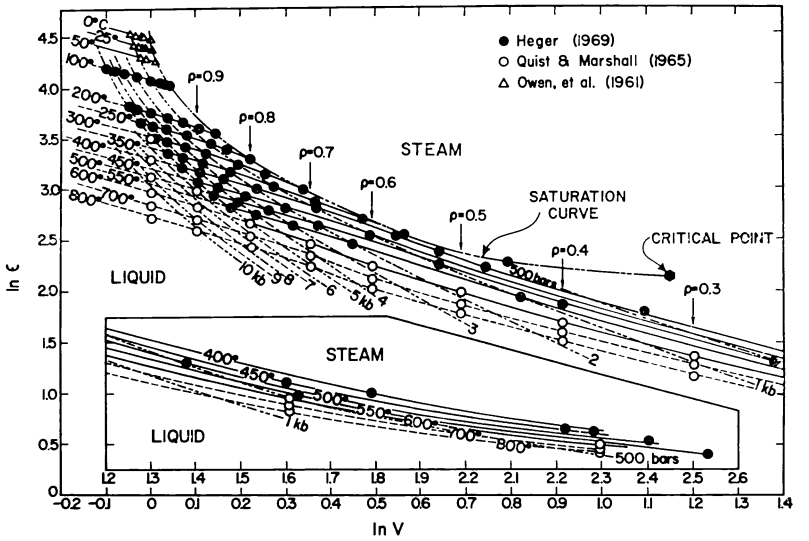

Fig. 1. Logarithm of the dielectric constant (ε) of H_2O as a function of the logarithm of the specific volume (V) of H_2O at constant temperature (solid curves) and constant pressure (dashed curves) calculated from regression equations (Helgeson and Kirkham, 1974a). The symbols represent values taken from the literature.

TABLE 1

A_γ in $kg^{1/2}mole^{-1/2}$ computed from equation (2)—see figures 2, 3, and 6

t	PRESSURE, KB							
(°C)	SAT	0.5	1	1.5	2	3	4	5
25	0.5092	0.4980	0.4882	(0.4807)	(0.4730)	(0.4606)	(0.4505)	(0.4417)
50	0.5336	0.5208	0.5096	(0.5013)	(0.4925)	(0.4784)	(0.4670)	(0.4570)
75	0.5639	0.5486	0.5353	(0.5251)	(0.5149)	(0.4987)	(0.4860)	(0.4748)
100	0.5998	0.5809	0.5649	0.5522	0.5402	0.5214	0.5070	0.4947
125	0.6416	0.6177	0.5983	0.5828	0.5686	0.5463	0.5299	0.5161
150	0.6898	0.6592	0.6352	0.6168	0.5998	0.5732	0.5541	0.5387
175	0.7454	0.7057	0.6756	0.6538	0.6334	0.6016	0.5795	0.5621
200	0.8099	0.7576	0.7196	0.6934	0.6692	0.6315	0.6057	0.5863
225	0.8860	0.8159	0.7673	0.7353	0.7068	0.6625	0.6327	0.6111
250	0.9785	0.8822	0.8192	0.7795	0.7461	0.6946	0.6605	0.6366
275	1.0960	0.9595	0.8762	0.8263	0.7873	0.7280	0.6894	0.6629
300	1.2555	1.0529	0.9398	0.8766	0.8308	0.7630	0.7195	0.6905
325	1.4943	1.1705	1.0126	0.9317	0.8774	0.8001	0.7515	0.7198
350	1.9252	1.3267	1.0981	0.9934	0.9282	0.8399	0.7857	0.7513
375		1.5464	1.2007	1.0639	0.9845	0.8832	0.8228	0.7854
400		1.8789	1.3262	1.1453	1.0476	0.9305	0.8632	0.8225
425		2.4301	1.4811	1.2402	1.1188	0.9823	0.9069	0.8625
450		3.3553	1.6723	1.3504	1.1988	1.0384	0.9536	0.9049
475		4.5059	1.9065	1.4768	1.2873	1.0977	1.0017	0.9480
500		5.5075	2.1872	1.6181	1.3822	1.1575	1.0485	0.9889
525			(2.5092)	(1.7685)	(1.4782)	(1.2127)	(1.0890)	(1.0228)
550			(2.8476)	(1.9151)	(1.5648)	(1.2551)	(1.1158)	(1.0428)
575			(3.1486)	(2.0366)	(1.6259)	(1.2735)	(1.1199)	(1.0406)
600			(3.3281)	(2.0960)	(1.6400)	(1.2556)	(1.0919)	(1.0081)

TABLE 2

B_γ in $(kg^{1/2}mole^{-1/2}\ cm^{-1}) \times 10^{-8}$ computed from equation (3)—see figures 4, 5, and 7

t	PRESSURE, KB							
(°C)	SAT	0.5	1	1.5	2	3	4	5
25	0.3283	0.3282	0.3281	(0.3281)	(0.3280)	(0.3297)	(0.3297)	(0.3280)
50	0.3325	0.3321	0.3317	(0.3315)	(0.3312)	(0.3308)	(0.3306)	(0.3304)
75	0.3371	0.3364	0.3358	(0.3353)	(0.3349)	(0.3342	(0.3337)	0.3334
100	0.3422	0.3411	0.3402	0.3395	0.3388	0.3378	0.3372	0.3366
125	0.3476	0.3461	0.3448	0.3439	0.3430	0.3416	0.3407	0.3401
150	0.3533	0.3512	0.3496	0.3483	0.3472	0.3455	0.3443	0.3435
175	0.3592	0.3565	0.3544	0.3528	0.3514	0.3493	0.3479	0.3469
200	0.3655	0.3618	0.3592	0.3573	0.3556	0.3530	0.3514	0.3503
225	0.3721	0.3673	0.3639	0.3616	0.3596	0.3566	0.3547	0.3535
250	0.3792	0.3729	0.3686	0.3658	0.3635	0.3601	0.3580	0.3567
275	0.3871	0.3787	0.3733	0.3699	0.3673	0.3634	0.3611	0.3598
300	0.3965	0.3850	0.3780	0.3739	0.3710	0.3667	0.3643	0.3629
325	0.4085	0.3921	0.3829	0.3780	0.3747	0.3700	0.3674	0.3661
350	0.4256	0.4004	0.3882	0.3822	0.3784	0.3734	0.3707	0.3694
375		0.4104	0.3940	0.3867	0.3823	0.3769	0.3741	0.3729
400		0.4230	0.4004	0.3915	0.3865	0.3806	0.3777	0.3766
425		0.4386	0.4076	0.3968	0.3909	0.3845	0.3815	0.3804
450		0.4548	0.4154	0.4024	0.3956	0.3885	0.3853	0.3843
475		0.4625	0.4237	0.4083	0.4004	0.3924	0.3890	0.3880
500		0.4620	0.4321	0.4141	0.4050	0.3960	0.3923	0.3912
525			(0.4397)	(0.4193)	(0.4089)	(0.3986)	(0.3944)	(0.3932)
550			(0.4454)	(0.4231)	(0.4113)	(0.3995)	(0.3948)	(0.3934)
575			(0.4472)	(0.4240)	(0.4109)	(0.3978)	(0.3924)	(0.3907)
600			(0.4428)	(0.4203)	(0.4064)	(0.3922)	(0.3863)	(0.3842)

TABLE 3

A_H in kcal $kg^{1/2}mole^{-3/2}$ computed from equations (2), (5), and (7)—see figures 8 through 10 and 13

t	PRESSURE, KB						
(°C)	SAT	0.5	1	2	3	4	5
25	0.692	0.65	0.62	(0.56)	(0.51)	(0.47)	(0.44)
50	1.049	0.97	0.90	(0.80)	(0.73)	(0.68)	(0.63)
75	1.471	1.33	1.23	(1.07)	(0.97)	(0.90)	(0.84)
100	1.981	1.76	1.61	1.38	1.24	1.14	(1.06)
125	2.610	2.27	2.04	1.71	1.52	1.39	(1.29)
150	3.403	2.88	2.54	2.08	1.82	1.65	(1.53)
175	4.427	3.61	3.10	2.49	2.14	1.92	(1.78)
200	5.805	4.50	3.75	2.94	2.47	2.21	(2.04)
225	7.773	5.63	4.51	3.44	2.83	2.51	(2.31)
250	10.815	7.13	5.43	4.00	3.24	2.84	(2.62)
275	15.981	9.27	6.60	4.66	3.71	3.24	(2.98)
300	25.894	12.48	8.15	5.45	4.27	3.71	(3.42)
325	49.072	17.54	10.28	6.42	4.96	4.29	(3.96)
350	135.177	25.93	13.25	7.63	5.82	5.01	(4.63)
375			17.39	9.16	6.87	5.88	(5.43)
400			23.07	11.05	8.12	6.90	(6.35)
425			30.67	13.34	9.54	8.00	(7.32)
450			(40.53)	(15.96)	(11.00)	(9.05)	(8.19
475			(52.73)	(18.67)	(12.22)	(9.77)	(8.68)
500			(66.41)	(20.92)	(12.69)	(9.68)	(8.34)
525			(78.48)	(21.84)	(11.67)	(8.17)	(6.59)
550			(82.22)	(19.20)	(8.02)	(4.25)	(2.56)
575			(67.48)	(11.02)	(0.60)	(-2.76)	(-4.26)
600			(24.13)	(-4.54)	(-11.10)	(-12.99)	(-13.81)

TABLE 4

B_H in (cal $kg^{1/2}cm^{-1}mole^{-3/2}$) $\times 10^{-9}$ computed from equations (3), (6), and (8)—see figures 11, 12, and 14

t	PRESSURE, KB						
(°C)	SAT	0.5	1	2	3	4	5
25	12.60	11.6	10.8	(9.5)	(8.5)	(7.7)	(7.0)
50	16.89	15.7	14.8	(13.3)	(12.1)	(11.2)	(10.5)
75	21.65	20.1	18.9	(17.1)	(15.7)	(14.7)	(13.9)
100	26.77	24.7	23.1	20.8	19.2	18.0	(17.1)
125	32.28	29.4	27.3	24.3	22.3	21.0	(20.1)
150	38.27	34.2	31.3	27.5	25.2	23.7	(22.7)
175	44.99	39.1	35.2	30.5	27.7	26.0	(25.0)
200	52.95	44.2	39.0	33.2	29.8	28.1	(27.1)
225	63.23	49.9	42.7	35.7	31.8	30.0	(29.2)
250	77.90	56.9	46.8	38.2	33.9	32.1	(31.4)
275	101.06	66.3	51.6	41.0	36.2	34.5	(34.2)
300	141.64	79.7	57.9	44.4	39.2	37.7	(37.8)
325	224.59	99.4	66.6	48.8	43.2	41.9	(42.4)
350	472.54	128.7	78.3	54.7	48.4	47.3	(48.2)
375			93.6	62.1	54.9	53.8	(55.1)
400			112.4	71.0	62.5	61.1	(62.6)
425			133.7	80.9	70.1	68.0	(69.5)
450			(155.2)	(90.3)	(76.2)	(72.8)	(73.8)
475			(172.9)	(96.5)	(77.6)	(72.1)	(72.0)
500			(179.3)	(94.3)	(69.4)	(61.0)	(59.2)
525			(161.7)	(76.9)	(44.8)	(32.9)	(28.5)
550			(101.9)	(30.8)	(-5.6)	(-20.8)	(-27.8)
575			(-22.5)	(-56.2)	(-91.4)	(-108.0)	(-117.1)
600			(-233.9)	(-196.0)	(-219.1)	(-232.9)	(-242.2)

bars where interregional regression discrepancies (Helgeson and Kirkham, 1974a) may introduce higher uncertainties. Uncertainties in the values of the Debye-Hückel parameters involving successive derivatives of ln ε and ln V increase with differentiation, but errors caused by overfitting the dielectric constant and density data have been minimized (Helgeson and Kirkham, 1974a). Values shown for temperatures < 100°C at pressures above a kilobar as well as those for temperatures above 550°C were obtained by extrapolation. The more uncertain values are shown parenthetically in the tables and represented by dashed curves in the figures.

ACTIVITY COEFFICIENT

Taking account of the ion size parameter (å, which is commonly expressed in angstroms), the Debye-Hückel equation for the mean activity coefficient ($\gamma_\pm$) of a completely dissociated binary electrolyte consisting of υ ions (mole of solute)$^{-1}$ with charges Z_+ and Z_- can be written as

$$\log \gamma_\pm = -\frac{|Z_+Z_-|A_\gamma I^{1/2}}{1 + \text{å}B_\gamma I^{1/2}} \tag{1}$$

where I is the ionic strength in molality (m) units of concentration ($I = (\upsilon/2)|Z_+Z_-|m$) and A_γ and B_γ are defined by

$$A_\gamma \equiv \frac{(2\pi N)^{1/2}\, e^3\, \rho^{1/2}}{2.302585(1000)^{1/2}\,(\varepsilon kT)^{3/2}} = \frac{1.824829238 \times 10^6\, \rho^{1/2}}{(\varepsilon T)^{3/2}} \tag{2}$$

and (for eq 1 with å expressed in cm)

$$B_\gamma \equiv \left(\frac{8\pi N \rho e^2}{1000\, \varepsilon kT}\right)^{1/2} = \frac{50.29158649 \times 10^8\, \rho^{1/2}}{(\varepsilon T)^{1/2}} \tag{3}$$

where $\pi = 3.14159265$, N refers to Avogadro's number (6.02252×10^{23} mole^{-1}), e stands for the absolute electronic charge (4.80298 esu), ρ is the density in g cm^{-3} and ε the dielectric constant of H_2O, T designates temperature on the thermodynamic scale in °K, and k is Boltzmann's constant (1.38054×10^{-16} erg (°K)$^{-1}$). A_γ and B_γ in equations (2) and (3) thus have dimensions of kg$^{1/2}$ mole$^{-1/2}$ and kg$^{1/2}$ mole$^{-1/2}$ cm^{-1}, respectively.

If $\text{å}B_\gamma$ is set to unity in equation (1), the expression reduces to the Guntelberg (1926) equation, but if $\text{å}B_\gamma$ is taken to be equal to 1.5 the relation becomes the Scatchard (1936) equation. Extension of equation (1) or one of its modifications to high concentrations at low temperatures requires additional terms in an ascending power function of I, such as that used by Lietzke and Stoughton (1962). The simplest of these was proposed originally by Hückel; that is,

$$\log \gamma_\pm = -\frac{|Z_+Z_-|A_\gamma I^{1/2}}{1 + \text{å}B_\gamma I^{1/2}} + b_\gamma I \tag{4}$$

where b_γ is an empirical parameter characteristic of the electrolyte. If $\mathring{a}B_\gamma$ is set to unity in equation (4), it reduces to the Guggenheim (1935) equation. Similarly, if $\mathring{a}B_\gamma$ is equated to one and b_γ is set to $0.2A_\gamma|Z_+Z_-|$, the expression reduces to the Davies (1938) equation. Owing to changes in ρ, ε, and the degree of ion association with increasing temperature and pressure, modified forms of the Debye-Hückel equation and/or its extensions such as the Guntelberg, Scatchard, Guggenheim, and Davies equations are limited in their applicability at high temperatures and pressures.

Values of A_γ and B_γ computed from equations (2) and (3) are listed in tables 1 and 2 and plotted in figures 2 through 5, where it can be seen that both A_γ and B_γ decrease to a decreasing degree as pressure increases isothermally (figs. 2 and 4) but increase with increasing temperature to $\sim$ 500°C at constant pressure. At higher temperatures, the isobars in figures 3 and 5 pass through extrema as the density contribution to A_γ and B_γ becomes more important than the electrostatic contribution. Because the dielectric constant of H_2O decreases as density decreases, either isothermally or isobarically (fig. 1), whether A_γ and B_γ increase or decrease with increasing temperature and/or pressure depends on the extent to which $(\varepsilon T)^{3/2}$ and $(\varepsilon T)^{1/2}$ increase or decrease relative to the corresponding increase or decrease in $\rho^{1/2}$. The dielectric constant of H_2O decreases by 50 to 70 units as temperature increases isobarically from 0° to $\sim$ 300°C in the liquid phase region below 5 kb, but the corresponding decrease in density is only 0.3 g cm^{-3} or less. Consequently, A_γ and B_γ increase. In contrast, at high temperatures (and in the steam phase region where the dielectric constant approaches unity at low pressures), the specific volume of H_2O increases dramatically with increasing temperature and/or decreasing pressure, which overcomes the effect of the negative change in the dielectric constant on the temperature and pressure dependence of A_γ and B_γ. As a result, A_γ and B_γ maximize at high temperatures and decrease with further isobaric increase in temperature. Because (εT) is raised to a lower power in equation (3) than in equation (2), the isobars for B_γ in figure 5 maximize at slightly lower temperature than those for A_γ in figure 3. Although not defined by the calculations, the isotherms for A_γ and B_γ in figures 2 and 4 should also exhibit maxima at high temperatures and low pressures (of the order of a few hundred bars).

The dielectric constant of H_2O increases by about 10 units as pressure increases isothermally from saturation pressures to $\sim$ 5 kb. Because the corresponding increase in density is slight, the isotherms in figures 2 and 4 decrease monotonically with increasing pressure and appear to approach constant values at high pressures. However, the isotherms may minimize as pressure increases above 5 kb if the rate of increase in the dielectric constant diminishes relative to the rate of increase in density at high pressures.

Perturbation by the critical phenomenon of A_γ and B_γ as functions of temperature and pressure is evident in figures 6 and 7, where the com-

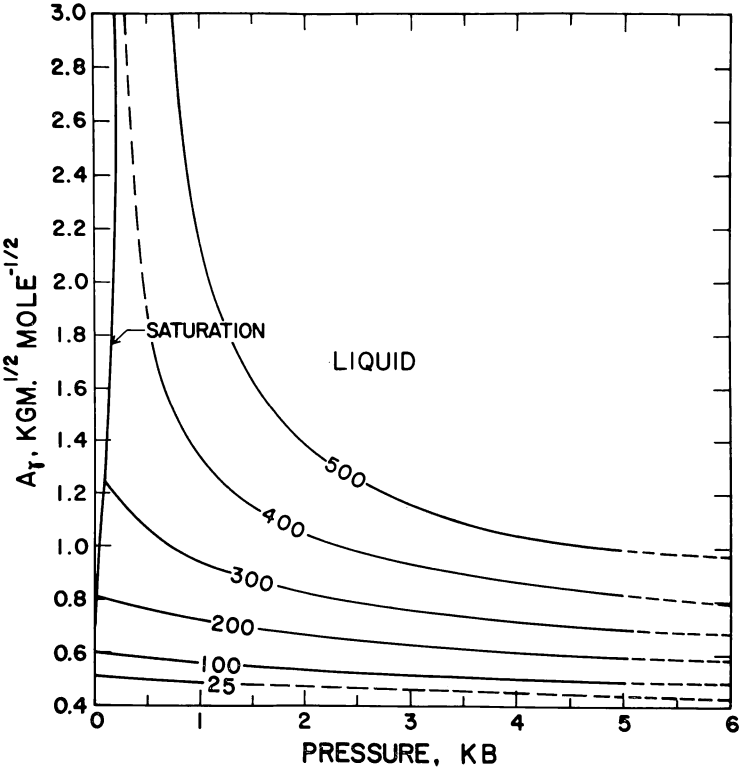

Fig. 2. A_γ (table 1) as a function of pressure at constant temperature (labeled in °C) computed from equation (2).

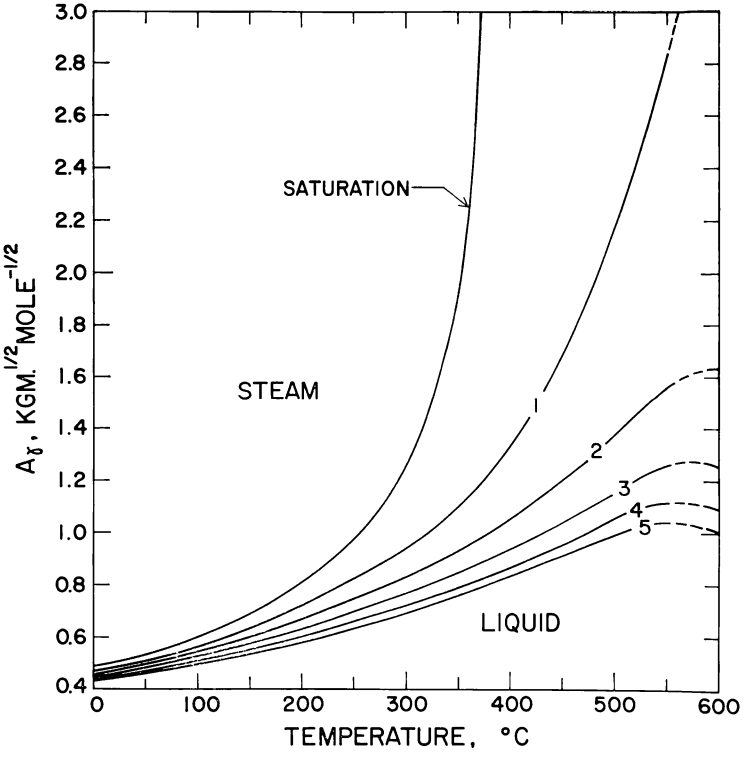

Fig. 3. A_γ (table 1) as a function of temperature at constant pressure (labeled in kb) computed from equation (2).

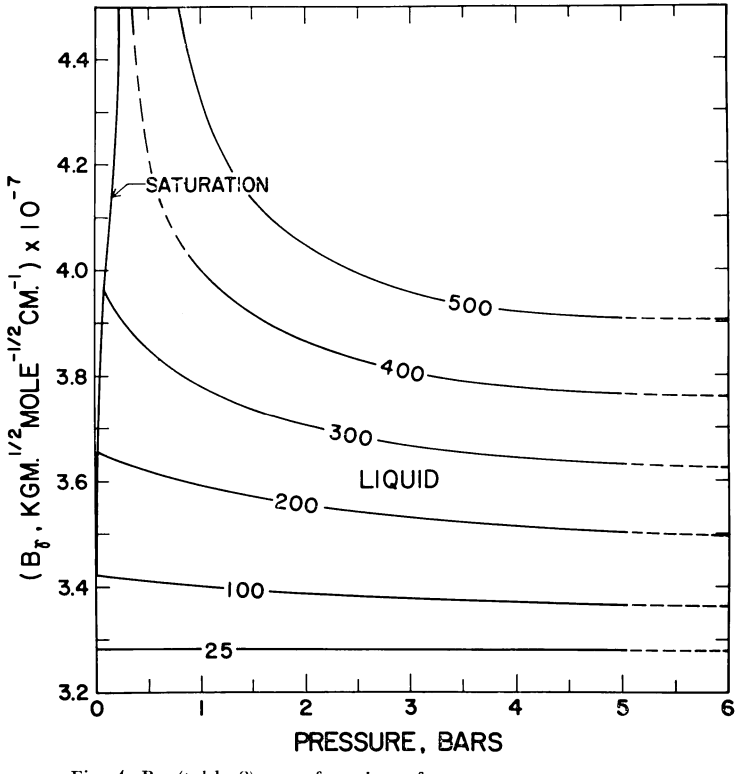

Fig. 4. B_γ (table 2) as a function of pressure at constant temperature (labeled in °C) computed from equation (3).

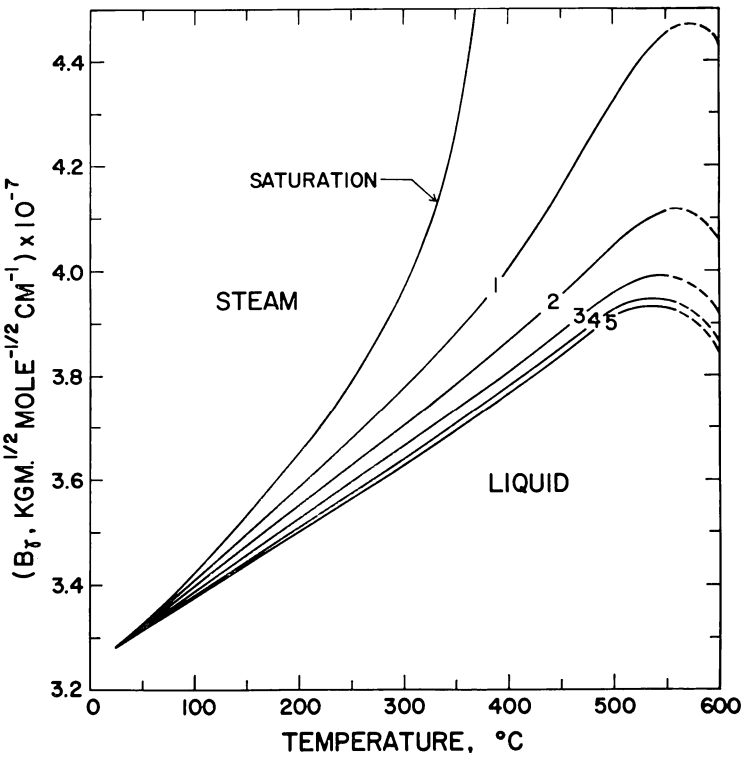

Fig. 5. B_γ (table 2) as a function of temperature at constant pressure (labeled in kb) computed from equation (3).

bined effects of increasing temperature and pressure on A_γ can be compared with the corresponding effects on B_γ. It can be seen that the configurations of the isopleths in the two diagrams are comparable. However, because the electrostatic contribution to A_γ and B_γ dominates the change in these variables over most of the pressure-temperature region considered, $(\partial P/\partial T)_{A\gamma} < (\partial P/\partial T)_{B\gamma}$; that is, as pressure and temperature increase at constant A_γ, B_γ increases. Nevertheless, an increase in temperature from 0° to ~ 300°C along the saturation curve causes corresponding increases in A_γ and B_γ which are approximately equivalent to those resulting from an increase in temperature from 0° to ~ 500°C at 5 kb.

ENTHALPY

The partial derivatives of equations (2) and (3) with respect to temperature at constant pressure can be written as

$$\left(\frac{\partial A_\gamma}{\partial T}\right)_P = -\frac{3A_\gamma}{2}\left(\left(\frac{\partial \ln \varepsilon}{\partial T}\right)_P + \frac{1}{T} + \frac{\alpha}{3}\right) \tag{5}$$

and

$$\left(\frac{\partial B_\gamma}{\partial T}\right)_P = -\frac{B_\gamma}{2}\left(\left(\frac{\partial \ln \varepsilon}{\partial T}\right)_P + \frac{1}{T} + \alpha\right) \tag{6}$$

where α stands for the coefficient of isobaric thermal expansion $(-(\partial \ln \rho/\partial T)_P)$. Following the definitions and notation adopted by Lewis and Randall (1961)[1]

$$A_H = 2(2.303)RT^2\left(\frac{\partial A_\gamma}{\partial T}\right)_P \tag{7}$$

and by analogy,

$$B_H = 2(2.303)RT^2\left(\frac{\partial B_\gamma}{\partial T}\right)_P \tag{8}$$

and

$$\mathring{a}_H = 2(2.303)RT^2\left(\frac{\partial \mathring{a}}{\partial T}\right)_P \tag{9}$$

Taking account of equation (1) we can thus write

$$\bar{L}_2 \equiv \bar{H}_2 - \bar{H}^\circ_2 = -2.303\upsilon RT^2\left(\frac{\partial \log \gamma_\pm}{\partial T}\right)_P$$

$$= \frac{\omega A_H I^{1/2}}{1 + \mathring{a}B_\gamma I^{1/2}} - \frac{\omega A_\gamma I(\mathring{a}B_H + B_\gamma \mathring{a}_H)}{(1 + \mathring{a}B_\gamma I^{1/2})^2} \tag{10}$$

[1] For the sake of brevity, 2.303 is shown in equation (7) and subsequent equations, but 2.302585 was used for ln 10 in the calculations.

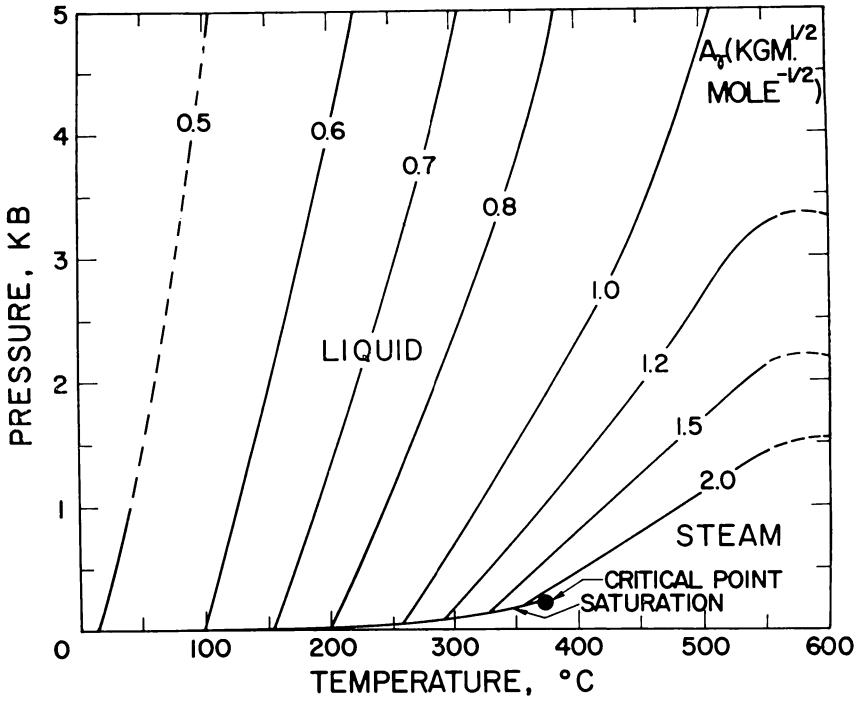

Fig. 6. Isopleths of A_γ (labeled in $kg^{1/2}mole^{-1/2}$) as a function of pressure and temperature (table 1 and figs. 2 and 3).

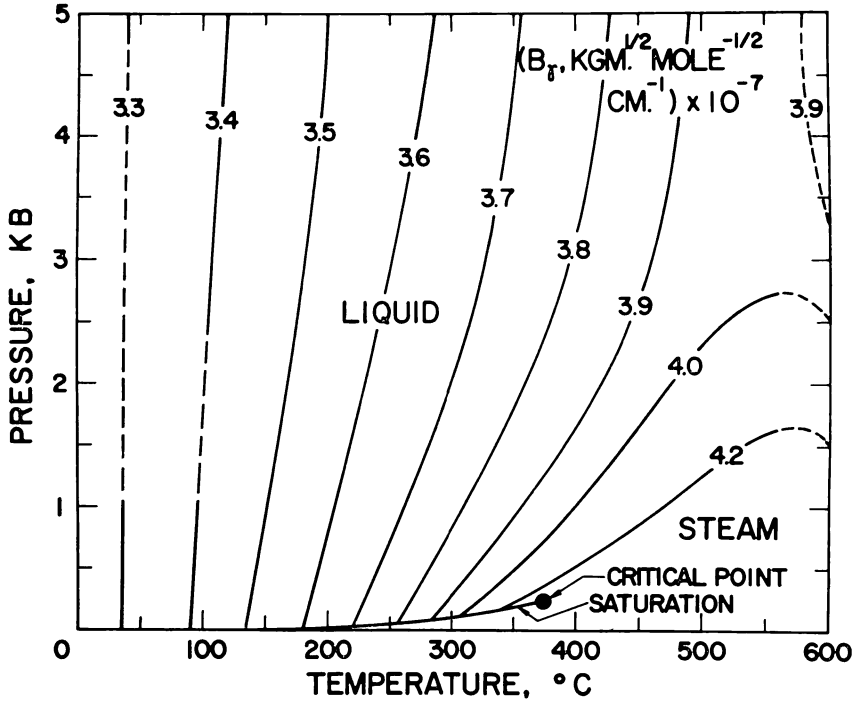

Fig. 7. Isopleths of B_γ (labeled in $(kg^{1/2}mole^{-1/2}cm^{-1}) \times 10^{-7}$) as a function of pressure and temperature (table 2 and figs. 4 and 5).

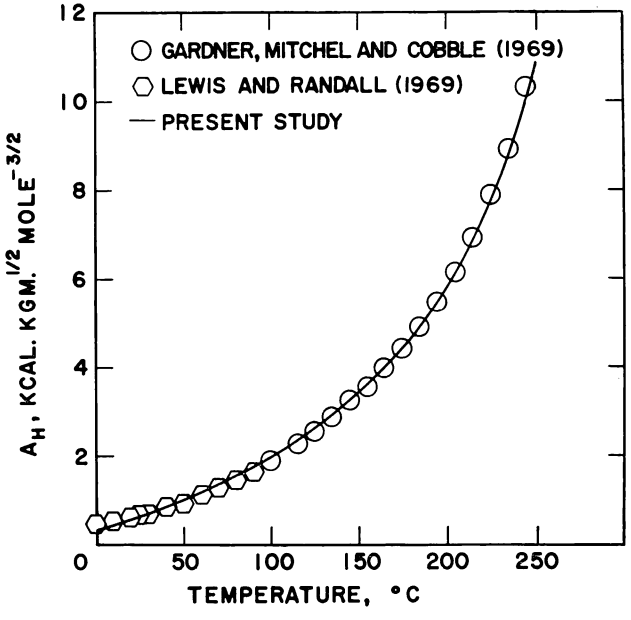

Fig. 8. A_H for the steam-saturated liquid phase as a function of temperature computed (curve) in the present study (table 17) compared with corresponding values taken from the literature.

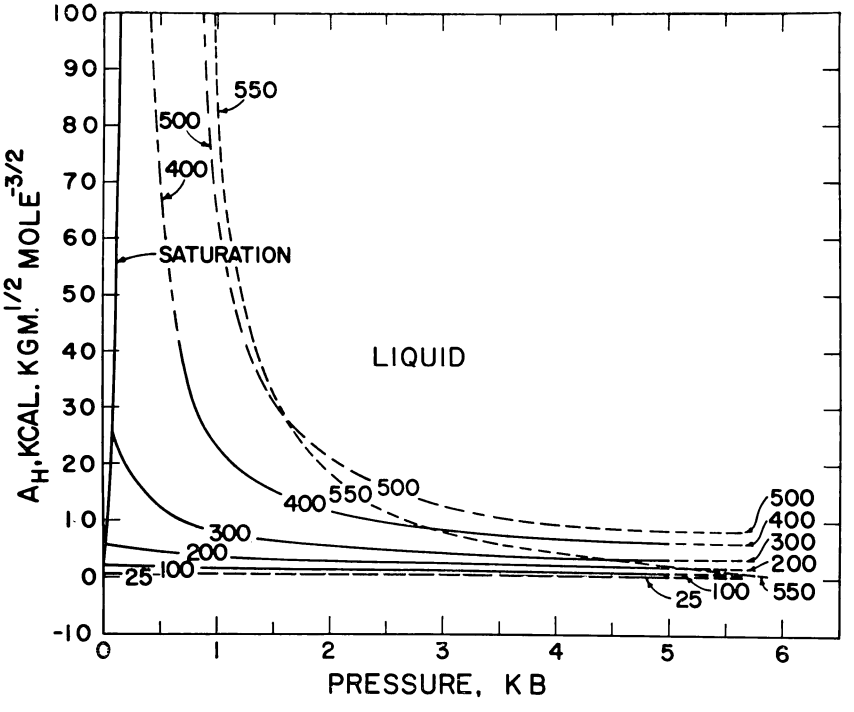

Fig. 9. A_H (table 3) as a function of pressure at constant temperature (labeled in °C) computed from equations (2), (5), and (7).

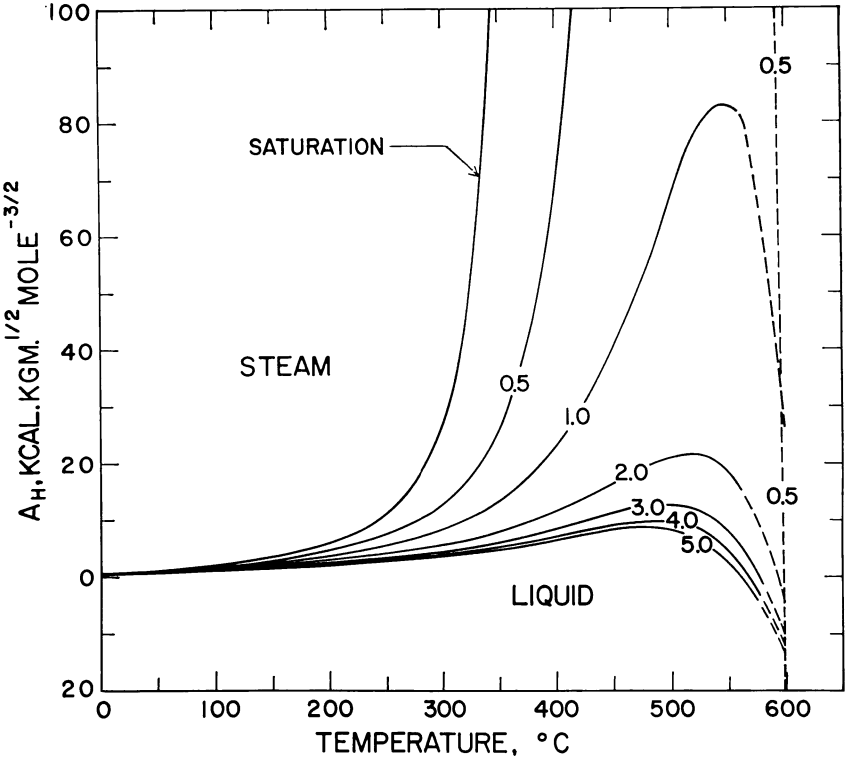

Fig. 10. A_H (table 3) as a function of temperature at constant pressure (labeled in kb) computed from equations (2), (5), and (7).

where $\bar{L}_2$ is the relative partial molal enthalpy of the solute (designated by the subscript 2) at constant temperature and pressure and

$$\omega = \frac{\upsilon|Z_+Z_-|}{2} = \frac{I}{m} \tag{11}$$

Extension of equation (1) to higher concentrations by addition of a $b_\gamma I$ term (eq 4) results in a corresponding term in equation (10) equal to $-\upsilon b_H I/2$, where

$$b_H = 2(2.303)RT^2\left(\frac{\partial b_\gamma}{\partial T}\right)_P \tag{12}$$

If $\mathring{a}B_\gamma$ is then taken to be independent of temperature and set to unity (as in the Guggenheim (1935) modification), it follows that

$$\bar{L}_2 = \frac{\omega A_H I^{1/2}}{1 + I^{1/2}} - \frac{\upsilon b_H I}{2} \tag{13}$$

which is consistent with the equation commonly used to represent the

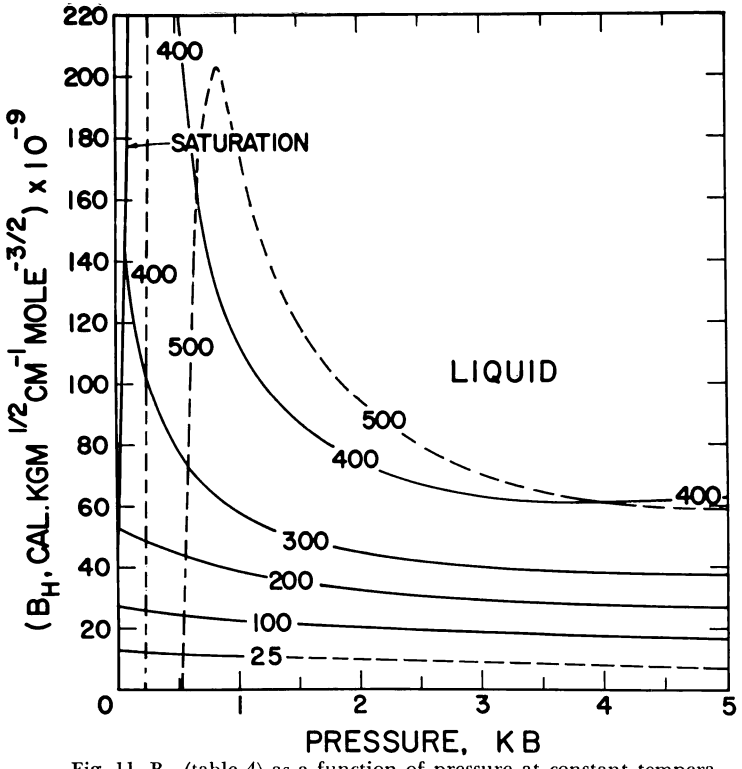

Fig. 11. B_H (table 4) as a function of pressure at constant temperature (labeled in °C) computed from equations (3), (6), and (8).

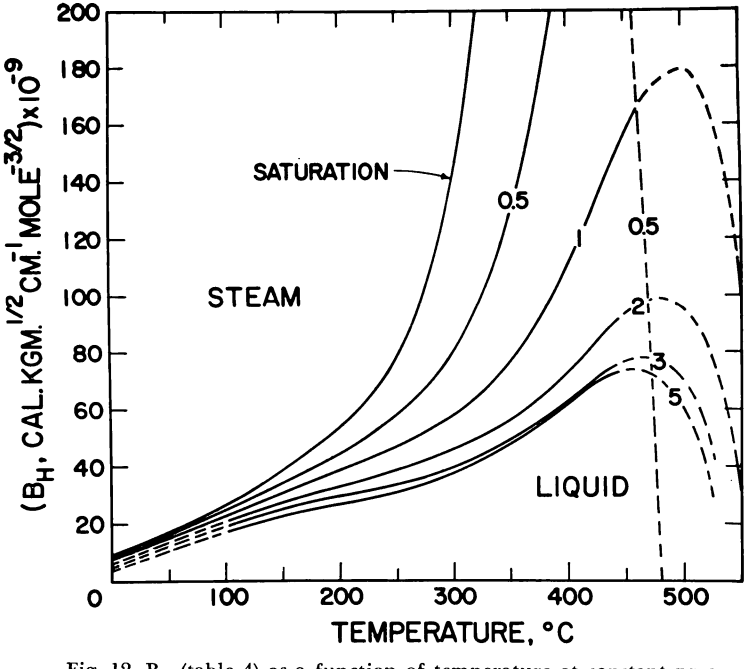

Fig. 12. B_H (table 4) as a function of temperature at constant pressure (labeled in kb) computed from equations (3), (6), and (8).

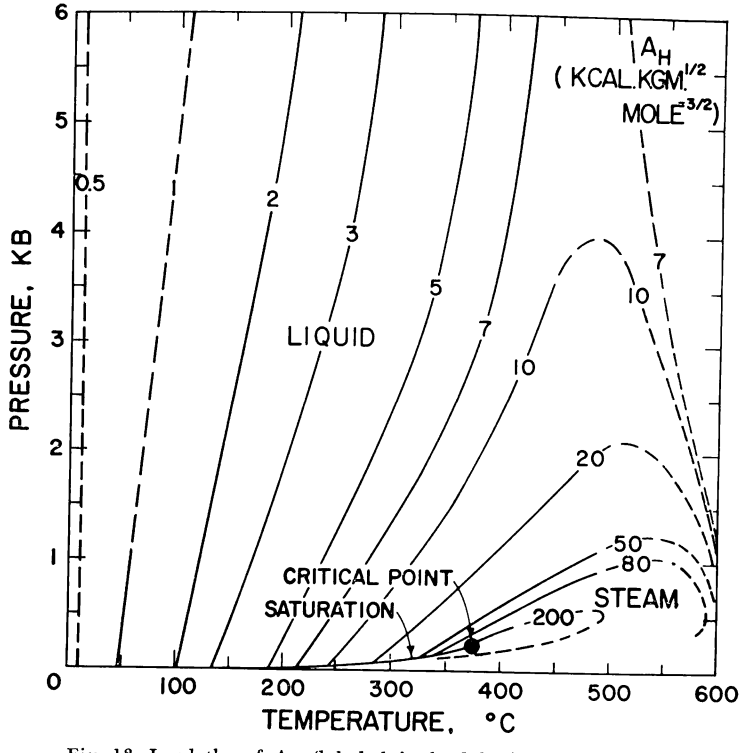

Fig. 13. Isopleths of A_H (labeled in kcal kg$^{1/2}$mole$^{-3/2}$) as a function of pressure and temperature (table 3 and figs. 9 and 10).

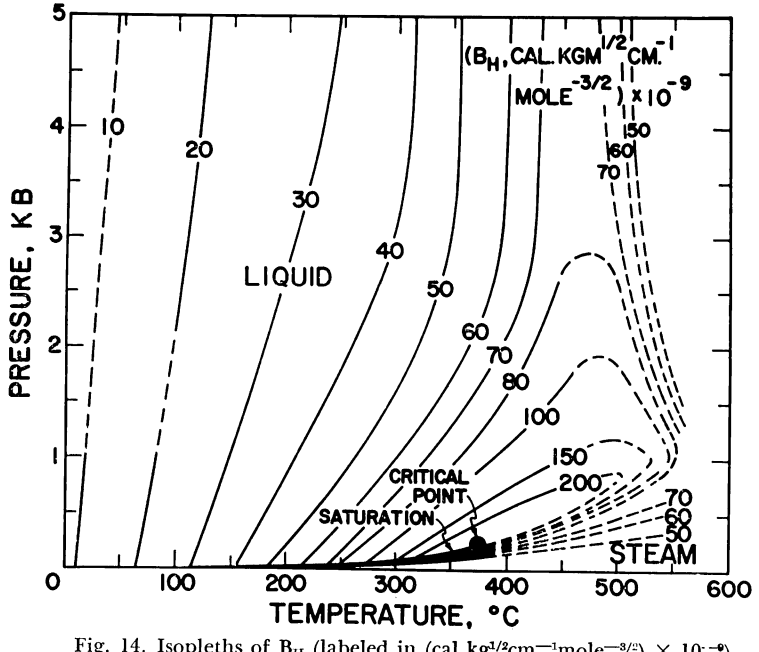

Fig. 14. Isopleths of B_H (labeled in (cal kg$^{1/2}$cm^{-1}mole$^{-3/2}$) $\times$ 10^{-9}) as a function of pressure and temperature (table 4 and figs. 11 and 12).

TABLE 5

A_J in cal $kg^{1/2}mole^{-3/2}$ $(°K)^{-1}$ computed from equations (2), (5), (16), and (18)—see figures 15 through 17 and 20

t	PRESSURE, KB						
(°C)	SAT	0.5	1	2	3	4	5
25	13.22	12	11	(9)	(8)	(8)	(7)
50	15.44	14	12	(10)	(9)	(9)	(8)
75	18.45	16	14	(12)	(10)	(9)	(9)
100	22.57	19	16	13	11	10	(9)
125	28.17	22	19	14	12	10	(10)
150	35.93	27	21	15	12	11	(10)
175	47.41	32	24	17	13	11	(10)
200	66.01	40	28	18	14	12	(11)
225	99.05	52	33	21	15	13	(12)
250	163.21	71	41	24	17	14	(13)
275	302.15	103	53	29	20	17	(16)
300	660.79	158	72	35	25	21	(20)
325	1964.42	256	100	44	30	26	(24)
350	13018.24	434	140	55	38	32	(29)
375			194	68	46	38	(35)
400			263	83	53	43	(38)
425			347	98	58	44	(38)
450			(442)	(107)	(55)	(37)	(29)
475			(529)	(103)	(38)	(16)	(6)
500			(546)	(67)	(-6)	(-29)	(-39)

TABLE 6

B_J in (cal $kg^{1/2}cm^{-1}mole^{-3/2}$ $(°K)^{-1}$) $\times 10^{-8}$ computed from equations (3), (6), (17), and (19)—see figures 18, 19, and 21

t	PRESSURE, KB						
(°C)	SAT	0.5	1	2	3	4	5
25	1.59	1.6	1.5	(1.5)	(1.4)	(1.4)	(1.4)
50	1.82	1.7	1.6	(1.6)	(1.5)	(1.4)	(1.4)
75	1.98	1.8	1.7	(1.6)	(1.4)	(1.4)	(1.3)
100	2.12	1.8	1.7	1.4	1.3	1.3	(1.2)
125	2.29	1.9	1.6	1.3	1.2	1.1	(1.1)
150	2.53	1.9	1.6	1.2	1.1	1.0	(1.0)
175	2.92	2.0	1.5	1.1	0.9	0.9	(0.9)
200	3.63	2.1	1.5	1.0	0.8	0.8	(0.8)
225	5.00	2.5	1.5	1.0	0.8	0.8	(0.8)
250	7.69	3.2	1.7	1.0	0.8	0.9	(1.0)
275	13.25	4.4	2.2	1.2	1.0	1.1	(1.2)
300	26.23	6.4	2.9	1.6	1.4	1.4	(1.6)
325	67.34	9.5	4.0	2.0	1.8	1.9	(2.1)
350	353.14	14.1	5.4	2.6	2.3	2.4	(2.6)
375			6.9	3.3	2.8	2.8	(2.9)
400			8.1	3.8	3.1	2.9	(3.0)
425			8.8	4.0	2.9	2.5	(2.4)
450			(8.2)	(3.3)	(1.7)	(1.1)	(0.8)
475			(5.5)	(1.2)	(-1.0)	(-2.0)	(-2.5)
500			(-1.2)	(-3.5)	(-6.1)	(-7.4)	(-8.2)

TABLE 7

A_E in kcal $kg^{1/2}mole^{-3/2}$ computed from equations (2), (26), and (28)—see figures 22 through 24 and 27

t	PRESSURE, KB						
(°C)	SAT	0.5	1	2	3	4	5
25	0.582	0.52	0.47	(0.40)	(0.35)	(0.32)	(0.29)
50	0.773	0.70	0.64	(0.56)	(0.50)	(0.46)	(0.42)
75	0.972	0.88	0.81	(0.71)	(0.65)	(0.60)	(0.56)
100	1.167	1.06	0.97	0.86	0.78	0.73	(0.69)
125	1.346	1.21	1.11	0.98	0.90	0.85	(0.81)
150	1.493	1.33	1.22	1.08	1.00	0.95	(0.92)
175	1.591	1.40	1.28	1.15	1.07	1.04	(1.02)
200	1.623	1.42	1.29	1.17	1.12	1.11	(1.12)
225	1.569	1.36	1.25	1.17	1.16	1.18	(1.22)
250	1.409	1.22	1.15	1.14	1.19	1.27	(1.35)
275	1.115	1.01	1.02	1.11	1.25	1.39	(1.53)
300	0.632	0.72	0.87	1.11	1.35	1.57	(1.77)
325	-0.179	0.34	0.72	1.17	1.53	1.84	(2.11)
350	-1.801	-0.14	0.62	1.32	1.81	2.22	(2.57)
375			0.58	1.58	2.20	2.71	(3.14)
400			0.65	1.96	2.70	3.29	(3.80)
425			0.83	2.41	3.23	3.89	(4.48)
450			(1.09)	(2.78)	(3.65)	(4.37)	(5.02)
475			(1.19)	(2.78)	(3.66)	(4.41)	(5.13)
500			(0.44)	(1.79)	(2.74)	(3.58)	(4.36)
525			(-2.98)	(-1.20)	(0.12)	(1.16)	(2.06)
550			(-12.96)	(-7.68)	(-5.19)	(-3.64)	(-2.50)
575			(-36.14)	(-19.39)	(-14.12)	(-11.46)	(-9.82)
600			(-79.58)	(-37.31)	(-26.88)	(-22.26)	(-19.74)

TABLE 8

B_E in (cal $kg^{1/2}cm^{-1}mole^{-3/2}$) $\times 10^{-9}$ computed from equations (3), (27), and (29)—see figures 25, 26, and 28

t	PRESSURE, KB						
(°C)	SAT	0.5	1	2	3	4	5
25	12.51	11.5	10.6	(9.4)	(8.4)	(7.7)	(7.1)
50	16.06	14.9	14.0	(12.6)	(11.6)	(10.8)	(10.3)
75	19.37	18.1	17.0	(15.5)	(14.4)	(13.7)	(13.2)
100	22.20	20.7	19.5	17.9	16.9	16.2	(15.7)
125	24.31	22.6	21.4	19.7	18.7	18.2	(17.9)
150	25.49	23.7	22.4	20.8	20.0	19.7	(19.7)
175	25.57	23.7	22.4	21.2	20.7	20.8	(21.1)
200	24.41	22.5	21.5	20.8	20.9	21.5	(22.3)
225	21.96	20.4	19.8	19.8	20.8	22.1	(23.6)
250	18.20	17.2	17.3	18.6	20.6	22.9	(25.2)
275	13.13	13.3	14.5	17.3	20.8	24.3	(27.6)
300	6.66	8.8	11.6	16.6	21.7	26.5	(31.0)
325	-1.63	3.8	9.1	16.7	23.6	30.0	(35.8)
350	-13.27	-1.4	7.3	17.9	26.8	34.9	(42.1)
375			6.4	20.5	31.3	41.0	(49.7)
400			6.6	24.1	36.8	48.0	(58.0)
425			7.7	28.1	42.1	54.6	(65.9)
450			(9.0)	(30.6)	(45.5)	(58.8)	(71.1)
475			(8.8)	(28.8)	(43.6)	(57.2)	(70.0)
500			(2.9)	(17.5)	(31.2)	(44.6)	(57.4)
525			(-17.4)	(-11.1)	(1.4)	(14.0)	(26.3)
550			(-67.6)	(-67.3)	(-55.0)	(-42.9)	(-31.4)
575			(-171.1)	(-163.3)	(-147.0)	(-133.9)	(-122.9)
600			(-353.0)	(-308.2)	(-279.9)	(-262.5)	(-250.7)

apparent molal enthalpy of the solute at constant temperature and pressure (ϕ_H) as a function of ionic strength; that is,

$$\phi_H = \bar{H}^\circ_2 + \omega A_H I^{1/2}\left((1 + I^{1/2})^{-1} - \frac{\sigma(I^{1/2})}{3}\right) - \frac{b_H \upsilon I}{4} \qquad (14)$$

where

$$\sigma(I^{1/2}) = \frac{3}{I^{3/2}}\left(1 + I^{1/2} - \frac{1}{1 + I^{1/2}} - 2 \ln (1 + I^{1/2}) \right) \qquad (15)$$

The term $\upsilon b_H I/2$ in equation (13) is numerically equivalent to Lewis and Randall's (1961) $2(2.303)RT^2 (\partial B/\partial T)_P\, m_{\upsilon_+\upsilon_-}$.

Values of A_H and B_H computed from equations (5) through (8) are given in tables 3 and 4 and plotted in figures 8 through 12. A_H values computed by Lewis and Randall (1961) and Gardner, Mitchell, and Cobble (1969) can be compared with those generated in this study for temperatures from 0° to 250°C in figure 8. The curve in figure 8 is in close agreement with the values calculated by Gardner, Mitchell, and Cobble but departs systematically to a slight extent from the low temperature values of Lewis and Randall (1961), which are based on the dielectric constant data of Malmberg and Maryott (1956) and densities taken from Dorsey (1940).

As expected from the isobaric behavior of A_γ and B_γ as functions of temperature in figures 3 and 5, the isobars in figures 10 and 12 pass through extrema at high temperatures, and the temperature corresponding to the maximum maximizes in the vicinity of a kilobar as pressure increases from the steam region to 5 kb. Note in figure 11 that the high temperature isotherms maximize at low pressures. With increasing pressure above ~ a kilobar at constant temperature, A_H and B_H decrease monotonically and approach constant values at high pressures.

The dependence of A_H and B_H on temperature and pressure is largely controlled by the behavior and relative magnitude of α compared to $(\partial \ln \varepsilon/\partial T)_P$, which are of opposite sign and approach ∞ and $-\infty$, respectively, at the critical point. The coefficient of isobaric thermal expansion increases at low temperatures with increasing temperature at constant pressure and the isobars maximize at or above the critical temperature. In contrast, $(\partial \ln \varepsilon/\partial T)_P$ becomes less negative with increasing temperature at constant pressure at both low and high temperatures, owing to isobaric extrema in the vicinity of 200° to 300°C and the minimum at the critical point (Helgeson and Kirkham, 1974a). As a consequence, $(\partial \ln \varepsilon/\partial T)_P$ controls the behavior of A_H and B_H at low temperatures, but α dominates the behavior of these functions at high temperatures (especially at low pressures), which causes A_H and B_H to become negative at high temperatures. Accordingly, the isopleths in figures 13 and 14 wrap around the critical point in a configuration similar to that exhibited by corresponding isopleths for α. Because α is divided by 3 in equation (5), the contours

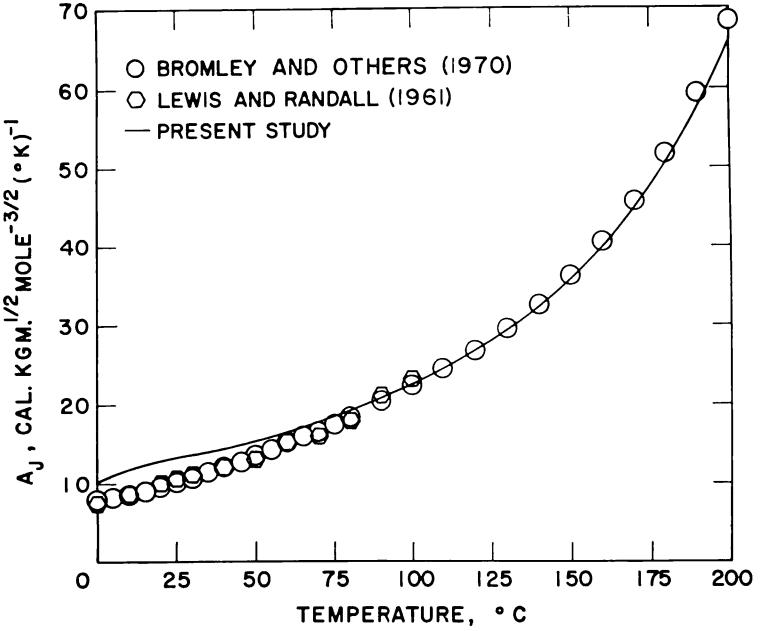

Fig. 15. A_J for the steam-saturated liquid phase as a function of temperature computed (curve) in the present study (table 17) compared with corresponding values taken from the literature.

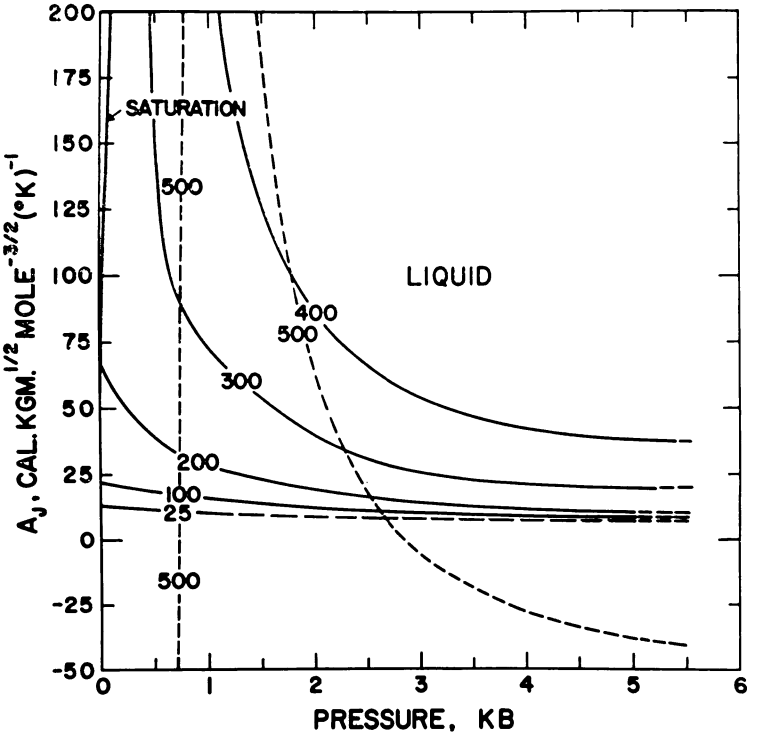

Fig. 16. A_J (table 5) as a function of pressure at constant temperature (labeled in °C) computed from equations (2), (5), (16), and (18).

around the critical point in figure 18 are not as convoluted as they are in figure 19.

It can be deduced from figures 9 through 14 that A_H and B_H as functions of temperature and pressure describe positive saddle-shaped asymptotic surfaces about the critical region. Nevertheless, in the immediate vicinity of the critical point, A_H and B_H should decrease and approach $-3(2.303)RT\ A_\gamma$ and $-2.303RT\ B_\gamma$, respectively. The configuration described by isopleths of A_H and B_H in the critical region should thus be similar to that defined by the contours of a precipitous volcano with a deep central vent (not shown in figs. 13 and 14).

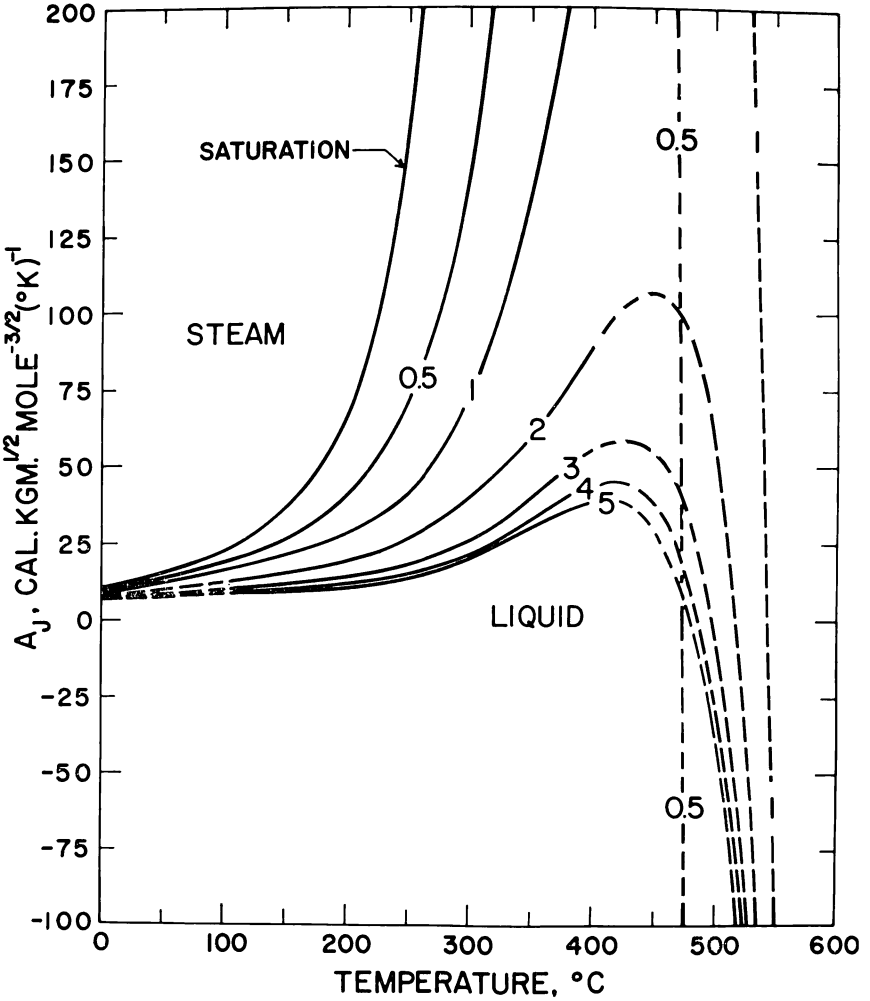

Fig. 17. A_J (table 5) as a function of temperature at constant pressure (labeled in kb) computed from equations (2), (5), (16), and (18).

HEAT CAPACITY AT CONSTANT PRESSURE

Differentiating equations (7) and (8) with respect to temperature at constant pressure leads to

$$A_J = \left(\frac{\partial A_H}{\partial T}\right)_P = 2(2.303)R\left(2T\left(\frac{\partial A_\gamma}{\partial T}\right)_P + T^2\left(\frac{\partial^2 A_\gamma}{\partial T^2}\right)_P\right)$$

$$= \frac{2A_H}{T} + 2(2.303)RT^2\left(\frac{\partial^2 A_\gamma}{\partial T^2}\right)_P \tag{16}$$

and

$$B_J = \left(\frac{\partial B_H}{\partial T}\right)_P = 2(2.303)R\left(2T\left(\frac{\partial B_\gamma}{\partial T}\right)_P + T^2\left(\frac{\partial^2 B_\gamma}{\partial T^2}\right)_P\right)$$

$$= \frac{2B_H}{T} + 2(2.303)RT^2\left(\frac{\partial^2 A_\gamma}{\partial T^2}\right)_P \tag{17}$$

where (from eqs 5 and 6)

$$\left(\frac{\partial^2 A_\gamma}{\partial T^2}\right)_P = \frac{1}{A_\gamma}\left(\frac{\partial A_\gamma}{\partial T}\right)_P^2 - \frac{3A_\gamma}{2}\left(\left(\frac{\partial^2 \ln \varepsilon}{\partial T^2}\right)_P - \frac{1}{T^2} + \frac{1}{3}\left(\frac{\partial \alpha}{\partial T}\right)_P\right) \tag{18}$$

and

$$\left(\frac{\partial^2 B_\gamma}{\partial T^2}\right)_P = \frac{1}{B_\gamma}\left(\frac{\partial B_\gamma}{\partial T}\right)_P^2 - \frac{B_\gamma}{2}\left(\left(\frac{\partial^2 \ln \varepsilon}{\partial T^2}\right) - \frac{1}{T^2} + \left(\frac{\partial \alpha}{\partial T}\right)_P\right) \tag{19}$$

The relative partial molal heat capacity of the solute at constant pressure ($\bar{J}_2$) consistent with equations (1) and (10) can thus be expressed as

$$\bar{J}_2 = \bar{C}_{P,2} - \bar{C}^\circ_{P,2} = \left(\frac{\partial \bar{L}_2}{\partial T}\right)_P$$

$$= 2.303\upsilon R\left(2T\left(\frac{\partial \log \gamma_\pm}{\partial T}\right)_P + T^2\left(\frac{\partial^2 \log \gamma_\pm}{\partial T^2}\right)_P\right)$$

$$= \frac{\omega A_J I^{1/2}}{1 + \mathring{a}B_\gamma I^{1/2}} - \frac{\omega I(A_H(\mathring{a}B_H + B_\gamma \mathring{a}_H) + A_\gamma \mathring{a}_H B_H)}{2.303RT^2(1 + \mathring{a}B_\gamma I^{1/2})^2}$$

$$- \frac{\omega A_\gamma I(\mathring{a}B_J + B_\gamma \mathring{a}_J)}{(1 + \mathring{a}B_\gamma I^{1/2})^2} + \frac{\omega A_\gamma I^{3/2}(\mathring{a}B_H + B_\gamma \mathring{a}_H)^2}{2.303RT^2(1 + \mathring{a}B_\gamma I^{1/2})^3} \tag{20}$$

or from equation (13) as

$$\bar{J}_2 = \frac{\omega A_J I^{1/2}}{1 + I^{1/2}} - \frac{\upsilon b_J I}{2} \tag{21}$$

which is consistent with

$$\phi_{C_P} = C^\circ_{P,2} + \omega A_J I^{1/2}\left((1 + I^{1/2})^{-1} - \frac{\sigma(I^{1/2})}{3}\right) - \frac{\upsilon b_J I}{4} \qquad (22)$$

where ϕ_{C_P} is the apparent molal heat capacity of the solute at constant temperature and pressure,

$$\mathring{a}_J = \left(\frac{\partial \mathring{a}_H}{\partial T}\right)_P = 2(2.303)R\left(2T\left(\frac{\partial \mathring{a}}{\partial T}\right)_P + T^2\left(\frac{\partial^2 \mathring{a}}{\partial T^2}\right)_P\right)$$

$$= \frac{2\mathring{a}_H}{T} + 2(2.303)RT^2\left(\frac{\partial^2 \mathring{a}}{\partial T^2}\right)_P \qquad (23)$$

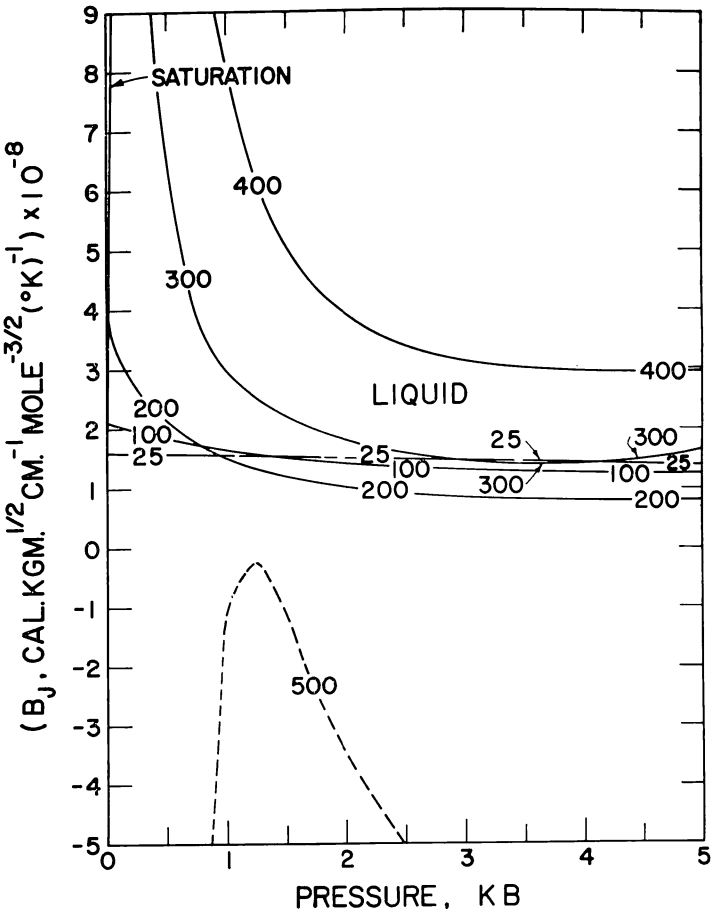

Fig. 18. B_J (table 6) as a function of pressure at constant temperature (labeled in °C) computed from equations (3), (6), (17), and (19).

and

$$b_J = \left(\frac{\partial b_H}{\partial T}\right)_P = 2(2.303)R\left(2T\left(\frac{\partial b_\gamma}{\partial T}\right)_P + T^2\left(\frac{\partial^2 b_\gamma}{\partial T^2}\right)_P\right)$$

$$= \frac{2b_H}{T} + 2(2.303)RT^2\left(\frac{\partial^2 b_\gamma}{\partial T^2}\right)_P \qquad (24)$$

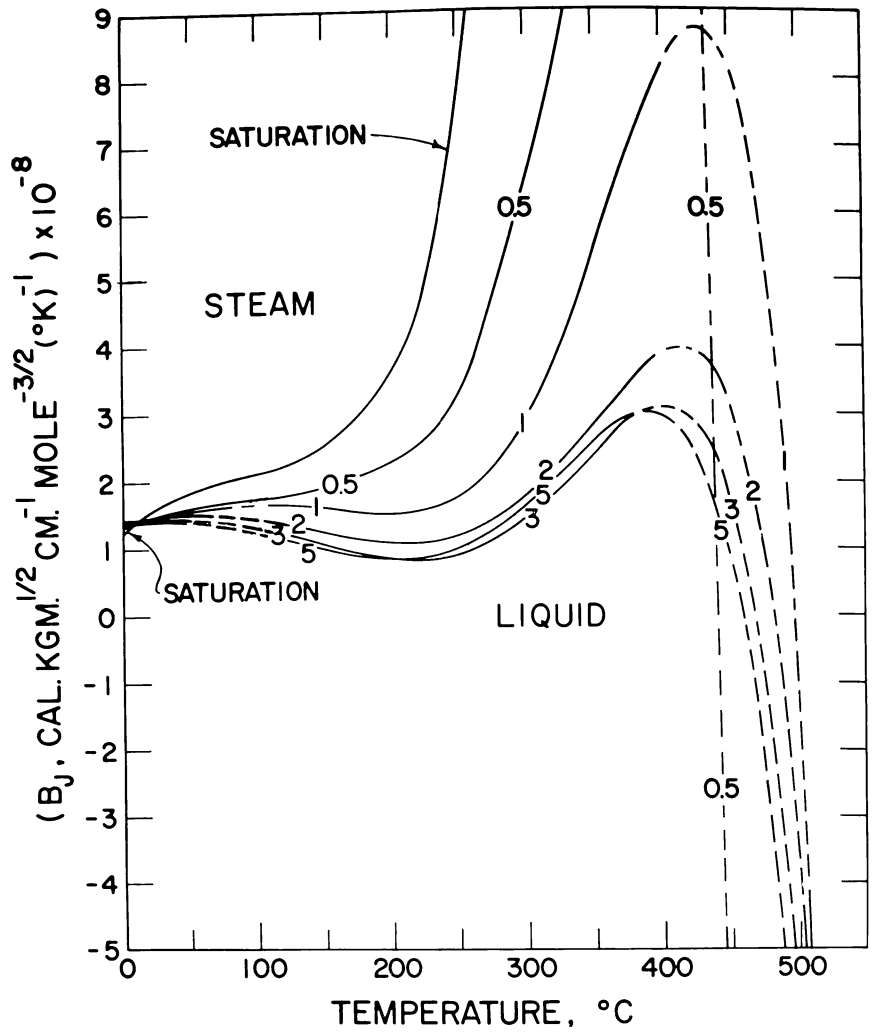

Fig. 19. B_J (table 6) as a function of temperature at constant pressure (labeled in kb) computed from equations (3), (6), (17), and (19).

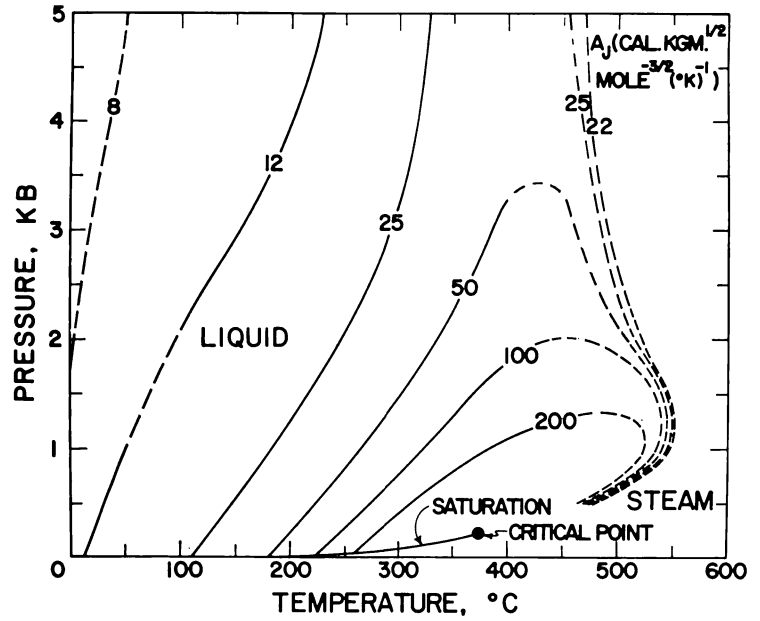

Fig. 20. Isopleths of A_J (labeled in cal $kg^{1/2}mole^{-3/2}(°K)^{-1}$) as a function of pressure and temperature (table 5 and figs. 16 and 17).

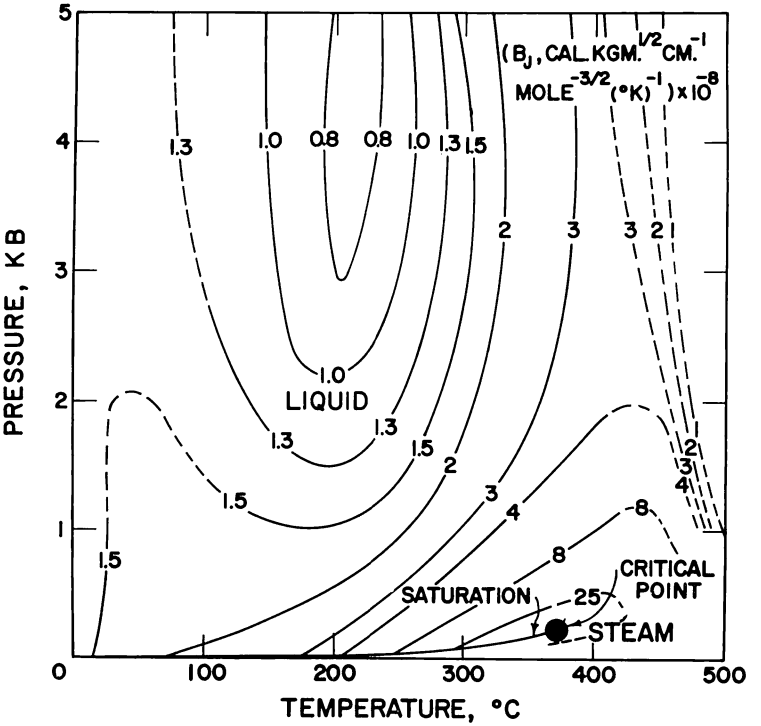

Fig. 21. Isopleths of B_J (labeled in (cal $kg^{1/2}cm^{-1}mole^{-3/2}(°K)^{-1}$) $\times 10^{-8}$) as a function of pressure and temperature (table 6 and figs. 18 and 19).

The term $\upsilon b_J I/4$ in equation (22), which corresponds to the partial derivative of equation (14), is numerically equivalent to $2.303RT^2\ m\upsilon_+\upsilon_-(2(\partial B/\partial T)_P/T + (\partial^2 B/\partial T^2)_P)$ in the comparable equation given by Lewis and Randall (1961).

Values of A_J and B_J computed from equations (16) through (19) are given in tables 5 and 6 and plotted in figures 15 through 19. It can be seen in figure 15 that the values of A_J computed in this study are in close agreement with those reported by Bromley and others (1970) and Lewis and Randall (1961) from 90° to 200°C along the saturation curve, but at lower temperatures the curve in figure 15 departs to higher values of A_J than those reported in the literature. The discrepancies result from the high sensitivity of A_J to $(\partial^2 \ln \varepsilon/\partial T^2)_P$ and the fact that the low temperature values taken from the literature were obtained by fitting dielectric constants reported by Malmberg and Maryott (1956) in contrast to the curve in figure 15, which is based on composite regression of data given by Owen and others (1961), Oshry (ms), and Heger (ms). The curve in figure 15 is consistent with that in figure 8, but Malmberg and Maryott's (1956) data are not closely consistent with the values of the dielectric constant reported by Oshry (ms) at higher temperatures (Helgeson and Kirkham, 1974a).

As expected from the behavior of the isobars in figures 10 and 12, those in figures 17 and 19 exhibit extrema between the temperature corresponding to the critical point and 450°C. Note also that the temperatures represented by the extrema maximize with increasing pressure. It

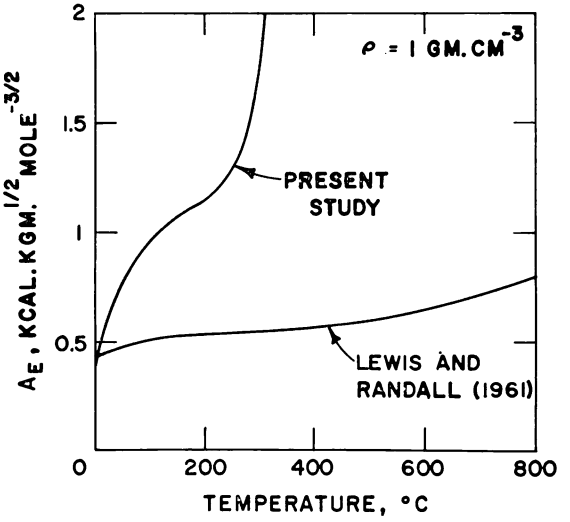

Fig. 22. A_E for a density of H_2O of one g cm^{-3} computed in the present study compared with corresponding values taken from the literature.

can be seen in figures 16 and 18 that both A_J and B_J maximize with increasing pressure at constant temperature $\gtrsim$ the critical temperature at pressures ranging from the critical pressure to ~ a kilobar at 500°C. Note that the isopleths in figures 20 and 21 wrap around the critical point, as they do for A_H and B_H in figures 13 and 14. In contrast to those for α, β, and C_P of H_2O (which approach infinity at the critical point), the isopleths for A_J and B_J in the immediate vicinity of the critical point should describe a "volcanic vent" configuration (not shown in figs. 20 and 21) like (but offset from) those of A_H and B_H. It can be seen in figure 21 that the isopleths for B_J minimize at ~ 200°C and high pressures. No corresponding minima in the A_J isopleths are apparent in figure 20.

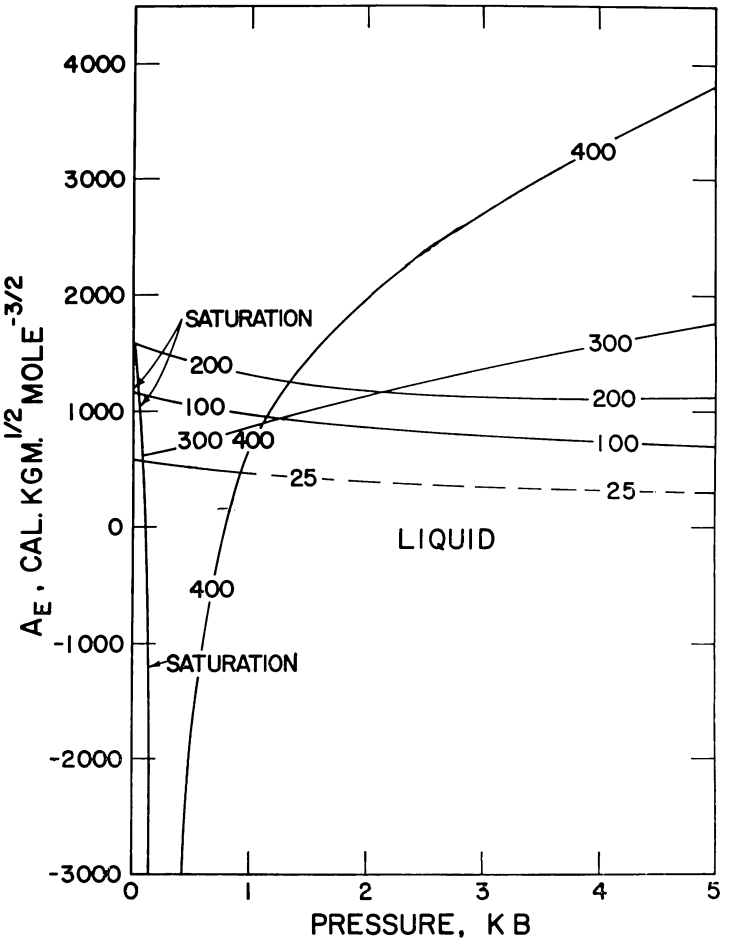

Fig. 23. A_E (table 7) as a function of pressure at constant temperature (labeled in °C) computed from equations (2), (26), and (28).

INTERNAL ENERGY

The Debye-Hückel parameters for the relative partial molal internal energy of the solute at constant *temperature* and *volume* ($\bar{E}_2 - \bar{E}^\circ_2$) defined by

$$\bar{E}_2 - \bar{E}^\circ_2 = -2.303_v RT^2 \left(\frac{\partial \log \gamma_\pm}{\partial T}\right)_\rho \tag{25}$$

can be expressed as

$$A_E = 2(2.303)RT^2 \left(\frac{\partial A_\gamma}{\partial T}\right)_\rho \tag{26}$$

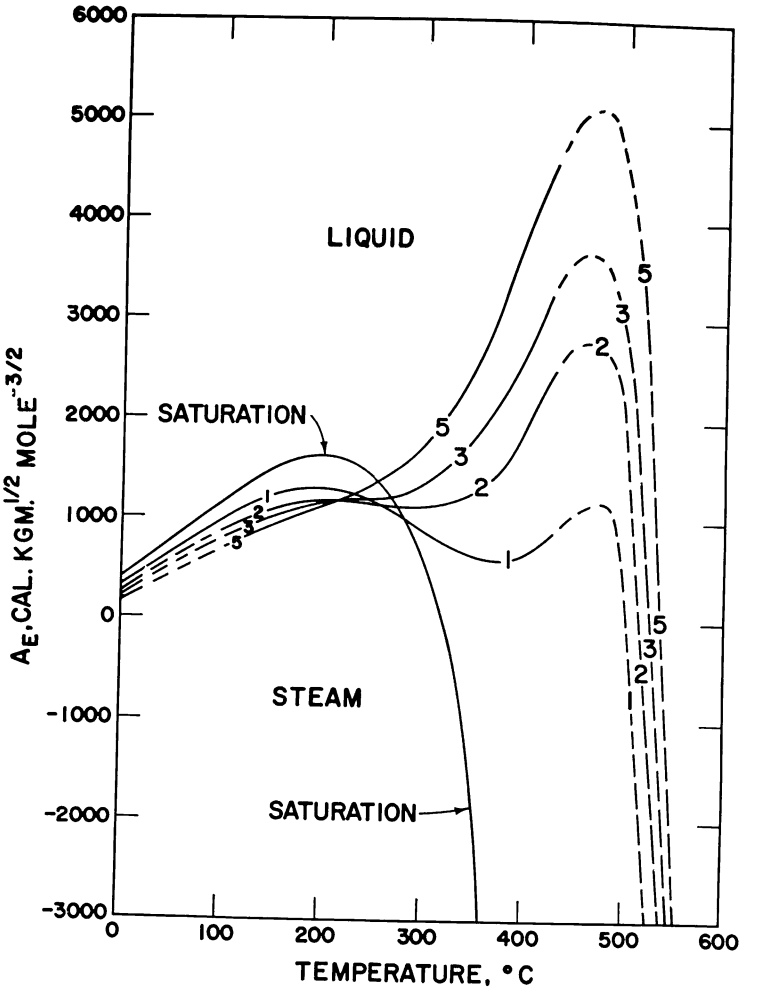

Fig. 24. A_E (table 7) as a function of temperature at constant pressure (labeled in kb) computed from equations (2), (26), and (28).

and

$$B_E = 2(2.303)RT^2\left(\frac{\partial B_\gamma}{\partial T}\right)_\rho \tag{27}$$

where (from eqs 2and 3)

$$\left(\frac{\partial A_\gamma}{\partial T}\right)_\rho = -\frac{3A_\gamma}{2}\left(\left(\frac{\partial \ln \varepsilon}{\partial T}\right)_\rho + \frac{1}{T}\right) \tag{28}$$

and

$$\left(\frac{\partial B_\gamma}{\partial T}\right)_\rho = -\frac{B_\gamma}{2}\left(\left(\frac{\partial \ln \varepsilon}{\partial T}\right)_\rho + \frac{1}{T}\right) = \frac{B_\gamma}{3A_\gamma}\left(\frac{\partial A_\gamma}{\partial T}\right)_\rho \tag{29}$$

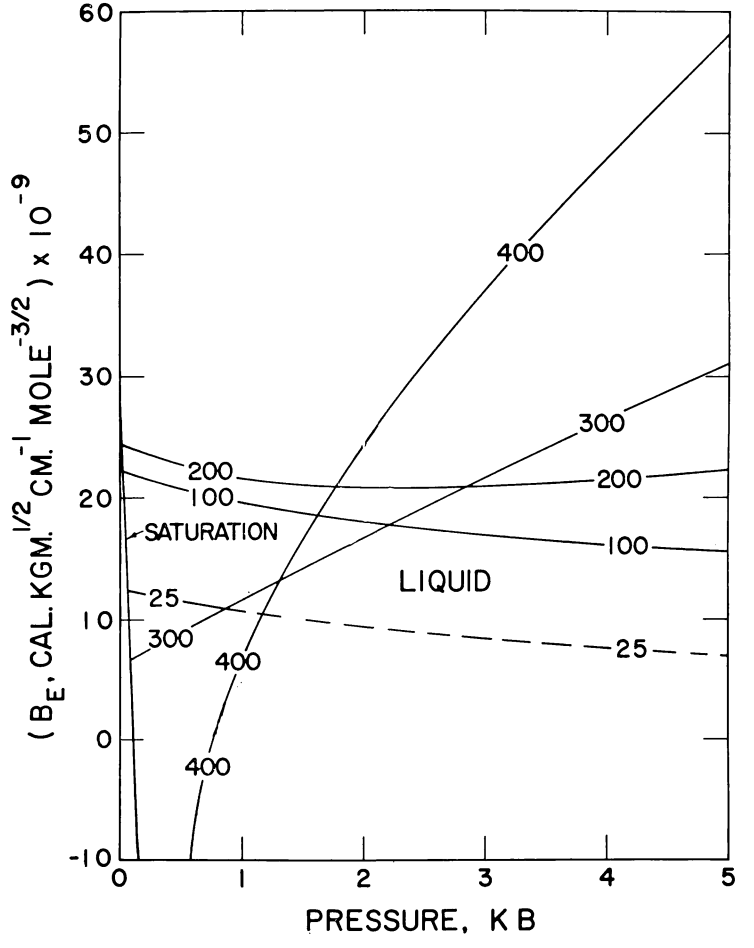

Fig. 25. B_E (table 8) as a function of pressure at constant temperature (labeled in °C) computed from equations (3), (27), and (29).

Hence

$$B_E = \frac{A_E B_\gamma}{3A_\gamma} \tag{30}$$

The internal energy analogs of equations (10), (13), and (14) for constant temperature and volume can now be written as

$$\tilde{E}_2 - \tilde{E}^\circ_2 = \frac{\omega A_E I^{1/2}}{1 + \mathring{a}B_\gamma I^{1/2}} - \frac{\omega A_\gamma I(\mathring{a}B_E + B_\gamma \mathring{a}_E)}{(1 + \mathring{a}B_\gamma I^{1/2})^2} \tag{31}$$

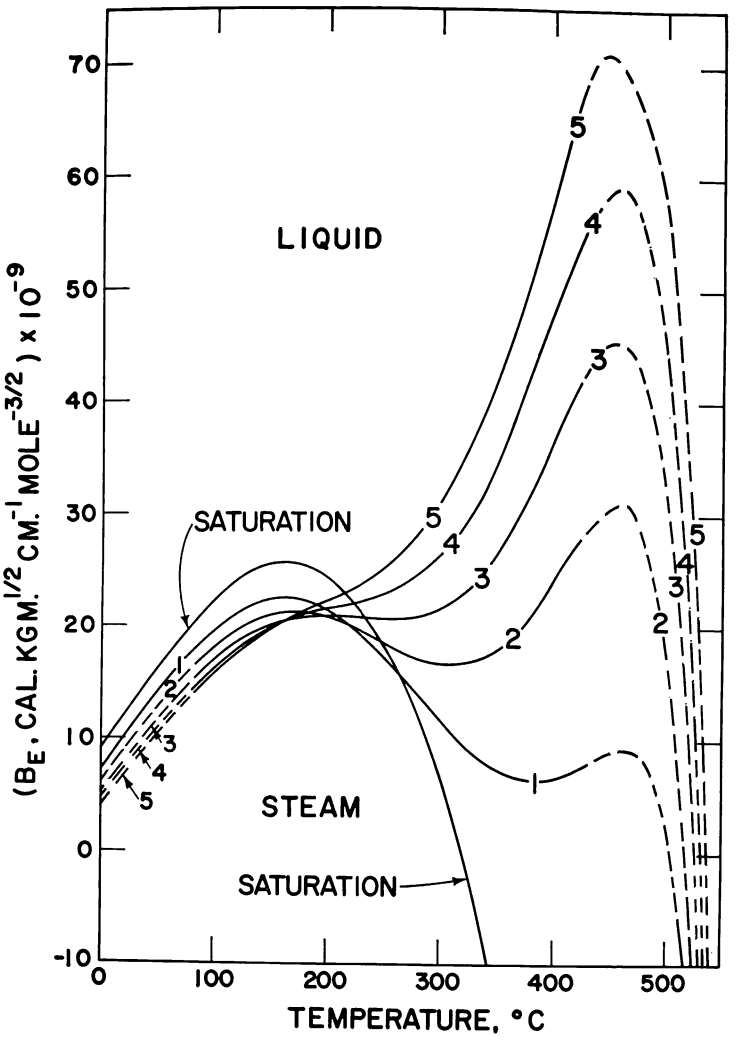

Fig. 26. B_E (table 8) as a function of temperature at constant pressure (labeled in kb) computed from equations (3), (27), and (29).

TABLE 9

A_{C_V} in cal $kg^{1/2}mole^{-3/2}$ $(°K)^{-1}$ computed from equations (2), (28), (37), and (39)—see figures 29 through 31 and 34

t	PRESSURE, KB						
(°C)	SAT	0.5	1	2	3	4	5
25	6.61	6.1	5.8	(5.3)	(5.0)	(4.9)	(4.8)
50	6.20	5.8	5.5	(5.1)	(4.9)	(4.8)	(4.8)
75	5.29	5.0	4.7	(4.5)	(4.5)	(4.5)	(4.6)
100	3.75	3.6	3.6	3.6	3.8	4.0	(4.3)
125	1.52	1.7	1.9	2.4	3.0	3.5	(3.9)
150	-1.42	-0.7	0.0	1.1	2.1	2.9	(3.7)
175	-4.99	-3.4	-2.2	-0.2	1.4	2.6	(3.7)
200	-9.02	-6.2	-4.1	-1.2	1.1	2.8	(4.3)
225	-13.26	-8.7	-5.5	-1.5	1.5	3.8	(5.6)
250	-17.44	-10.3	-5.9	-0.8	3.0	5.8	(8.0)
275	-21.32	-10.8	-4.8	1.3	5.7	8.9	(11.4)
300	-24.85	-9.5	-2.0	5.0	9.7	13.1	(15.9)
325	-28.50	-6.0	3.0	10.3	14.9	18.5	(21.5)
350	-35.41	0.5	10.0	16.7	20.9	24.4	(27.5)
375			18.8	23.5	26.8	30.1	(33.3)
400			28.5	29.1	31.1	33.9	(37.1)
425			36.5	30.5	30.9	33.2	(36.4)
450			(36.6)	(22.5)	(21.8)	(23.7)	(26.9)
475			(15.2)	(-3.4)	(-3.3)	(-0.8)	(2.5)
500			(-56.1)	(-60.0)	(-53.6)	(-48.4)	(-44.1)

TABLE 10

B_{C_V} in (cal $kg^{1/2}cm^{-1}mole^{-3/2}$ $(°K)^{-1}$) $\times 10^{-8}$ computed from equations (3), (29), (38), and (40)—see figures 32, 33, and 35

t	PRESSURE, KB						
(°C)	SAT	0.5	1	2	3	4	5
25	1.30	1.2	1.2	(1.2)	(1.1)	(1.1)	(1.1)
50	1.13	1.1	1.1	(1.0)	(1.0)	(1.1)	(1.1)
75	0.85	0.8	0.8	(0.9)	(0.9)	(0.9)	(1.0)
100	0.49	0.5	0.5	0.6	0.7	0.8	(0.9)
125	0.04	0.1	0.2	0.3	0.5	0.6	(0.7)
150	-0.47	-0.3	-0.2	0.1	0.3	0.5	(0.6)
175	-1.00	-0.7	-0.5	-0.2	0.1	0.4	(0.6)
200	-1.52	-1.1	-0.8	-0.3	0.1	0.4	(0.7)
225	-1.97	-1.4	-1.0	-0.4	0.2	0.6	(0.9)
250	-2.32	-1.5	-0.9	-0.2	0.4	0.9	(1.3)
275	-2.54	-1.2	-0.7	0.1	0.9	1.4	(1.9)
300	-2.62	-0.7	-0.3	0.7	1.5	2.1	(2.6)
325	-2.60	0.0	-0.4	1.4	2.2	2.9	(3.4)
350	-2.63		1.2	2.2	3.0	3.6	(4.2)
375			2.0	3.0	3.7	4.3	(4.9)
400			2.9	3.5	4.1	4.6	(5.2)
425			3.3	3.5	3.8	4.3	(4.8)
450			(3.0)	(2.4)	(2.5)	(2.8)	(3.3)
475			(1.1)	(-0.4)	(-0.6)	(-0.4)	(-0.1)
500			(-3.7)	(-5.9)	(-6.2)	(-6.2)	(-6.1)

TABLE 11

A_V in $cm^3kg^{1/2}mole^{-3/2}$ computed from equations (2), (48), and (51)—see figures 36 through 38 and 41

t	PRESSURE, KB						
(°C)	SAT	0.5	1	2	3	4	5
25	2.75	2.37	2.13	(1.67)	(1.35)	(1.10)	(0.90)
50	3.43	2.94	2.65	(2.09)	(1.67)	(1.35)	(1.11)
75	4.48	3.77	3.33	(2.58)	(2.04)	(1.65)	(1.35)
100	6.03	4.93	4.24	3.21	2.49	2.00	(1.63)
125	8.29	6.52	5.43	4.01	3.04	2.41	(1.95)
150	11.60	8.72	7.01	5.04	3.71	2.89	(2.31)
175	16.56	11.77	9.08	6.34	4.51	3.44	(2.72)
200	24.21	16.06	11.83	7.97	5.48	4.08	(3.17)
225	36.56	22.22	15.51	9.99	6.62	4.79	(3.65)
250	57.81	31.34	20.47	12.45	7.94	5.58	(4.17)
275	97.83	45.34	27.29	15.43	9.48	6.46	(4.72)
300	184.17	67.85	36.83	19.03	11.25	7.43	(5.31)
325	419.46	106.14	50.45	23.41	13.30	8.52	(5.94)
350	1504.78	176.05	70.18	28.79	15.68	9.73	(6.62)
375			99.06	35.46	18.48	11.11	(7.36)
400			141.49	43.87	21.79	12.70	(8.20)
425			203.66	54.58	25.76	14.56	(9.15)
450			(294.23)	(68.29)	(30.57)	(16.76)	(10.27)
475			(424.14)	(85.86)	(36.39)	(19.36)	(11.58)
500			(603.15)	(108.10)	(43.38)	(22.43)	(13.14)
525			(830.08)	(131.18)	(52.05)	(27.27)	(14.96)
550			(1080.52)	(160.58)	(61.08)	(31.20)	(16.92)
575			(1305.01)	(190.49)	(70.13)	(35.06)	(18.88)
600			(1439.53)	(215.40)	(77.59)	(38.17)	(20.51)

TABLE 12

B_V in $(cm^2kg^{1/2}mole^{-3/2}) \times 10^{-6}$ computed from equations (3), (49), and (52)—see figures 39, 40, and 42

t	PRESSURE, KB						
(°C)	SAT	0.5	1	2	3	4	5
25	-2.07	-2.15					
50	-10.32	-9.08	-8.16	(-5.98)	(-4.07)	(-2.49)	(-1.13)
75	-20.47	-17.43	-15.34	(-11.31)	(-8.07)	(-5.59)	(-3.54)
100	-33.92	-27.99	-23.99	-17.47	-12.52	-8.97	(-6.11)
125	-52.24	-41.59	-34.59	-24.74	-17.52	-12.61	(-8.80)
150	-77.61	-59.23	-47.68	-33.41	-23.14	-16.48	(-11.54)
175	-113.39	-82.31	-63.89	-43.72	-29.40	-20.52	(-14.21)
200	-165.21	-112.85	-84.02	-55.81	-36.27	-24.61	(-16.68)
225	-243.18	-153.94	-109.20	-69.71	-43.67	-28.62	(-18.80)
250	-366.91	-232.08	-140.98	-85.42	-51.48	-32.42	(-20.43)
275	-578.63	-327.84	-181.59	-102.90	-59.55	-35.85	(-21.43)
300	-984.09	-475.22	-234.24	-122.21	-67.77	-38.82	(-21.68)
325	-1926.64	-715.90	-303.34	-143.56	-76.09	-41.26	(-21.13)
350	-5336.98	-1142.27	-394.50	-167.43	-84.57	-43.18	(-19.76)
375			-514.09	-194.60	-93.43	-44.68	(-17.61)
400			-668.02	-226.23	-103.08	-46.01	(-14.85)
425			-860.20	-263.90	-114.17	-47.56	(-11.76)
450			-1090.55	-309.61	-127.63	-49.92	(-8.78)
475			(-1350.36)	(-365.70)	(-144.62)	(-53.85)	(-6.51)
500			(-1612.73)	(-434.46)	(-166.41)	(-60.24)	(-5.73)
525			(-1825.03)	(-500.56)	(-195.74)	(-73.44)	(-7.30)
550			(-1924.25)	(-586.25)	(-228.70)	(-87.15)	(-11.85)
575			(-1871.34)	(-670.91)	(-264.95)	(-103.97)	(-19.51)
600			(-1652.62)	(-737.60)	(-298.70)	(-121.51)	(-29.37)

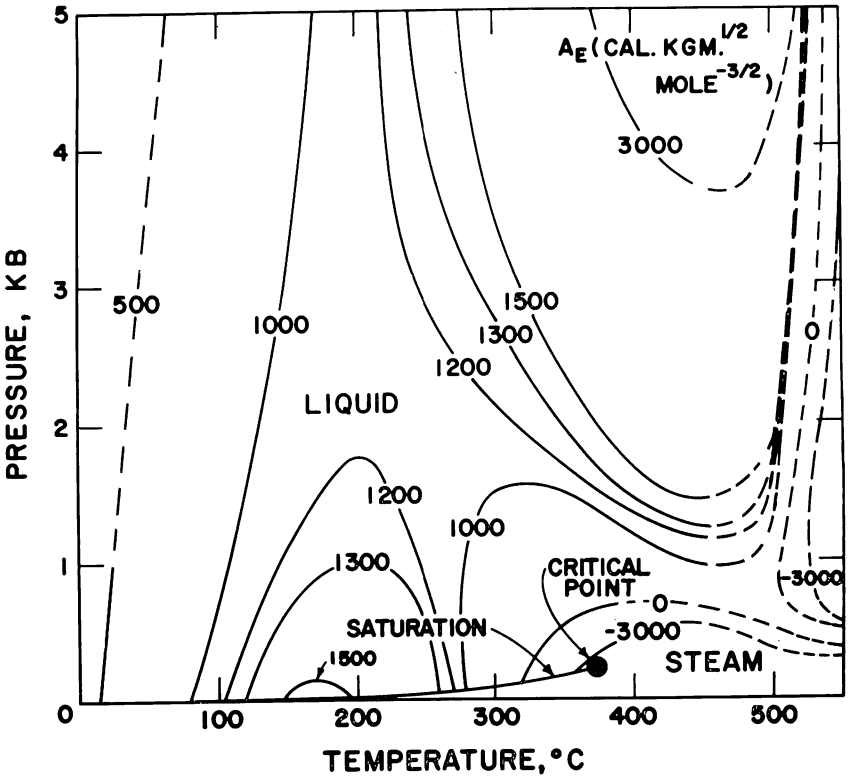

Fig. 27. Isopleths of A_E (labeled in cal $kg^{1/2}mole^{-3/2}$) as a function of pressure and temperature (table 7 and figs. 23 and 24).

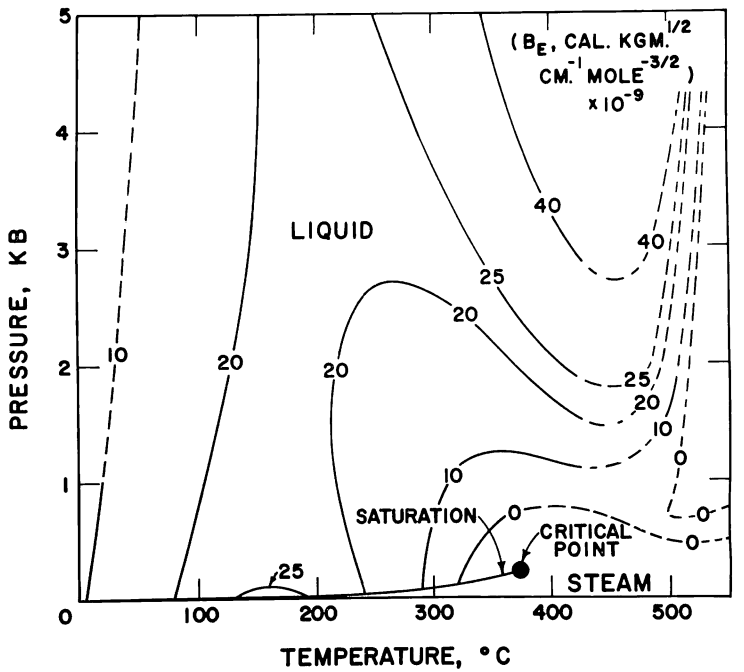

Fig. 28. Isopleths of B_E (labeled in (cal $kg^{1/2}cm^{-1}mole^{-3/2}$) $\times$ 10^{-9}) as a function of pressure and temperature (table 8 and figs. 25 and 26).

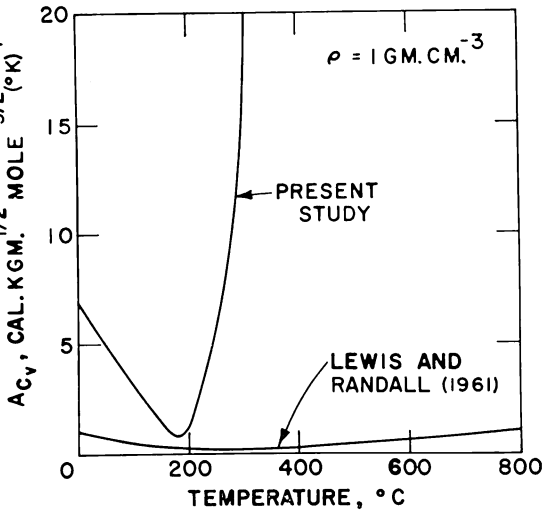

Fig. 29. A_{C_V} for a density of H_2O of one g cm^{-3} computed in the present study compared with corresponding values taken from the literature.

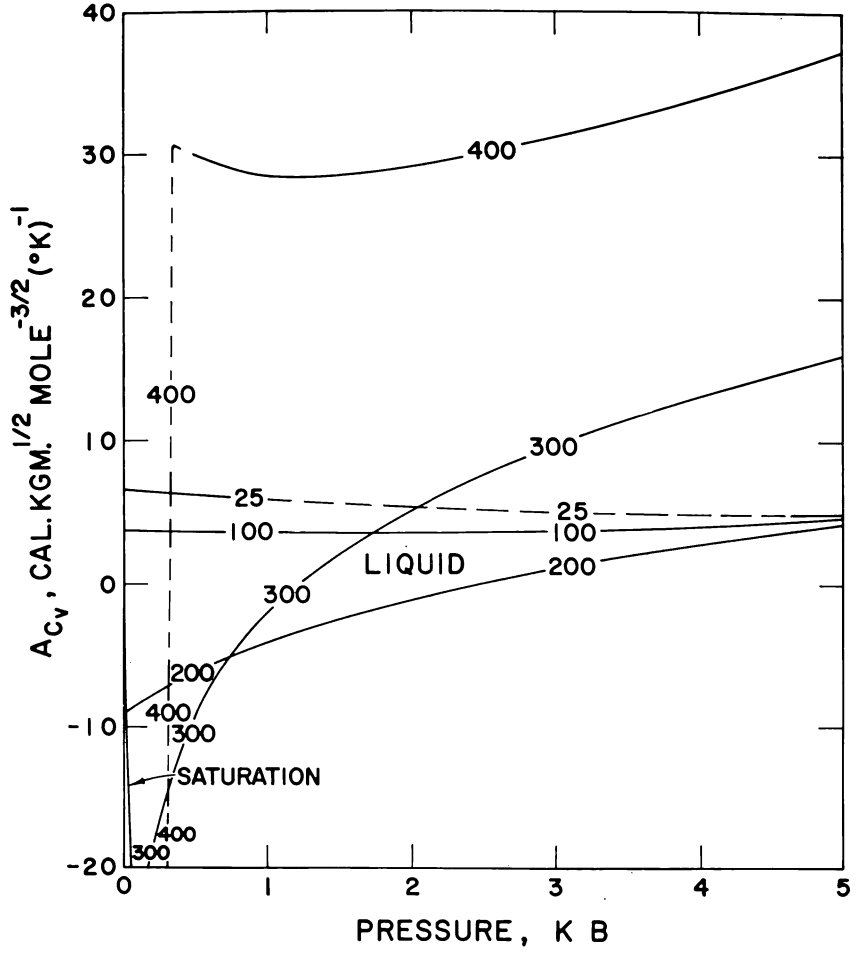

Fig. 30. A_{C_V} (table 9) as a function of pressure at constant temperature (labeled in °C) computed from equations (2), (28), (37), and (39).

$$\bar{E}_2 - \bar{E}^\circ_2 = \frac{\omega A_E I^{1/2}}{1 + I^{1/2}} - \frac{\upsilon b_E I}{2} \tag{32}$$

and

$$\phi_E = \bar{E}^\circ_2 + \omega A_E I^{1/2}\left((1+ I^{1/2})^{-1} - \frac{\sigma(I^{1/2})}{3}\right) - \frac{b_E \upsilon I}{4} \tag{33}$$

where ϕ_E is the apparent molal internal energy of the solute at constant temperature and volume,

$$\mathring{a}_E = 2(2.303)RT^2\left(\frac{\partial \mathring{a}}{\partial T}\right)_\rho \tag{34}$$

and

$$b_E = 2(2.303)RT^2\left(\frac{\partial b_\gamma}{\partial T}\right)_\rho \tag{35}$$

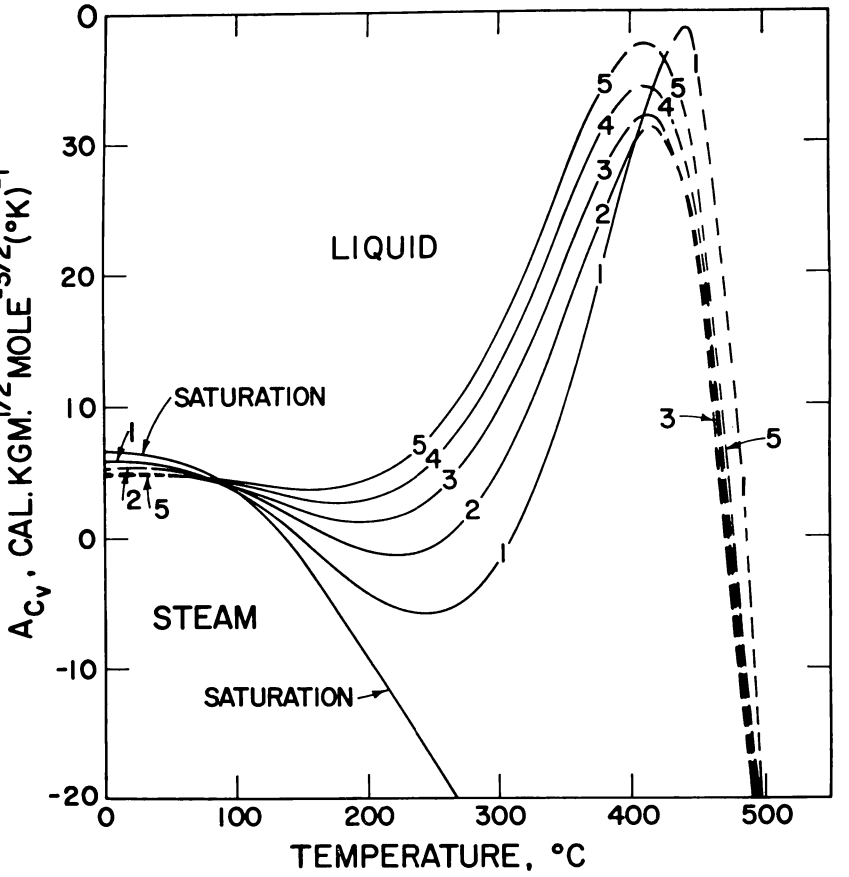

Fig. 31. A_{C_V} (table 9) as a function of temperature at constant pressure (labeled in kb) computed from equations (2), (28), (37), and (39).

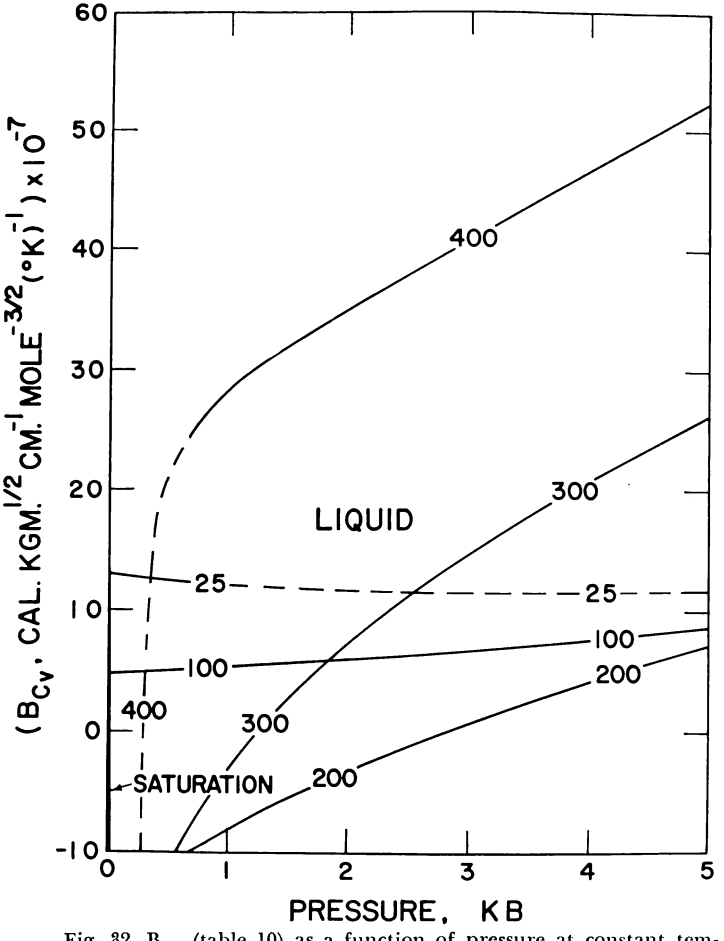

Fig. 32. B_{C_V} (table 10) as a function of pressure at constant temperature (labeled in °C) computed from equations (3), (29), (38), and (40).

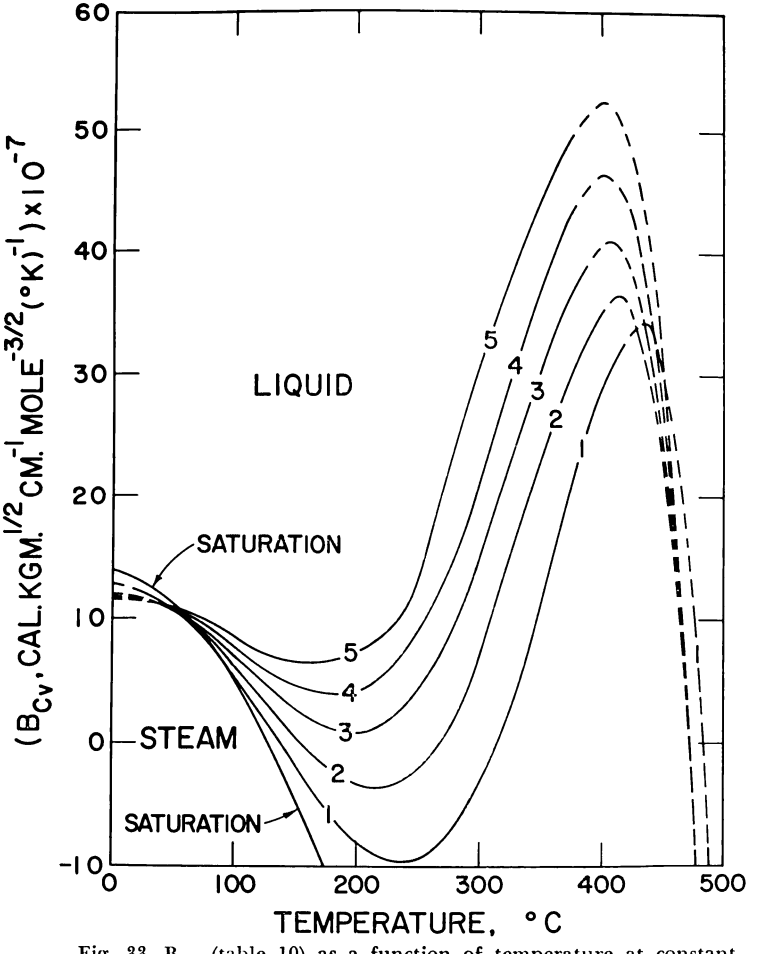

Fig. 33. B_{C_V} (table 10) as a function of temperature at constant pressure (labeled in kb) computed from equations (3), (29), (38), and (40).

Values of A_E and B_E computed from equations (26) through (29) are shown in tables 7 and 8 and plotted in figures 22 through 26. A_E as a function of temperature at $\rho = 1$ g cm^{-3} is shown in figure 27, where values computed in this study can be compared with those given by Lewis and Randall (1961), which are based on Franck's (1956) early estimates of the dielectric constant of H_2O at high pressures and temperatures. Franck's dielectric constants were obtained from graphic fits of the Kirkwood equation (Kirkwood, 1939; Oster and Kirkwood, 1943) to relatively low temperature-pressure data. Computer regression (Helgeson and Kirkham, 1974a) of more extensive data including Heger's (ms) recent measurements at high pressures and temperatures yields dielectric constants that differ from Franck's early estimates by as much as 10 percent or more and values of $(\partial \ln \varepsilon/\partial T)_\rho$ that differ by more than 30 percent from corresponding finite difference derivatives calculated by Pitzer and Brewer (Lewis and Randall, 1961) from Franck's data. Because $(\partial \ln \varepsilon/\partial T)_\rho$ is negative, these differences are magnified in equations (28) and (29) by addition of $1/T$, which causes the large departure of the two curves in figure 22.

It can be seen in figures 24 and 26 that the low pressure isobars for A_E and B_E pass through two extrema as functions of temperature, one between 100° and 200°C, and the other in the vicinity of 450°C. The latter extrema also are present in the high pressure isobars, which exhibit increasingly precipitous maxima with increasing pressure. As a consequence of the configuration of the isobars in figures 24 and 26, the isotherms for A_E and B_E in figures 23 and 24 cross each other and exhibit maxima and minima in the steam phase region at 500°C and low pressures. Note that the saturation curves in figures 23 and 24 also maximize. The extrema in A_E and B_E, none of which coincides with the critical point (where $(\partial \ln \varepsilon/\partial T)_\rho \neq -\infty = (\partial \ln \varepsilon/\partial T)_P$), are contoured by the isopleths in figures 27 and 28, which describe surfaces somewhat like warped Spanish saddles.

HEAT CAPACITY AT CONSTANT VOLUME

The relative partial molal heat capacity of the solute at constant volume $(\tilde{C}_{V,2} - \tilde{C}^\circ_{V,2})$ is defined by the isochoric partial derivative of equation (25) with respect to temperature; that is,

$$\tilde{C}_{V,2} - \tilde{C}^\circ_{V,2} = \left(\frac{\partial \tilde{E}_2}{\partial T}\right)_\rho - \left(\frac{\partial \tilde{E}^\circ_2}{\partial T}\right)_\rho$$

$$= -2.303\upsilon R\left(2T\left(\frac{\partial \log \gamma_\pm}{\partial T}\right)_\rho + T^2\left(\frac{\partial^2 \log \gamma_\pm}{\partial T^2}\right)_\rho\right) \quad (36)$$

Similarly, the Debye-Hückel parameters for $\tilde{C}_{V,2} - \tilde{C}^\circ_{V,2}$ (that is, A_{C_V} and

B_{C_V}) are given by corresponding derivatives of equations (26) and (27), which appear as

$$A_{C_V} = \left(\frac{\partial A_E}{\partial T}\right)_\rho = 2(2.303)R\left(2T\left(\frac{\partial A_\gamma}{\partial T}\right)_\rho + T^2\left(\frac{\partial^2 A_\gamma}{\partial T^2}\right)_\rho\right) = \frac{2A_E}{T} + 2(2.303)RT^2\left(\frac{\partial^2 A_\gamma}{\partial T^2}\right)_\rho \quad (37)$$

and

$$B_{C_V} = \left(\frac{\partial B_E}{\partial T}\right)_\rho = 2(2.303)R\left(2T\left(\frac{\partial B_\gamma}{\partial T}\right)_\rho + T^2\left(\frac{\partial^2 B_\gamma}{\partial T^2}\right)_\rho\right) = \frac{2B_E}{T} + 2(2.303)RT^2\left(\frac{\partial^2 B_\gamma}{\partial T^2}\right)_\rho \quad (38)$$

where (from eqs 28 and 29),

$$\left(\frac{\partial^2 A_\gamma}{\partial T^2}\right)_\rho = \frac{1}{A_\gamma}\left(\frac{\partial A_\gamma}{\partial T}\right)_\rho^2 - \frac{3A_\gamma}{2}\left(\left(\frac{\partial^2 \ln \varepsilon}{\partial T^2}\right)_\rho - \frac{1}{T^2}\right) \quad (39)$$

and

$$\left(\frac{\partial^2 B_\gamma}{\partial T^2}\right)_\rho = \frac{1}{B_\gamma}\left(\frac{\partial B_\gamma}{\partial T}\right)_\rho^2 - \frac{B_\gamma}{2}\left(\left(\frac{\partial^2 \ln \varepsilon}{\partial T^2}\right)_\rho - \frac{1}{T^2}\right) = \frac{B_\gamma}{3A_\gamma}\left(\frac{\partial^2 A_\gamma}{\partial T^2}\right)_\rho + \frac{1}{3A_\gamma}\left(\frac{\partial B_\gamma}{\partial T}\right)_\rho\left(\frac{\partial A_\gamma}{\partial T}\right)_\rho - \frac{B_\gamma}{3A_\gamma^2}\left(\frac{\partial A_\gamma}{\partial T}\right)_\rho^2 \quad (40)$$

Hence

$$B_{C_V} = \frac{A_E B_E A_\gamma - A_E^2 B_\gamma}{6A_\gamma^2(2.303)RT^2} + \frac{B_\gamma A_{C_V}}{3A_\gamma} \quad (41)$$

The Debye-Hückel equation for $\tilde{C}_{V,2} - \tilde{C}^\circ_{V,2}$ analogous to equation (20) can now be written as

$$\tilde{C}_{V,2} - \tilde{C}^\circ_{V,2} = \frac{\omega A_{C_V} I^{1/2}}{1 + \mathring{a}B_\gamma I^{1/2}} - \frac{\omega I(A_E(\mathring{a}B_E + B_\gamma \mathring{a}_E) + A_\gamma \mathring{a}_E B_E)}{2.303RT^2(1 + \mathring{a}B_\gamma I^{1/2})^2} - \frac{\omega A_\gamma I(\mathring{a}B_{C_V} + B_\gamma \mathring{a}_{C_V})}{(1 + \mathring{a}B_\gamma I^{1/2})^2} + \frac{\omega A_\gamma I^{3/2}(\mathring{a}B_E + B_\gamma \mathring{a}_E)^2}{2.303RT^2(1 + \mathring{a}B_\gamma I^{1/2})^3} \quad (42)$$

which reduces in the Guggenheim (1935) modification (eq 4 with $\mathring{a}B_\gamma = 1$) to

$$\tilde{C}_{V,2} - \tilde{C}^\circ_{V,2} = \frac{\omega A_{C_V} I^{1/2}}{1 + I^{1/2}} - \frac{\upsilon b_{C_V} I}{2} \quad (43)$$

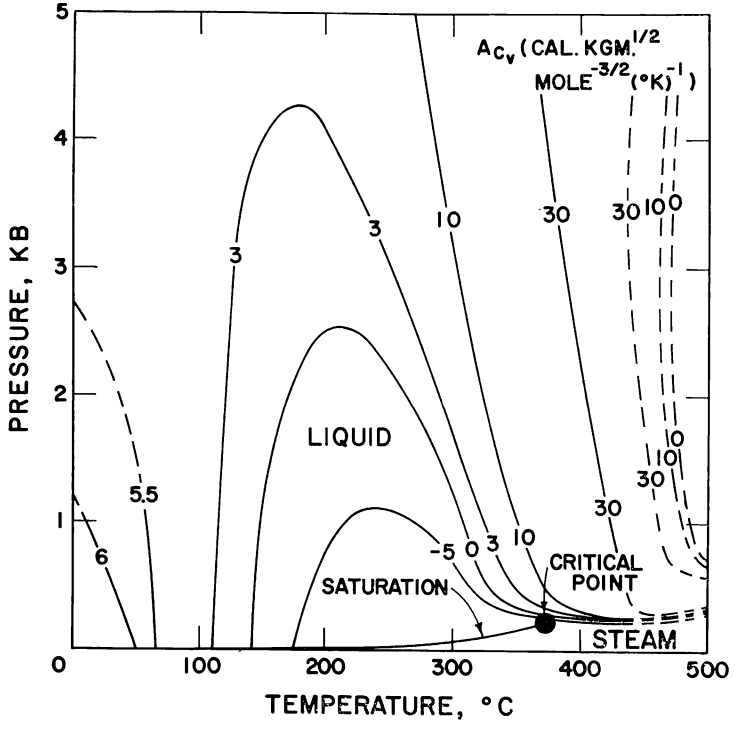

Fig. 34. Isopleths of A_{C_V} (labeled in cal $kg^{1/2}mole^{-3/2}(°K)^{-1}$) as a function of pressure and temperature (table 9 and figs. 30 and 31).

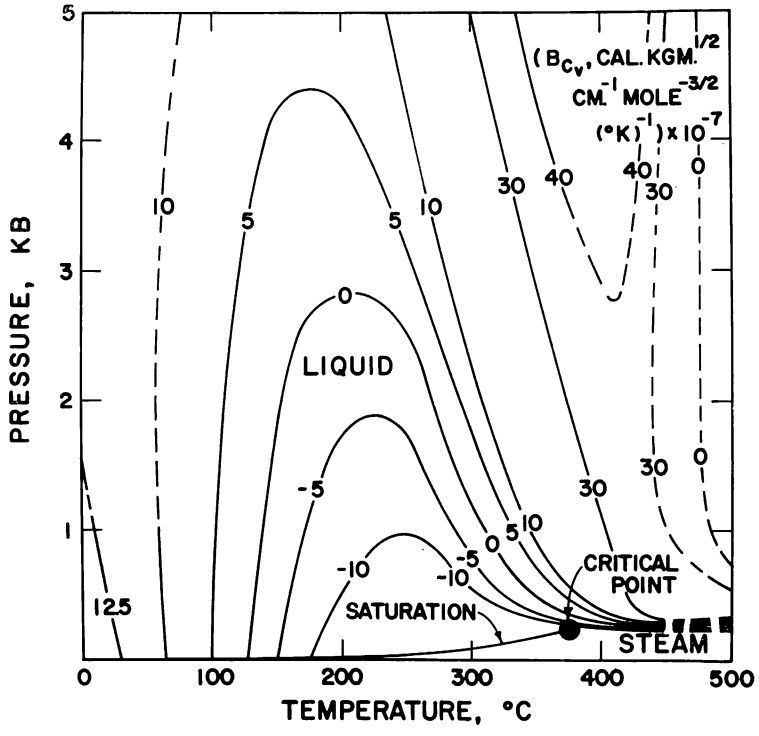

Fig. 35. Isopleths of B_{C_V} (labeled in cal $kg^{1/2}cm^{-1}mole^{-3/2}(°K)^{-1}$) $\times 10^{-7}$) as functions of pressure and temperature (table 10 and figs. 32 and 33).

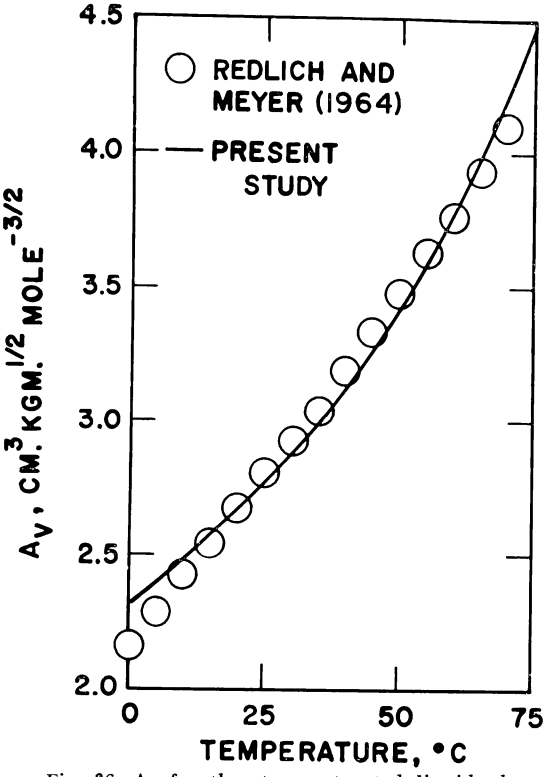

Fig. 36. A_V for the steam-saturated liquid phase as a function of temperature computed (curve) in the present study (table 17) compared with corresponding values taken from the literature.

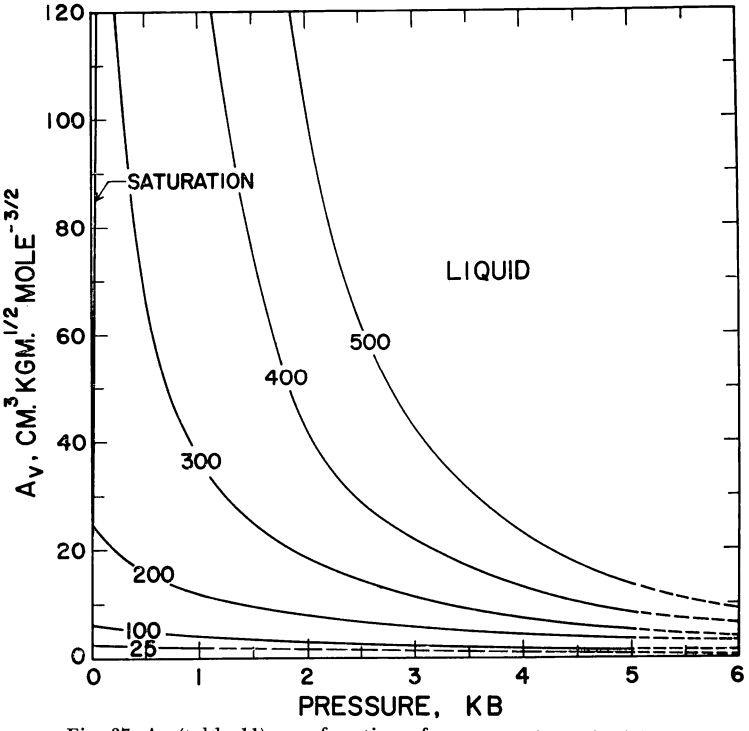

Fig. 37. A_V (table 11) as a function of pressure at constant temperature (labeled in °C) computed from equations (2), (48), and (51).

and thus

$$\phi_{C_V} = \tilde{C}^\circ_{V,2} + \omega A_{C_V} I^{1/2}\left((1 + I^{1/2})^{-1} - \frac{\sigma(I^{1/2})}{3}\right) - \frac{\upsilon b_{C_V} I}{4} \quad (44)$$

where ϕ_{C_V} is the apparent molal isochoric heat capacity of the solute at constant temperature,

$$\begin{aligned} \text{å}_{C_V} = \left(\frac{\partial \text{å}_E}{\partial T}\right)_\rho &= 2(2.303)R\left(2T\left(\frac{\partial \text{å}}{\partial T}\right)_\rho + T^2\left(\frac{\partial^2 \text{å}}{\partial T^2}\right)_\rho \right) \\ &= \frac{2\text{å}_E}{T} + 2(2.303)RT^2\left(\frac{\partial^2 \text{å}}{\partial T^2}\right)_\rho \end{aligned} \quad (45)$$

and

$$\begin{aligned} b_{C_V} = \left(\frac{\partial b_E}{\partial T}\right)_\rho &= 2(2.303)R\left(2T\left(\frac{\partial b_\gamma}{\partial T}\right)_\rho + T^2\left(\frac{\partial^2 b_\gamma}{\partial T^2}\right)_\rho \right) \\ &= \frac{2b_E}{T} + 2(2.303)RT^2\left(\frac{\partial^2 b_\gamma}{\partial T^2}\right)_\rho \end{aligned} \quad (46)$$

Equations (43) and (44) are the isochoric analogs of equations (21) and (22).

Values of A_{C_V} and B_{C_V} computed from equations (37) through (40) are shown in tables 9 and 10 and plotted in figures 29 through 33. It can be seen in figure 29 that (as a consequence of the difference in the curves shown in figure 22) the values of A_{C_V} computed in this study for $\rho = 1$ g cm^3 differ considerably from those given by Lewis and Randall (1961), which are based on Franck's (1956) early estimates of the dielectric constant at high pressures and temperatures. As indicated above, Franck's values have since been superseded (Heger, ms; Helgeson and Kirkham, 1974a).

The curves in figures 30 through 35 describe smooth high-temperature anticlinal and low-temperature synclinal surfaces, which in the case of B_{C_V} (figs. 32, 33, and 35) and A_{C_V} from $\sim$ 200° to $\sim$ 300°C (figs. 30, 31, and 34) plunge toward lower pressures. The high temperature anticlinal surface for A_{C_V} is doubly plunging toward $\sim$ a kilobar, which causes the angular hook in the 400°C isotherm in figure 30. At temperatures below $\sim$ 50° to 100°C and pressures $\lesssim$ 2 kb, both A_{C_V} and B_{C_V} are negative functions of pressure.

VOLUME

The partial derivative of equation (1) with respect to pressure at constant temperature can be written as

$$\begin{aligned} \bar{V}_2 - \bar{V}^\circ_2 &= 2.303\upsilon RT\left(\frac{\partial \log \gamma_\pm}{\partial P}\right)_T \\ &= \frac{\omega A_V I^{1/2}}{1 + \text{å}B_\gamma I^{1/2}} + \frac{\omega A_\gamma I(\text{å}B_V + B_\gamma \text{å}_V)}{(1 + \text{å}B_\gamma I^{1/2})^2} \end{aligned} \quad (47)$$

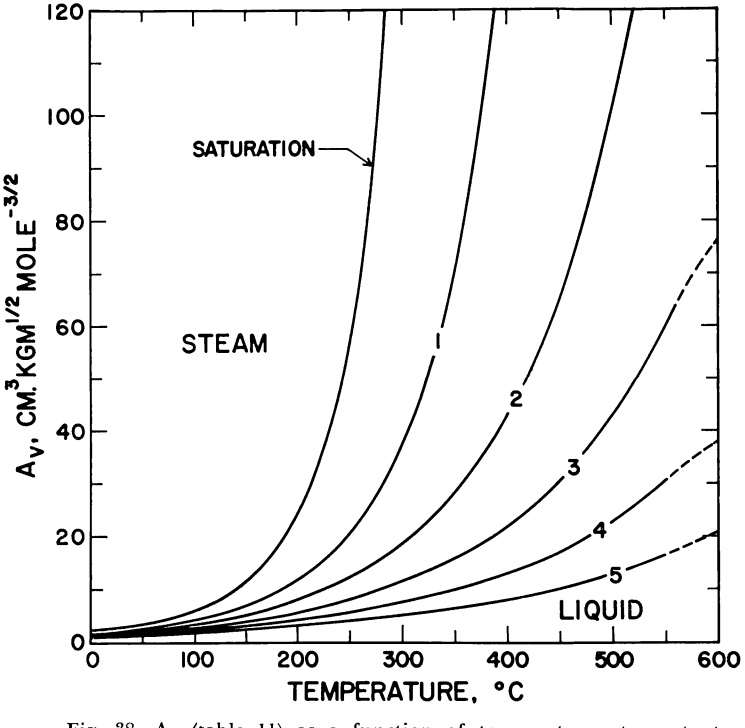

Fig. 38. A_V (table 11) as a function of temperature at constant pressure (labeled in kb) computed from equations (2), (48), and (51).

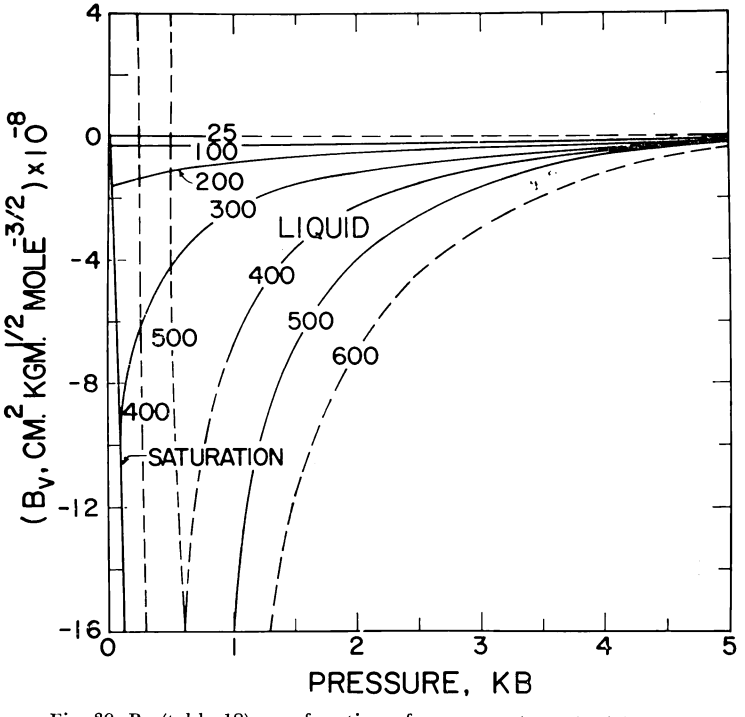

Fig. 39. B_V (table 12) as a function of pressure at constant temperature (labeled in °C) computed from equations (3), (49), and (52).

where $\bar{V}_2 - \bar{V}^\circ_2$ is the relative partial molal volume of the solute at constant pressure and temperature, and A_V, B_V, and $\mathring{a}_V$ stand for the Debye-Hückel parameters defined by

$$A_V = -2(2.303)RT\left(\frac{\partial A_\gamma}{\partial P}\right)_T \tag{48}$$

$$B_V = 2(2.303)RT\left(\frac{\partial B_\gamma}{\partial P}\right)_T \tag{49}$$

and

$$\mathring{a}_V = 2(2.303)RT\left(\frac{\partial \mathring{a}}{\partial P}\right)_T \tag{50}$$

where (from eqs 2 and 3)

$$\left(\frac{\partial A_\gamma}{\partial P}\right)_T = \frac{A_\gamma}{2}\left(\beta - 3\left(\frac{\partial \ln \varepsilon}{\partial P}\right)_T\right) \tag{51}$$

and

$$\left(\frac{\partial B_\gamma}{\partial P}\right)_T = \frac{B_\gamma}{2}\left(\beta - \left(\frac{\partial \ln \varepsilon}{\partial P}\right)_T\right) \tag{52}$$

where β is the coefficient of isothermal compressibility $(-(\partial \ln V/\partial P)_T)$ of H_2O. If equation (1) is extended to higher concentrations by addition of a $b_\gamma I$ term (eq 4), a corresponding term $(\upsilon b_V I/2$, where $b_V = 2(2.303)RT(\partial b_\gamma/\partial P)_T)$ appears in equation (47). For electrolytes in which $\mathring{a}B_\gamma$ can be regarded as unity at all pressures, the resulting equation reduces to

$$\bar{V}_2 - \bar{V}^\circ_2 = \frac{\omega A_V I^{1/2}}{1 + I^{1/2}} + \frac{\upsilon b_V I}{2} \tag{53}$$

which is consistent with the Guggenheim (1935) equation (eq 4 with $\mathring{a}B_\gamma$ set to unity) and

$$\phi_V = \bar{V}^\circ_2 + \omega A_V I^{1/2}\left((1 + I^{1/2})^{-1} - \frac{\sigma(I^{1/2})}{3}\right) + \frac{b_V \upsilon I}{4} \tag{54}$$

where ϕ_V stands for the apparent molal volume of the solute at constant temperature and pressure. If equation (53) is further simplified by inserting 1 for $(1 + I^{1/2})$ in the denominator of Debye-Hückel term, the expression reduces to

$$\bar{V}_2 - \bar{V}^\circ_2 = \omega A_V I^{1/2} + \frac{\upsilon b_V I}{2} \tag{55}$$

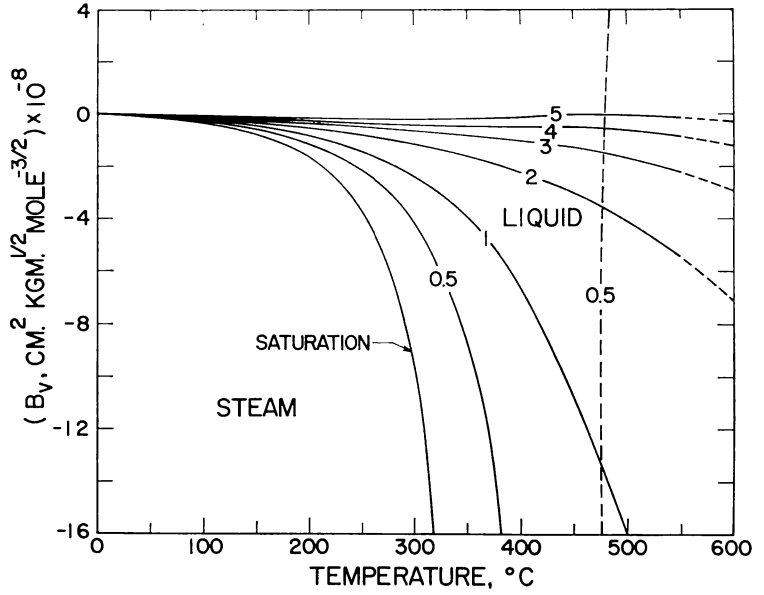

Fig. 40. B_V (table 12) as a function of temperature at constant pressure (labeled in kb) computed from equations (3), (49), and (52).

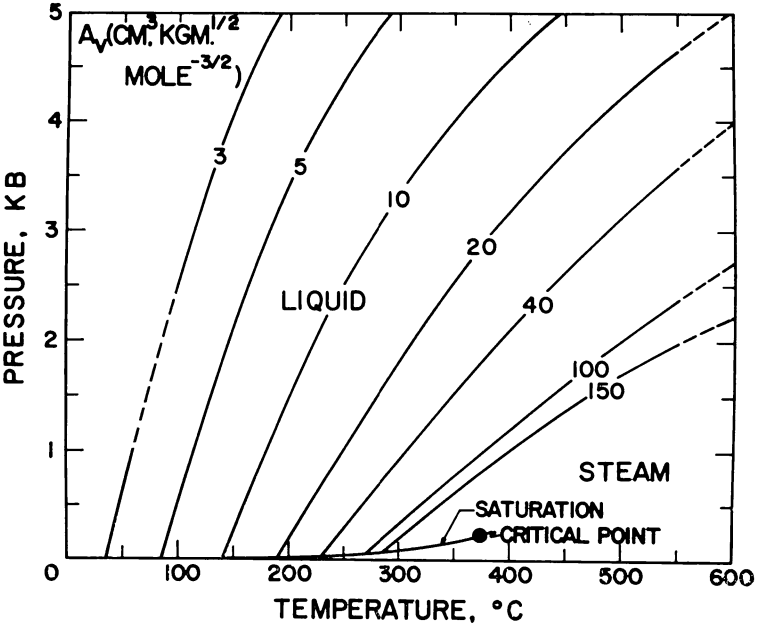

Fig. 41. Isopleths of A_V (labeled in $cm^3kg^{1/2}mole^{-3/2}$) as a function of pressure and temperature (table 11 and figs. 37 and 38).

which is consistent with the Redlich-Meyer (1964) equation for the apparent molal volume; that is,

$$\phi_V = \bar{V}^\circ_2 + S_V m^{1/2} + b^*_V m \tag{56}$$

where

$$S_V = \frac{2A_V\omega^{3/2}}{3} \tag{57}$$

and

$$b^*_V = \frac{\upsilon b_V \omega}{4} \tag{58}$$

If b_V is then set to zero, equation (56) reduces to the molal equivalent of the Masson (1929) equation.

Comparison of A_V values computed in this study with those calculated from Redlich and Meyer's (1964) k values ($A_V = 3/2\ k\rho^{1/2}$) from 0° to 70°C at 1 bar can be made in figure 36, where it can be seen that the two sets of calculations are in close agreement. Nevertheless, the curve in figure 36 departs slightly toward higher values of A_V from those based on Redlich and Meyer's k values as temperature decreases below 20°C and increases above 60°C. Redlich and Meyer computed their k values using Kell and Whalley's (1965) compressibilities (which are in close agreement with compressibilities generated from the equation of state given by Keenan and others, 1969) and values of $(\partial \ln \varepsilon/\partial P)_T$ taken from Owen and others (1961), who represented the dependence of the dielectric constant on temperature and pressure from 0° to 70°C and 1 bar to 1 kb with a quadratic power function. The discrepancy between the distribution of the symbols and the curve in figure 36 arises from differences of ~ 5 percent or less in values of $(\partial \ln \varepsilon/\partial P)_T$ computed by Owen and his coworkers at the edges of their pressure-temperature fit region and those generated by composite regression (Helgeson and Kirkham, 1974a) of data taken from Owen and others (1961), Oshry (ms), and Heger (ms) for temperatures and pressures from 0° to 550°C and 0.001 to 5 kb.

Values of A_V and B_V computed from equations (48), (49), (51), and (52) are shown in tables 11 and 12 and plotted in figures 37 through 40. Comparison of figures 37 and 38 with figures 39 and 40 indicates that (apart from the difference in sign stipulated by eqs 48 and 49) A_V and B_V exhibit much the same dependence on pressure and temperature except in the steam phase region at high temperatures and low pressures.

It can be seen in figure 1 that $\ln \varepsilon$ is nearly a linear function of $\ln V$ at constant temperature, and that the slopes of the isotherms are close to -1. As a consequence, $(\partial \ln \varepsilon/dP)_T$ at high temperatures is almost proportional and nearly equivalent in magnitude to β, both of which are positive and approach ∞ at the critical point. It follows from equations (49) and (52) that B_V is a sensitive function of the relative magnitude of β and $(\partial \ln \varepsilon/dP)_T$. Except in the steam phase region at high temperatures and low pressures, $(\partial \ln \varepsilon/\partial P)_T > \beta$, which causes B_V to be negative over

most of the temperature/pressure region considered (figs. 39 and 40). However, at high temperatures and low pressures where $\beta > (\partial \ln \varepsilon/\mathrm{dP})_T$, B_V is positive, which causes the low pressure isobars in figure 40 and the high temperature isotherms in figure 39 to pass through precipitous minima at high temperatures and low pressures, respectively. As a consequence, the isopleths for B_V wrap around the critical point in figure 42. The same behavior is not exhibited by A_V in figure 41, because β is always smaller than $3(\partial \ln \varepsilon/\partial P)_T$ in equation (51) for the pressure/temperature region considered. Hence A_V decreases monotonically as a function of pressure at constant temperature (fig. 37) and also increases monotonically as an isobaric function of temperature (fig. 38). At high pressures, $A_V \rightarrow B_V \rightarrow (\partial A_V/\partial P)_T \rightarrow (\partial B_V/\partial P)_T \rightarrow 0$ as pressure increases at constant temperature (figs. 37 and 39). Similarly, $A_V \rightarrow B_V \rightarrow (\partial A_V/\partial T)_P \rightarrow (\partial B_V/\partial T)_P \rightarrow 0$ as temperature decreases at constant pressure and low temperatures (figs. 38 and 40).

COMPRESSIBILITY

The relative partial molal compressibility ($\bar{\kappa}_2 - \bar{\kappa}^\circ_2$) of an electrolyte is given by

$$\bar{\kappa} - \bar{\kappa}^\circ_2 = -\left(\left(\frac{\partial \bar{V}_2}{\partial P}\right)_T - \left(\frac{\partial \bar{V}^\circ_2}{\partial P}\right)_T\right) = -2.303\nu RT\left(\frac{\partial^2 \log \gamma_\pm}{\partial P^2}\right)_T \tag{59}$$

Hence, for electrolytes described by equation (1),

$$\bar{\kappa}_2 - \bar{\kappa}^\circ_2 = -\frac{\omega A_\kappa I^{1/2}}{1 + \mathring{a}B_\gamma I^{1/2}} + \frac{\omega I(A_V(\mathring{a}B_V + B_\gamma \mathring{a}_V) + A_\gamma \mathring{a}_V B_V)}{2.303RT\,(1 + \mathring{a}B_\gamma I^{1/2})^2} + \frac{\omega A_\gamma I(\mathring{a}B_\kappa + B_\gamma \mathring{a}_\kappa)}{(1 + \mathring{a}B_\gamma I^{1/2})^2} - \frac{\omega A_\gamma I^{3/2}(\mathring{a}B_V + B_\gamma \mathring{a}_V)^2}{2.303RT\,(1 + \mathring{a}B_\gamma I^{1/2})^3} \tag{60}$$

where

$$A_\kappa = \left(\frac{\partial A_V}{\partial P}\right)_T = -2(2.303)RT\left(\frac{\partial^2 A_\gamma}{\partial P^2}\right)_T, \tag{61}$$

$$B_\kappa = \left(\frac{\partial B_V}{\partial P}\right)_T = 2(2.303)RT\left(\frac{\partial^2 B_\gamma}{\partial P^2}\right)_T, \tag{62}$$

and

$$\mathring{a}_\kappa = \left(\frac{\partial \mathring{a}_V}{\partial P}\right)_T = 2(2.303)RT\left(\frac{\partial^2 \mathring{a}}{\partial P^2}\right)_T \tag{63}$$

where (from eqs 51 and 52)

$$\left(\frac{\partial^2 A_\gamma}{\partial P^2}\right)_T = \frac{1}{A_\gamma}\left(\frac{\partial A_\gamma}{\partial P}\right)^2_T + \frac{A_\gamma}{2}\left(\left(\frac{\partial \beta}{\partial P}\right)_T - 3\left(\frac{\partial^2 \ln \varepsilon}{\partial P^2}\right)_T\right) \tag{64}$$

and

$$\left(\frac{\partial^2 B_\gamma}{\partial P^2}\right)_T = \frac{1}{B_\gamma}\left(\frac{\partial B_\gamma}{\partial P}\right)_T^2 + \frac{B_\gamma}{2}\left(\left(\frac{\partial \beta}{\partial P}\right)_T - \left(\frac{\partial^2 \ln \varepsilon}{\partial P^2}\right)_T\right) \quad (65)$$

Extension of equation (1) to higher concentrations by addition of a $b_\gamma I$ term (eq 4) results in a corresponding extension of equation (60) by $-\upsilon b_\kappa I/2$, where

$$b_\kappa = 2(2.303)RT\left(\frac{\partial b_V}{\partial P}\right)_T \quad (66)$$

The partial derivatives of equations (53) through (56) with respect to pressure at constant temperature can now be written as

$$\bar{\kappa}_2 - \bar{\kappa}^\circ_2 = -\frac{\omega A_\kappa I^{1/2}}{1 + I^{1/2}} - \frac{\upsilon b_\kappa I}{2}, \quad (67)$$

$$\phi_\kappa = \bar{\kappa}^\circ_2 - \omega A_\kappa I^{1/2}\left((1 + I^{1/2})^{-1} - \frac{\sigma(I^{1/2})}{3}\right) - \frac{b_\kappa \upsilon I}{4}, \quad (68)$$

$$\bar{\kappa}_2 - \bar{\kappa}^\circ_2 = -\omega A_\kappa I^{1/2} - \frac{\upsilon b_\kappa I}{2}, \quad (69)$$

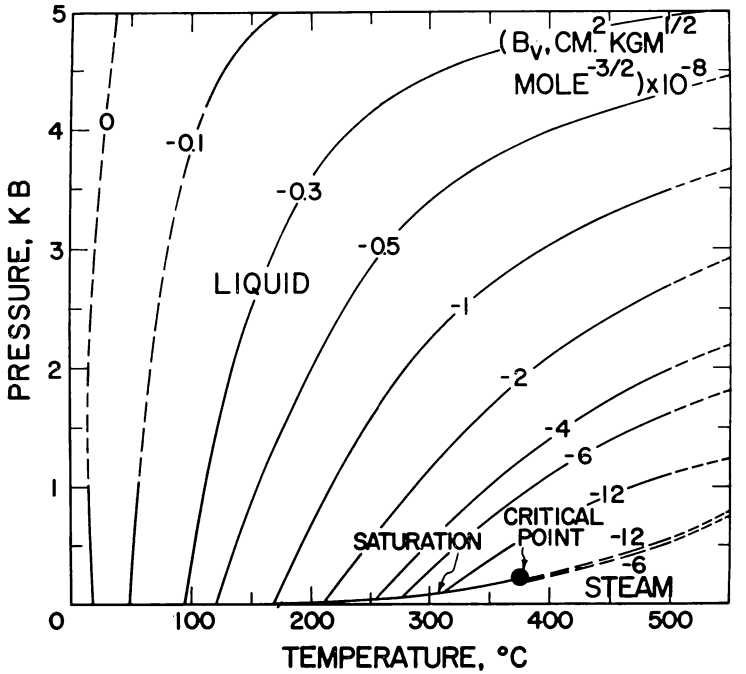

Fig. 42. Isopleths of B_V (labeled in ($cm^2 kg^{1/2} mole^{-3/2}$) $\times 10^{-8}$) as a function of pressure and temperature (table 12 and figs. 39 and 40).

TABLE 13

A_κ in $(cm^3 kg^{1/2} mole^{-3/2} bar^{-1}) \times 10^3$ computed from equations (2), (51), (61), and (64)—see figures 43, 44, and 47

t	PRESSURE, KB						
(°C)	SAT	0.5	1	2	3	4	5
25	-1.02	-0.6					
50	-1.33	-0.7					
75	-1.91	-1.1					
100	-2.95	-1.7	(-1.1)	(-0.9)	(-0.6)	(-0.4)	(-0.3)
125	-4.80	-2.3	-1.8	-1.2	-0.8	-0.6	(-0.4)
150	-8.08	-4.3	-2.8	-1.7	-1.0	-0.7	(-0.5)
175	-14.13	-6.8	-4.3	-2.3	-1.4	-0.9	(-0.6)
200	-25.86	-11.1	-6.5	-3.2	-1.8	-1.1	(-0.8)
225	-50.34	-18.5	-9.8	-4.4	-2.3	-1.4	(-1.0)
250	-106.98	-31.7	-15.1	-6.1	-3.0	-1.7	(-1.1)
275	-259.08	-56.4	-23.3	-8.4	-3.9	-2.2	(-1.4)
300	-772.23	-106.1	-36.6	-11.5	-5.0	-2.7	(-1.6)
325	-3353.74	-214.6	-58.3	-15.6	-6.4	-3.3	(-2.0)
350	-36221.30	-478.9	-94.4	-21.1	-8.1	-4.0	(-2.3)
375			-154.7	-28.5	-10.2	-4.8	(-2.8)
400			-255.8	-38.6	-12.9	-5.8	(-3.3)
425			-425.3	-52.3	-16.3	-7.1	(-3.9)
450			(-706.3)	(-71.0)	(-20.5)	-8.6	(-4.7)
475			(-1152.9)	(-96.5)	(-25.7)	-10.4	(-5.5)
500			(-1793.9)	(-130.5)	(-32.3)	(-12.6)	(-6.6)

TABLE 14

B_κ in $(cm^2 kg^{1/2} mole^{-3/2} bar^{-1}) \times 10^{-4}$ computed from equations (3), (52), (62), and (65)—see figures 45, 46, and 48

t	PRESSURE, KB						
(°C)	SAT	0.5	1	2	3	4	5
25	0.05	0.0					
50	0.31	0.2					
75	0.78	0.5					
100	1.54	0.9	(0.7)	(0.6)	(0.4)	(0.3)	(0.3)
125	2.83	1.7	1.2	0.9	0.6	0.5	(0.3)
150	5.04	2.8	1.9	1.3	0.8	0.6	(0.4)
175	8.95	4.6	3.0	1.8	1.1	0.8	(0.6)
200	16.19	7.4	4.5	2.4	1.4	1.0	(0.7)
225	30.40	12.0	6.8	3.3	1.9	1.2	(0.8)
250	60.96	19.6	10.0	4.5	2.4	1.6	(1.0)
275	135.88	32.9	14.8	5.9	3.0	1.8	(1.2)
300	361.08	57.1	21.9	7.7	3.7	2.1	(1.4)
325	1330.60	104.0	32.5	10.0	4.5	2.5	(1.6)
350	10974.44	202.3	48.1	12.7	5.4	2.9	(1.8)
375			70.7	16.1	6.5	3.4	(2.1)
400			102.5	20.2	7.7	3.9	(2.4)
425			145.0	25.3	9.2	4.5	(2.7)
450			(197.9)	(31.6)	(10.9)	(5.2)	(3.1)
475			(252.9)	(39.3)	(12.9)	(6.0)	(3.6)
500				(48.4)	(15.3)	(7.0)	(4.1)

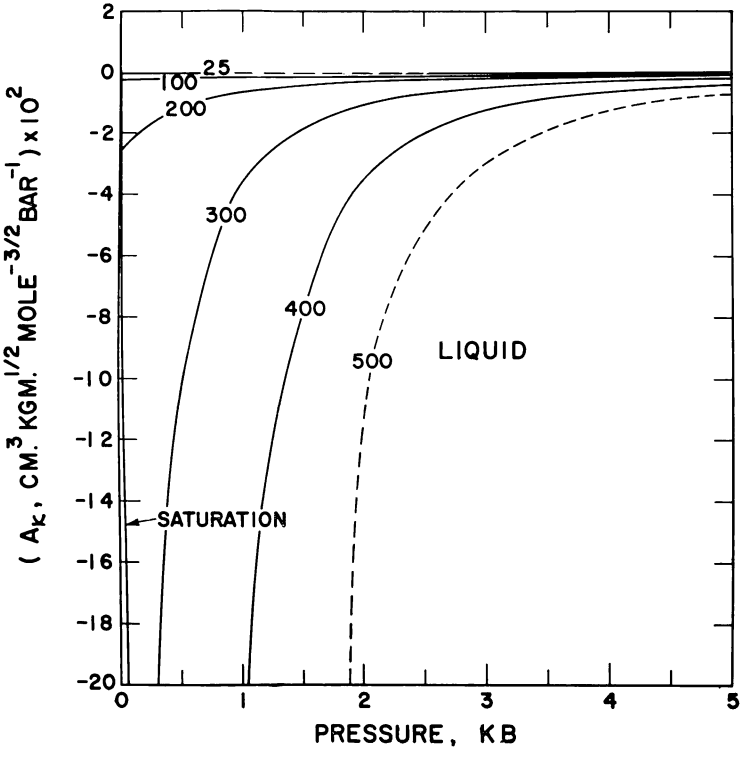

Fig. 43. A_K (table 13) as a function of pressure at constant temperature (labeled in °C) computed from equations (2), (51), (61), and (64).

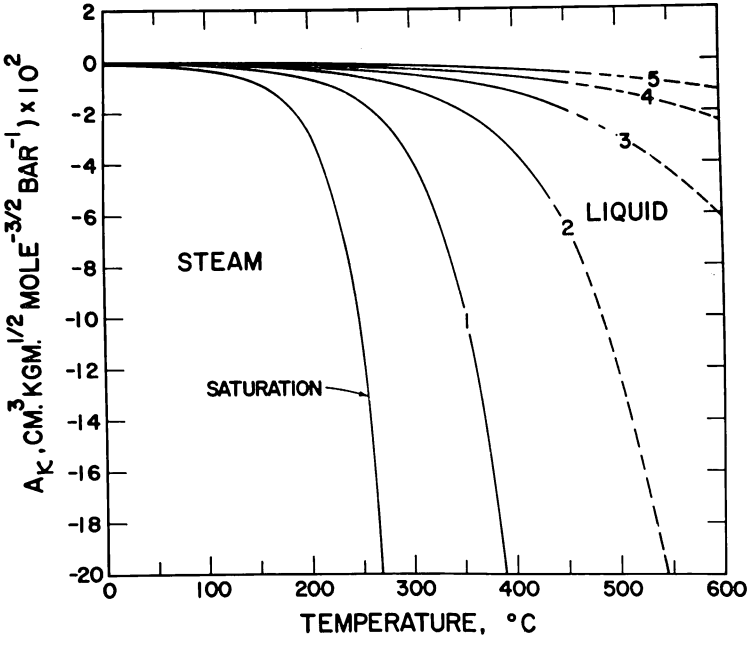

Fig. 44. A_K (table 13) as a function of temperature at constant pressure (labeled in kb) computed from equations (2), (51), (61), and (64).

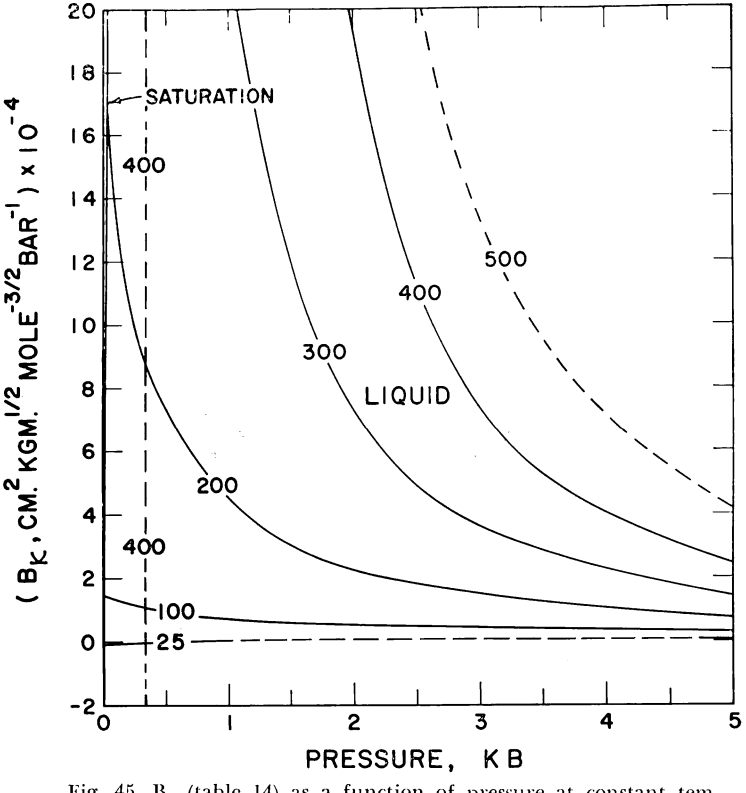

Fig. 45. B_κ (table 14) as a function of pressure at constant temperature (labeled in °C) computed from equations (3), (52), (62), and (65).

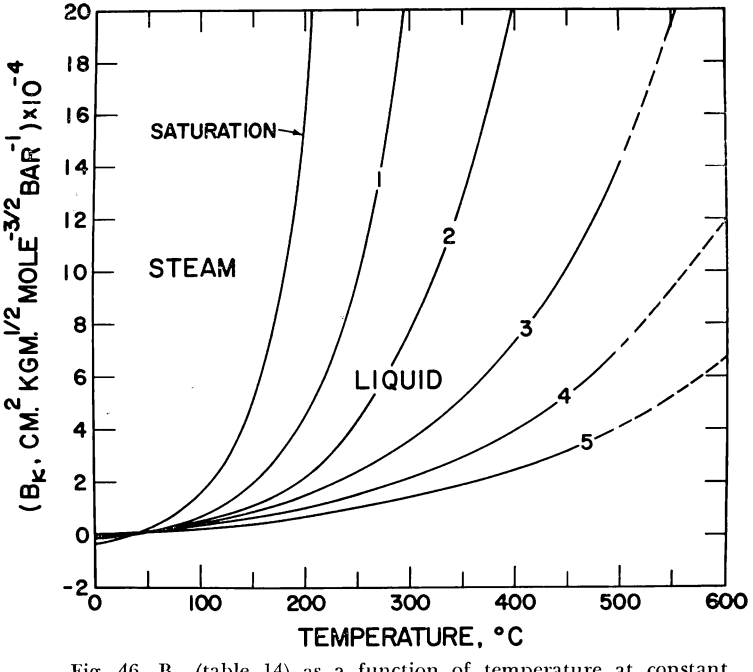

Fig. 46. B_κ (table 14) as a function of temperature at constant pressure (labeled in kb) computed from equations (3), (52), (62), and (65).

and

$$\phi_\kappa = \bar{\kappa}^\circ_2 + S_\kappa m^{1/2} + b^*_\kappa m \tag{70}$$

where ϕ_κ is the apparent molal compressibility of the solute $(-(\partial\phi_V/\partial P)_T$ at constant temperature and pressure,

$$S_\kappa = -\frac{2A_\kappa\omega^{3/2}}{3}\ , \tag{71}$$

and

$$b^*_\kappa = -\frac{\upsilon b_\kappa\omega}{4}\ . \tag{72}$$

With b_κ set to zero, equation (70) reduces to the molal equivalent of the Masson (1929) equation for the apparent molal compressibility.

Debye-Hückel compressibility parameters computed from equations (61), (62), (64), and (65) are shown in tables 13 and 14 and plotted in figures 43 through 46. Owing to the near-linear isothermal relation apparent in figure 1, the isothermal dependence of A_κ and B_κ on pressure (figs. 43 and 45) as well as their isobaric dependence on temperature (figs. 44 and 46) are essentially the same as the corresponding dependence of $-A_V$ and $-B_V$ on pressure and temperature, except at low temperatures.

Because $(\partial A_\gamma/\partial P)_T$ is squared in equation (64) and $(3|(\partial^2 \ln \varepsilon/\partial P^2)_T|) > |(\partial\beta/\partial P)_T|$, both of which are negative, A_κ is negative throughout the pressure-temperature region considered, and it becomes more negative with increasing temperature and decreasing pressure (figs. 43 and 44). Except at low temperatures and in the steam phase region at high temperatures and low pressures where $(\partial \ln \varepsilon/\partial P)_T < \beta$ and $|(\partial^2 \ln \varepsilon/\partial P^2)_T| < |(\partial B/\partial P)_T|$, B_κ is positive and becomes more positive with increasing temperature and decreasing pressure. At low temperatures ($\lesssim 25°C$ at 1 bar) B_κ is negative, but it becomes less so with increasing pressure and temperature. The precipitous minimum in B_V at high temperatures and low pressures is also exhibited by B_κ in the steam phase region (for much the same reason), which causes isopleths for B_κ at high temperatures and low pressures to curve around the critical point (not shown in fig. 48).

Because of the relations shown in figure 1, the configurations of the isopleths in figures 41 and 47, and 42 and 48, respectively, are similar, except at low temperatures where the isobars in figure 44 maximize and those in figure 46 cross each other as a consequence of the minima exhibited by β and $(\partial \ln \varepsilon/\partial P)_T$ as isobaric functions of temperature at low pressures and temperatures. Accordingly, the isopleths for A_κ in figure 47 pass through minima at low temperatures and pressures $\lesssim 2$ kb, and those for B_κ in figure 48 have negative slopes below $\sim 35°C$. At high pressures $A_\kappa \to (\partial A_\kappa/\partial P)_T \to 0$.

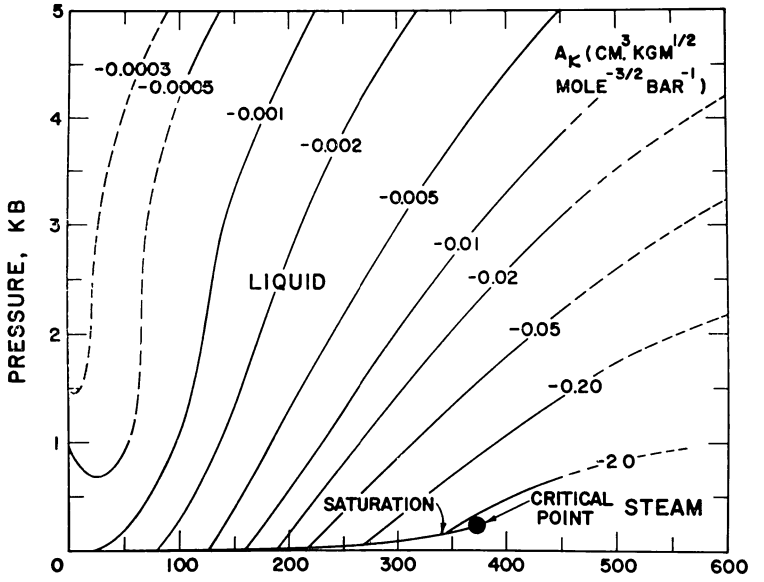

Fig. 47. Isopleths of A_κ (labeled in $cm^3kg^{1/2}mole^{-3/2}bar^{-1}$) as a function of pressure and temperature (table 13 and figs. 43 and 44). Temperature, °C.

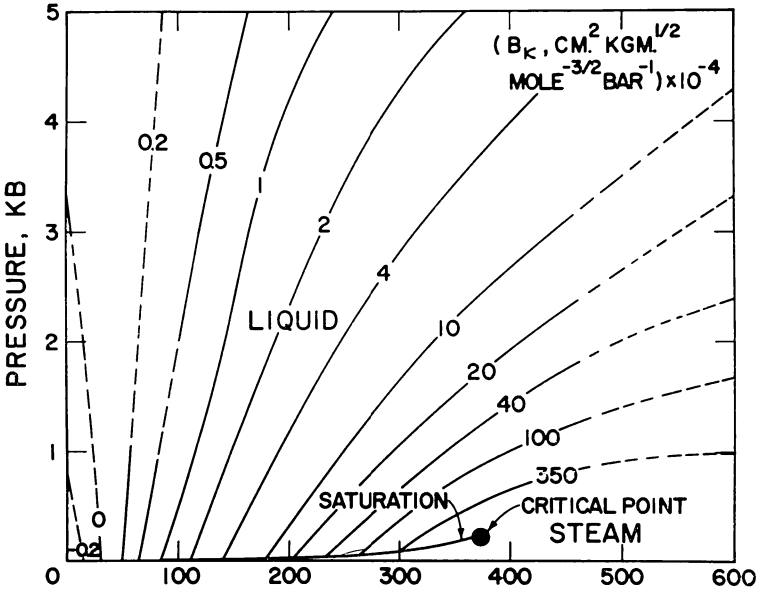

Fig. 48. Isopleths of B_κ (labeled in $(cm^2kg^{1/2}mole^{-3/2}bar^{-1}) \times 10^{-4}$) as a function of pressure and temperature (table 14 and figs. 45 and 46). Temperature, °C.

EXPANSIBILITY

The relative partial molal expansibility of an electrolyte at constant pressure and temperature ($\bar{E}x_2 - \bar{E}x^\circ_2$) can be expressed as

$$\begin{aligned}\bar{E}x_2 - \bar{E}x^\circ_2 &= \left(\frac{\partial \bar{V}_2}{\partial T}\right)_P - \left(\frac{\partial \bar{V}^\circ_2}{\partial T}\right)_P \\ &= 2.303R\left(\left(\frac{\partial \log \gamma_\pm}{\partial T}\right)_P + T\left(\frac{\partial^2 \log \gamma_\pm}{\partial T^2}\right)_P\right) \\ &= \frac{\bar{V}_2 - \bar{V}^\circ_2}{T} + 2.303RT\left(\frac{\partial^2 \log \gamma_\pm}{\partial T^2}\right)_P \qquad (73)\end{aligned}$$

which can be combined with the partial derivative of equation (47) to give

$$\begin{aligned}\bar{E}x_2 - \bar{E}x^\circ_2 = &\frac{\omega A_{Ex} I^{1/2}}{1 + \mathring{a}B_\gamma I^{1/2}} \\ &+ \frac{\omega I(A_H(\mathring{a}B_V + B_\gamma \mathring{a}_V) + A_\gamma(\mathring{a}_H B_V + B_H \mathring{a}_V) - A_V(\mathring{a}B_H + \mathring{a}_H B_\gamma))}{2(2.303)RT^2(1 + \mathring{a}B_\gamma I^{1/2})^2} \\ &+ \frac{\omega A_\gamma I(\mathring{a}B_{Ex} + B_\gamma \mathring{a}_{Ex})}{(1 + \mathring{a}B_\gamma I^{1/2})^2} - \frac{\omega A_\gamma I^{3/2}(\mathring{a}B_V + B_\gamma \mathring{a}_V)(\mathring{a}_H B_\gamma + \mathring{a}B_H)}{2.303RT^2(1 + \mathring{a}B_\gamma I^{1/2})^3} \qquad (74)\end{aligned}$$

where

$$\begin{aligned}A_{Ex} = \left(\frac{\partial A_V}{\partial T}\right)_P &= -2(2.303)R\left(\left(\frac{\partial A_\gamma}{\partial P}\right)_T + T\left(\frac{\partial\left(\frac{\partial A_\gamma}{\partial P}\right)_T}{\partial T}\right)_P\right) = \frac{A_V}{T} - \frac{1}{T}\left(\frac{\partial A_H}{\partial P}\right)_T, \qquad (75)\\ B_{Ex} = \left(\frac{\partial B_V}{\partial T}\right)_P &= 2(2.303)R\left(\left(\frac{\partial B_\gamma}{\partial P}\right)_T + T\left(\frac{\partial\left(\frac{\partial B_\gamma}{\partial P}\right)_T}{\partial T}\right)_P\right) = \frac{B_V}{T} + \frac{1}{T}\left(\frac{\partial B_H}{\partial P}\right)_T \qquad (76)\end{aligned}$$

and

$$\mathring{a}_{Ex} = \left(\frac{\partial \mathring{a}_V}{\partial T}\right)_P = 2(2.303)R\left(\left(\frac{\partial \mathring{a}}{\partial P}\right)_T + T\left(\frac{\partial\left(\frac{\partial \mathring{a}}{\partial P}\right)_T}{\partial T}\right)_P\right) = \frac{\mathring{a}_V}{T} + \frac{1}{T}\left(\frac{\partial \mathring{a}_H}{\partial P}\right)_T \qquad (77)$$

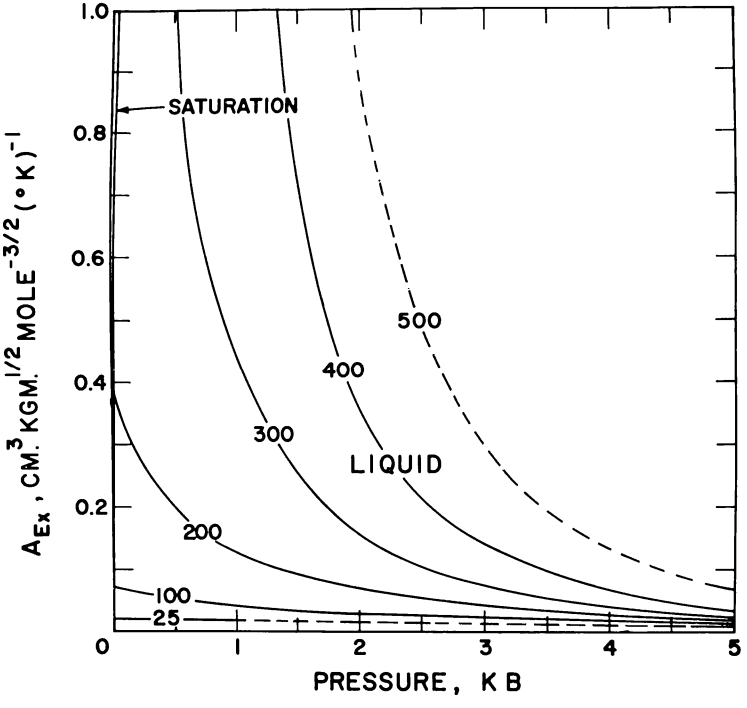

Fig. 49. A_{Ex} (table 15) as a function of pressure at constant temperature (labeled in °C) computed from equations (2), (5), (51), (75), and (78).

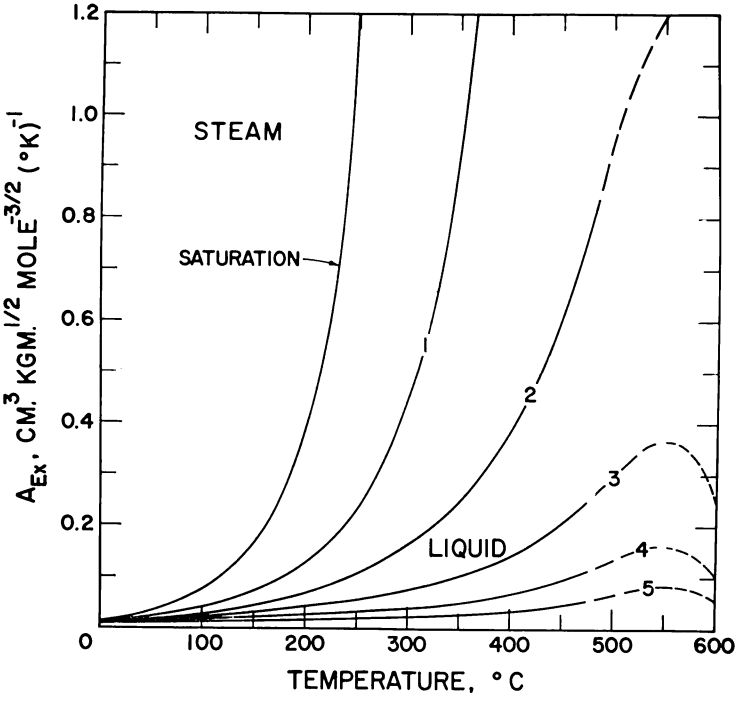

Fig. 50. A_{Ex} (table 15) as a function of temperature at constant pressure (labeled in kb) computed from equations (2), (5), (51), (75), and (78).

TABLE 15

A_{Ex} in $(cm^3 kg^{1/2} mole^{-3/2} (°K)^{-1} \times 10^2$ computed from equations (2), (5), (51), (75), and (78)—see figures 49, 50, and 53

t	PRESSURE, KB							
(°C)	SAT	0.5	1	1.5	2	3	4	5
25	2.08	1.8						
50	3.40	2.8						
75	5.10	3.9						
100	7.45	5.4	(4.1)	(3.5)	(2.8)	(2.0)	(1.6)	(1.2)
125	10.89	7.5	5.5	4.4	3.6	2.5	1.8	(1.4)
150	16.14	10.3	7.2	5.7	4.5	3.0	2.1	(1.6)
175	24.58	14.4	9.5	7.4	5.6	3.5	2.4	(1.8)
200	39.02	20.4	12.6	9.5	7.0	4.1	2.7	(1.9)
225	65.64	29.6	17.0	12.2	8.7	4.8	3.0	(2.1)
250	119.90	44.5	23.1	15.5	10.7	5.6	3.4	(2.2)
275	246.93	69.7	32.0	19.7	13.1	6.5	3.7	(2.3)
300	614.27	114.9	45.2	25.0	16.0	7.4	4.1	(2.4)
325	2160.46	201.2	65.0	32.0	19.6	8.6	4.5	(2.6)
350	17927.28	381.4	94.8	41.3	24.1	10.0	5.0	(2.8)
375			139.2	54.0	29.9	11.8	5.7	(3.1)
400			204.3	71.8	37.5	14.1	6.6	(3.4)
425			298.8	96.4	47.6	17.1	7.8	(4.0)
450			(433.2)	(129.9)	(60.7)	(20.7)	(9.3)	(4.7)
475			(613.2)	(173.2)	(77.5)	(25.1)	(11.1)	(5.5)
500			(819.0)	(224.8)	(97.7)	(29.9)	(13.0)	(6.5)

TABLE 16

B_{Ex} in $(cm^2 kg^{1/2} mole^{-3/2} (°K)^{-1}) \times 10^{-5}$ computed from equations (3), (6), (52), (76), and (79)—see figures 51, 52, and 54

t	PRESSURE, KB						
(°C)	SAT	0.5	1	2	3	4	5
25	-3.12	-2.6					
50	-3.58	-3.0					
75	-4.63	-3.7					
100	-6.24	-4.8	(-3.8)	(-2.7)	(-1.9)	(-1.4)	(-1.0)
125	-8.58	-6.2	-4.7	-3.1	-2.2	-1.6	(-1.1)
150	-12.01	-8.0	-5.8	-3.7	-2.4	-1.6	(-1.1)
175	-17.23	-10.6	-7.2	-4.3	-2.6	-1.7	(-1.1)
200	-25.59	-14.1	-9.0	-5.0	-2.8	-1.7	(-1.0)
225	-39.99	-19.1	-11.3	-5.8	-3.0	-1.6	(-0.8)
250	-67.13	-26.7	-14.3	-6.6	-3.1	-1.5	(-0.6)
275	-124.99	-38.5	-18.4	-7.4	-3.1	-1.3	(-0.2)
300	-274.07	-57.7	-24.0	-8.2	-3.2	-1.1	(0.0)
325	-814.22	-89.8	-31.6	-9.2	-3.2	-0.8	(-0.4)
350	-5197.56	-146.5	-41.7	-10.5	-3.3	-0.6	(-0.8)
375			-54.2	-11.7	-3.5	-0.4	(-1.1)
400			-69.1	-13.6	-3.9	-0.4	(-1.3)
425			-84.7	-16.2	-4.6	-0.6	(-1.4)
450			(-99.1)	(-19.6)	(-5.8)	(-1.0)	(-1.2)
475			(-107.1)	(-24.2)	(-7.4)	(-1.9)	(-0.8)
500			(-99.2)	(-29.7)	(-9.6)	(-3.0)	(0.0)

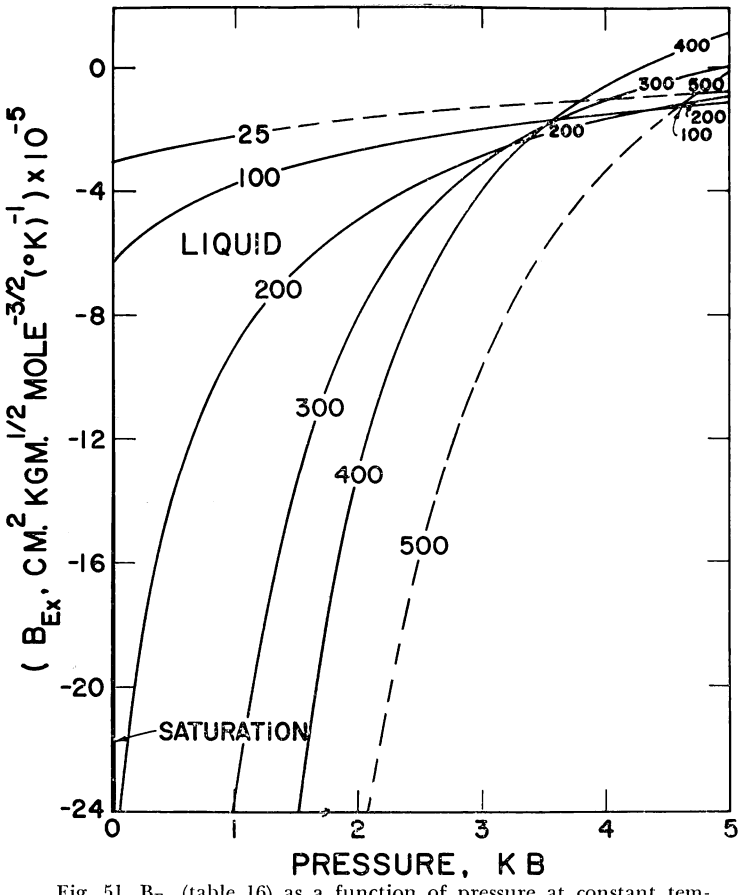

Fig. 51. B_{Ex} (table 16) as a function of pressure at constant temperature (labeled in °C) computed from equations (3), (6), (52), (76), and (79).

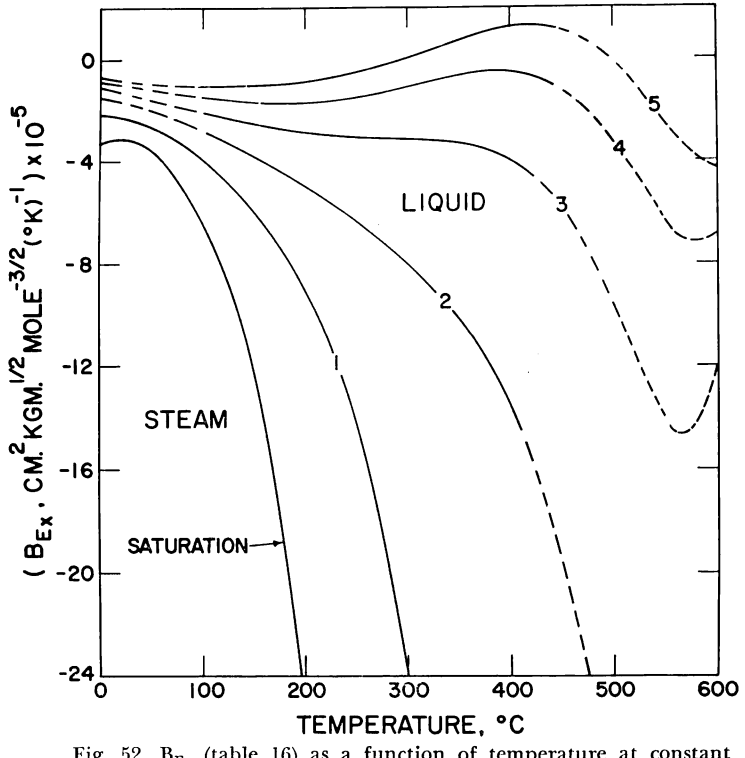

Fig. 52. B_{Ex} (table 16) as a function of temperature at constant pressure (labeled in kb) computed from equations (3), (6), (52), (76), and (79).

where (from eqs 51 and 52)

$$\left(\frac{\partial\left(\frac{\partial A_\gamma}{\partial P}\right)_T}{\partial T}\right)_P = \frac{1}{A_\gamma}\left(\frac{\partial A_\gamma}{\partial P}\right)_T\left(\frac{\partial A_\gamma}{\partial T}\right)_P + \frac{A_\gamma}{2}\left(\left(\frac{\partial \beta}{\partial T}\right)_P - 3\left(\frac{\partial\left(\frac{\partial \ln \varepsilon}{\partial P}\right)_T}{\partial T}\right)_P\right) = -\frac{A_V A_H}{4A_\gamma (2.303R)^2 T^3} + \frac{A_\gamma}{2}\left(\left(\frac{\partial \beta}{\partial T}\right)_P - 3\left(\frac{\partial\left(\frac{\partial \ln \varepsilon}{\partial P}\right)_T}{\partial T}\right)_P\right) \quad (78)$$

and

$$\left(\frac{\partial\left(\frac{\partial B_\gamma}{\partial P}\right)_T}{\partial T}\right)_P = \frac{1}{B_\gamma}\left(\frac{\partial B_\gamma}{\partial P}\right)_T\left(\frac{\partial B_\gamma}{\partial T}\right)_P + \frac{B_\gamma}{2}\left(\left(\frac{\partial \beta}{\partial T}\right)_P - \left(\frac{\partial\left(\frac{\partial \ln \varepsilon}{\partial P}\right)_T}{\partial T}\right)_P\right) = \frac{B_V B_H}{4A_\gamma (2.303R)^2 T^3} + \frac{A_\gamma}{2}\left(\left(\frac{\partial \beta}{\partial T}\right)_P - \left(\frac{\partial\left(\frac{\partial \ln \varepsilon}{\partial P}\right)_T}{\partial T}\right)_P\right) \quad (79)$$

Addition of a $b_\gamma I$ term to the right side of equation (1) to produce equation (4) results in a corresponding term ($\upsilon b_{Ex} I/2$) in equation (74), in which

$$b_{Ex} = 2(2.303)RT\left(\frac{\partial b_V}{\partial T}\right)_P = 2(2.303)R\left(\left(\frac{\partial b_\gamma}{\partial P}\right)_T + T\left(\frac{\partial\left(\frac{\partial b_\gamma}{\partial P}\right)_T}{\partial T}\right)_P\right) = \frac{b_V}{T} + \frac{1}{T}\left(\frac{\partial b_H}{\partial P}\right)_T \quad (80)$$

The expansibility analogs of equations (67) through (70) can now be written as

$$\bar{E}x_2 - \bar{E}x^\circ_2 = \frac{\omega A_{Ex} I^{1/2}}{1 + I^{1/2}} + \frac{\upsilon b_{Ex} I}{2}, \quad (81)$$

$$\phi_{Ex} = \bar{E}x^\circ_2 + \omega A_{Ex} I^{1/2}\left((1 + I^{1/2})^{-1} - \frac{\sigma(I^{1/2})}{3}\right) + \frac{b_{Ex}\upsilon I}{4}, \quad (82)$$

$$\bar{E}x_2 - \bar{E}x^\circ_2 = \omega A_{Ex} I^{1/2} + \frac{\upsilon b_{Ex} I}{2}, \quad (83)$$

and

$$\phi_{Ex} = \bar{E}x^{\circ}_2 + S_{Ex}\, m^{1/2} + b^*_{Ex} m \quad , \tag{84}$$

where ϕ_{Ex} is the apparent molal expansibility of the solute at constant temperature and pressure $((\partial\phi_V/\partial T)_P)$,

$$S_{Ex} = \frac{2A_{Ex}\omega^{3/2}}{3} \quad , \tag{85}$$

and

$$b^*_{Ex} = \frac{\upsilon b_{Ex}\omega}{4} \tag{86}$$

Setting $b_{Ex} = 0$ reduces equation (84) to the molal analog of the Masson (1929) equation for expansibility.

Values of A_{Ex} and B_{Ex} computed from equations (75), (76), (78), and (79) are shown in tables 15 and 16 and plotted in figures 49 through 52. Owing to the monotonic and negative isothermal dependence of A_V and A_H (both of which are positive) on pressure in figures 9 and 37, A_{Ex} is positive but exhibits a negative dependence on pressure (fig. 49). Similarly, as a consequence of the maxima in the isotherms in figure 10, A_{Ex} passes through an extremum as a function of temperature at constant

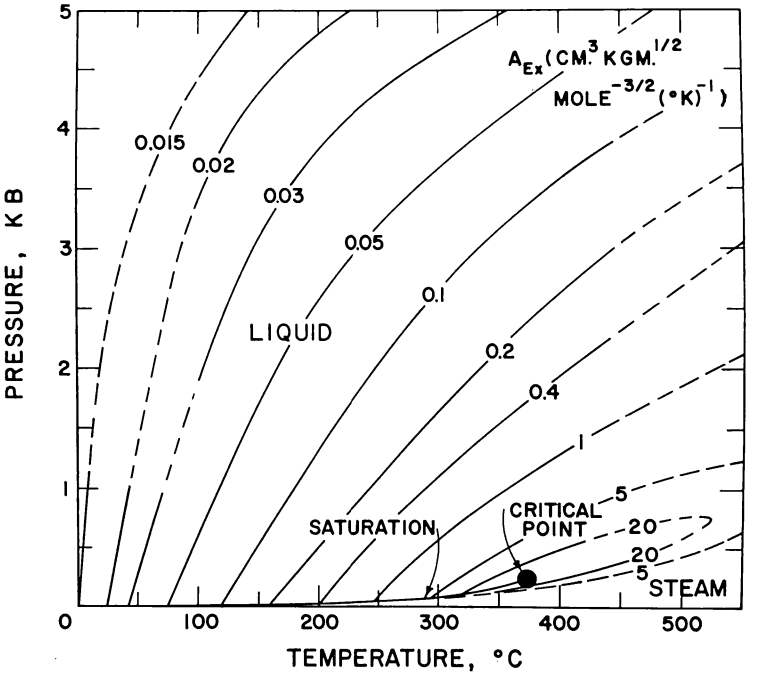

Fig. 53. Isopleths of A_{Ex} (labeled in $cm^3 kg^{1/2} mole^{-3/2}(°K)^{-1}$) as a function of pressure and temperature (table 15 and figs. 49 and 50).

TABLE 17

Summary of molal Debye-Hückel A (limiting law) parameters for the steam-saturated liquid phase

t[a]	P[b]	A_Y[c]	A_H[d]	A_j[e]	A_E[d]	A_{C_V}[e]	A_V[f]	A_K[g] × 10^3	A_{Ex}[h] × 10^2
0	0.006	0.4913	0.392	10.27	0.408	6.67	2.33	-0.56	1.49
5	0.009	0.4943	0.445	11.18	0.441	6.67	2.41	-0.73	1.43
10	0.012	0.4976	0.503	11.84	0.475	6.67	2.48	-0.84	1.50
15	0.017	0.5012	0.563	12.36	0.510	6.66	2.56	-0.91	1.65
20	0.023	0.5050	0.626	12.80	0.545	6.64	2.65	-0.97	1.85
25	0.032	0.5092	0.691	13.22	0.582	6.61	2.75	-1.02	2.08
30	0.042	0.5135	0.759	13.63	0.619	6.56	2.86	-1.07	2.32
35	0.056	0.5182	0.828	14.05	0.657	6.49	2.98	-1.12	2.57
40	0.074	0.5231	0.899	14.49	0.695	6.41	3.12	-1.18	2.84
45	0.096	0.5282	0.973	14.95	0.734	6.32	3.26	-1.25	3.11
50	0.123	0.5336	1.049	15.44	0.773	6.20	3.43	-1.33	3.40
55	0.158	0.5392	1.127	15.97	0.812	6.06	3.60	-1.42	3.70
60	0.199	0.5450	1.208	16.53	0.852	5.90	3.80	-1.52	4.02
65	0.250	0.5511	1.292	17.13	0.892	5.72	4.01	-1.63	4.36
70	0.312	0.5574	1.380	17.76	0.932	5.52	4.23	-1.76	4.72
75	0.386	0.5639	1.470	18.45	0.972	5.29	4.48	-1.91	5.10
80	0.474	0.5706	1.564	19.17	1.011	5.03	4.74	-2.07	5.51
85	0.578	0.5776	1.662	19.95	1.051	4.75	5.03	-2.26	5.94
90	0.701	0.5848	1.764	20.77	1.090	4.45	5.34	-2.46	6.41
95	0.845	0.5922	1.870	21.64	1.129	4.11	5.67	-2.70	6.91
100	1.013	0.5998	1.980	22.57	1.167	3.75	6.03	-2.95	7.45
105	1.208	0.6077	2.095	23.56	1.204	3.36	6.41	-3.25	8.03
110	1.433	0.6158	2.215	24.61	1.241	2.94	6.83	-3.57	8.66
115	1.691	0.6242	2.341	25.73	1.277	2.50	7.28	-3.93	9.35
120	1.985	0.6328	2.472	26.91	1.312	2.02	7.76	-4.34	10.08
125	2.321	0.6416	2.610	28.17	1.346	1.52	8.29	-4.80	10.89
130	2.701	0.6507	2.754	29.52	1.378	0.98	8.85	-5.31	11.76
135	3.130	0.6601	2.904	30.96	1.409	0.42	9.46	-5.89	12.71
140	3.613	0.6697	3.063	32.50	1.439	-0.16	10.12	-6.53	13.75
145	4.154	0.6796	3.228	34.15	1.467	-0.78	10.83	-7.26	14.89
150	4.758	0.6898	3.403	35.93	1.493	-1.42	11.60	-8.08	16.14
155	5.431	0.7003	3.586	37.85	1.517	-2.09	12.43	-9.01	17.51
160	6.178	0.7111	3.779	39.94	1.539	-2.78	13.34	-10.06	19.02
165	7.004	0.7222	3.983	42.21	1.559	-3.49	14.32	-11.25	20.69
170	7.916	0.7336	4.199	44.69	1.576	-4.23	15.39	-12.60	22.53
175	8.920	0.7454	4.427	47.41	1.591	-4.99	16.56	-14.13	24.58
180	10.021	0.7575	4.669	50.40	1.603	-5.76	17.82	-15.88	26.86
185	11.226	0.7700	4.926	53.71	1.613	-6.56	19.21	-17.89	29.40
190	12.543	0.7829	5.199	57.37	1.619	-7.36	20.72	-20.18	32.24
195	13.978	0.7962	5.491	61.45	1.622	-8.18	22.38	-22.82	35.43
200	15.537	0.8099	5.804	66.01	1.622	-9.02	24.21	-25.86	39.02
210	19.061	0.8387	6.501	76.87	1.612	-10.70	28.42	-33.47	47.65
220	23.177	0.8697	7.314	90.70	1.587	-12.41	33.56	-43.79	58.82
225	25.476	0.8860	7.773	99.05	1.568	-13.26	36.56	-50.34	65.64
230	27.947	0.9030	8.273	108.57	1.546	-14.11	39.90	-58.06	73.49
240	33.440	0.9391	9.421	132.00	1.487	-15.79	47.81	-78.13	93.11
250	39.728	0.9785	10.814	163.21	1.408	-17.44	57.81	-106.98	119.90
260	46.883	1.0218	12.533	205.53	1.309	-19.03	70.65	-149.54	157.34
270	54.984	1.0699	14.690	264.21	1.186	-20.57	87.45	-214.19	211.12
275	59.415	1.0960	15.980	302.15	1.115	-21.32	97.83	-259.08	246.93
280	64.113	1.1238	17.447	347.77	1.036	-22.05	109.89	-315.93	290.94
290	74.356	1.1850	21.053	470.95	0.853	-23.47	140.65	-483.00	414.21
300	85.805	1.2555	25.893	660.79	0.632	-24.65	184.17	-772.23	614.27
325	120.387	1.4943	49.072	1964.42	-0.178	-28.50	419.46	-3353.74	2160.46
350	165.125	1.9252	135.176	13018.24	-1.801	-35.41	1504.78	-36221.30	17927.28

[a] °C. [b] bar. [c] $kg^{1/2}\ mole^{-1/2}$. [d] $kcal\ kg^{1/2}\ mole^{-3/2}$. [e] $cal\ kg^{1/2}\ mole^{-3/2}(°K)^{-1}$.
[f] $cm^3\ kg^{1/2}\ mole^{-3/2}$. [g] $cm^3\ kg^{1/2}\ mole^{-3/2}\ bar^{-1}$. [h] $cm^3\ kg^{1/2}\ mole^{-3/2}\ (°K)^{-1}$.

TABLE 18

Summary of molal Debye-Hückel B parameters for the steam-saturated liquid phase

[a] t (°C)	[b] P (bar)	[c] $B_\gamma \times 10^{-7}$	[d] $B_H \times 10^{-9}$	[e] $B_J \times 10^{-8}$	[d] $B_E \times 10^{-9}$	[e] $B_{Cv} \times 10^{-7}$	[f] $B_V \times 10^{-8}$	[g] $B_\kappa \times 10^{-4}$	[h] $B_{Ex} \times 10^{-5}$
0	0.006	0.3247	9.04	1.25	9.00	1.40	5.94	-0.36	-3.36
5	0.009	0.3254	9.68	1.32	9.69	1.38	4.28	-0.32	-3.30
10	0.012	0.3261	10.36	1.39	10.39	1.37	2.65	-0.26	-3.22
15	0.017	0.3268	11.07	1.46	11.09	1.35	1.05	-0.19	-3.15
20	0.023	0.3275	11.82	1.53	11.80	1.33	-0.51	-0.12	-3.12
25	0.032	0.3283	12.60	1.59	12.51	1.30	-2.07	-0.05	-3.12
30	0.042	0.3291	13.41	1.65	13.23	1.27	-3.64	0.02	-3.16
35	0.056	0.3299	14.24	1.70	13.94	1.24	-5.24	0.09	-3.23
40	0.074	0.3307	15.11	1.74	14.65	1.21	-6.87	0.16	-3.32
45	0.096	0.3316	15.99	1.79	15.36	1.17	-8.56	0.23	-3.44
50	0.123	0.3325	16.89	1.82	16.06	1.13	-10.32	0.31	-3.58
55	0.158	0.3334	17.81	1.86	16.75	1.08	-12.15	0.39	-3.75
60	0.199	0.3343	18.75	1.89	17.43	1.03	-14.07	0.48	-3.94
65	0.250	0.3352	19.70	1.92	18.09	0.97	-16.09	0.57	-4.15
70	0.312	0.3362	20.67	1.95	18.74	0.92	-18.22	0.67	-4.38
75	0.386	0.3371	21.65	1.98	19.37	0.85	-20.47	0.78	-4.63
80	0.474	0.3381	22.65	2.01	19.98	0.79	-22.85	0.91	-4.90
85	0.578	0.3391	23.66	2.04	20.57	0.72	-25.38	1.04	-5.20
90	0.701	0.3401	24.68	2.06	21.14	0.64	-28.05	1.19	-5.52
95	0.845	0.3411	25.72	2.09	21.68	0.57	-30.90	1.36	-5.87
100	1.013	0.3422	26.77	2.12	22.20	0.49	-33.92	1.54	-6.24
105	1.208	0.3432	27.84	2.15	22.69	0.40	-37.14	1.75	-6.64
110	1.433	0.3443	28.93	2.19	23.14	0.32	-40.56	1.97	-7.07
115	1.691	0.3454	30.03	2.22	23.57	0.23	-44.21	2.23	-7.54
120	1.985	0.3465	31.14	2.26	23.96	0.13	-48.10	2.51	-8.04
125	2.321	0.3476	32.28	2.29	24.31	0.04	-52.24	2.82	-8.58
130	2.701	0.3487	33.43	2.33	24.63	-0.06	-56.66	3.17	-9.16
135	3.130	0.3498	34.61	2.38	24.90	-0.16	-61.39	3.57	-9.79
140	3.613	0.3510	35.80	2.42	25.14	-0.26	-66.43	4.00	-10.47
145	4.154	0.3521	37.02	2.48	25.34	-0.36	-71.83	4.49	-11.21
150	4.758	0.3533	38.27	2.53	25.49	-0.47	-77.61	5.04	-12.01
155	5.431	0.3545	39.54	2.59	25.60	-0.57	-83.79	5.65	-12.88
160	6.178	0.3556	40.85	2.66	25.66	-0.68	-90.42	6.33	-13.83
165	7.004	0.3568	42.19	2.74	25.68	-0.79	-97.53	7.11	-14.86
170	7.916	0.3580	43.57	2.82	25.65	-0.89	-105.17	7.97	-15.99
175	8.920	0.3592	44.99	2.92	25.57	-1.00	-113.39	8.95	-17.23
180	10.021	0.3605	46.46	3.03	25.44	-1.11	-122.23	10.06	-18.58
185	11.226	0.3617	47.98	3.15	25.26	-1.21	-131.76	11.31	-20.08
190	12.543	0.3629	49.56	3.29	25.03	-1.31	-142.05	12.73	-21.73
195	13.978	0.3642	51.22	3.45	24.75	-1.42	-153.17	14.34	-23.56
200	15.537	0.3655	52.95	3.63	24.41	-1.52	-165.21	16.19	-25.59
210	19.061	0.3681	56.70	4.07	23.59	-1.71	-192.46	20.70	-30.38
220	23.177	0.3707	60.91	4.65	22.55	-1.89	-224.76	26.69	-36.40
225	25.476	0.3721	63.23	5.00	21.96	-1.97	-243.18	30.40	-39.99
230	27.947	0.3734	65.72	5.40	21.31	-2.05	-263.37	34.72	-44.07
240	33.440	0.3762	71.30	6.39	19.86	-2.20	-309.99	45.69	-54.01
250	39.728	0.3792	77.90	7.69	18.20	-2.32	-366.91	60.96	-67.13
260	46.883	0.3822	85.80	9.43	16.33	-2.43	-437.32	82.69	-84.81
270	54.984	0.3855	95.43	11.77	14.25	-2.51	-525.73	114.46	-109.22
275	59.415	0.3871	101.06	13.25	13.13	-2.54	-578.63	135.88	-124.99
280	64.113	0.3889	107.34	14.99	11.95	-2.57	-638.73	162.40	-143.94
290	74.356	0.3926	122.35	19.55	9.43	-2.61	-786.27	237.54	-195.13
300	85.805	0.3965	141.64	26.23	6.66	-2.62	-984.09	361.08	-274.07
325	120.387	0.4085	224.59	67.34	-1.63	-2.60	-1926.64	1330.59	-814.22
350	165.125	0.4256	472.54	353.14	-13.27	-2.63	-5336.98	10974.44	-5197.56

[a] °C. [b] bar. [c] $kg^{1/2}\ cm^{-1}\ mole^{-3/2}$. [d] $cal\ kg^{1/2}\ cm^{-1}\ mole^{-3/2}$. [e] $cal\ kg^{1/2}\ cm^{-1}\ mole^{-3/2}\ (°K)^{-1}$. [f] $cm^2\ kg^{1/2}\ mole^{-3/2}$. [g] $cm^2\ kg^{1/2}\ mole^{-3/2}\ bar^{-1}$. [h] $cm^2\ kg^{1/2}\ mole^{-3/2}\ (°K)^{-1}$

pressure (fig. 50), and the isopleths for A_{Ex} in figure 53 wrap around the critical point. In contrast, B_{Ex} as an isobaric function of temperature exhibits extrema at pressures $\gtrsim 4$ kb as well as minima at higher temperatures (fig. 52). B_{Ex} is negative, except at high pressures > 4 kb from $\sim$ 300° to $\sim$ 500°C, where it maximizes as a function of temperature at constant pressure. Note also in figure 52 that B_{Ex} maximizes with decreasing temperature at constant pressure below a kilobar in the vicinity of 35°C in response to the influence of $(\partial \ln \varepsilon/\partial P)_T$ and β, which exhibit the same behavior. The high pressure extrema in figure 52 are manifested by the crossing isotherms in figure 51 and the high pressure minima in the isopleths shown in figure 54.

SUMMARY OF PARAMETERS FOR SATURATED LIQUID H_2O

Computed values of A_γ, B_γ, A_H, B_H, A_J, B_J, A_E, B_E, A_{C_V}, B_{C_V}, A_V, B_V, A_κ, B_κ, A_{Ex}, and B_{Ex} in liquid H_2O along the saturation curve are given in tables 17 and 18 at closely spaced intervals from 0° to 350°C to facilitate analysis of experimental data.

CONCLUDING REMARKS

Owing to the much greater increase in A_γ relative to the increase in B_γ with increasing temperature, activity coefficients computed from the Debye-Hückel equation (for a constant å) decrease with increasing temperature at constant ionic strength. At high temperatures and low pressures the decrease becomes dramatic as temperature increases and/or

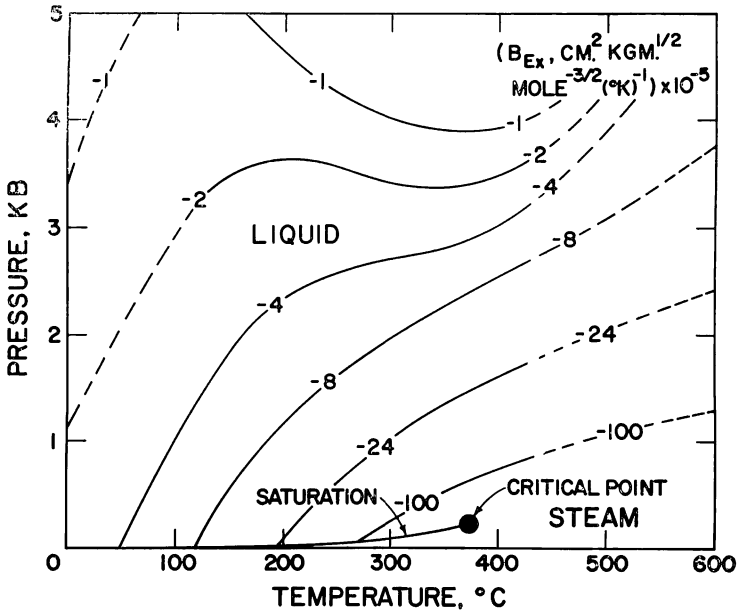

Fig. 54. Isopleths of B_{Ex} (labeled in $(cm^2 kg^{1/2} mole^{-3/2}(°K)^{-1}) \times 10^{-5}$) as a function of pressure and temperature (table 16 and figs. 51 and 52).

pressure decreases, which favors increasing mineral solubilities and decreasing degrees of formation of aqueous complexes. However, dissociation constants and b_γ become small at high temperatures (Quist and Marshall, 1966, 1968a, b, c, and d, 1969; Helgeson and James, 1968; Helgeson, 1967a, 1969) where true ionic strengths of 0.01 or less occur in concentrated electrolyte solutions owing to the high degrees of formation achieved by neutral complexes in a medium of relatively low dielectric constant. As a consequence, Debye-Hückel theory becomes increasingly applicable to solutions with progressively higher concentrations as temperature increases and/or pressure decreases. The increasing electrostatic contribution to ion association thus overcomes the effect of decreasing ionic activity coefficients on the formation of aqueous complexes with increasing temperature and/or decreasing pressure.

The tables and diagrams presented in the foregoing pages were generated with the aid of a comprehensive computer program which can be used to calculate all the high-temperature/pressure thermodynamic/electrostatic properties of H_2O (Helgeson and Kirkham, 1974a). Hopefully, such calculations will stimulate more experimental research on the thermodynamic properties of aqueous electrolytes at high pressures and temperatures. Precise density measurements under these conditions are needed to test and refine equations of state for electrolytes (Helgeson and Kirkham, 1975a). With the aid of the A_V and B_V values given above, standard state data can be extracted from such measurements to calculate the thermodynamic properties of aqueous species in hydrothermal solutions at high pressures and temperatures (Helgeson and Kirkham, 1975b).

ACKNOWLEDGMENTS

The work reported here was supported in part by NSF Grants GA 25314, GA 36023, GA 35888, and the donors of the Petroleum Research Fund, administered by the American Chemical Society, under PRF #5356-AC2. Additional funds provided by the Kennecott Copper Corporation, the Anaconda Company, and the Committee on Research at the University of California, Berkeley, are also acknowledged with thanks. We are indebted to Philip Lehot, David Bice, Yoshi Hidaka, David Pitou, Joan Delany, and Joachim Hampel for assistance with programming, plotting, drafting, and preparation of the manuscript. Our gratitude also to A. J. Ellis, J. W. Cobble, and C. W. Burnham for critical reviews of the paper, and to Debbie Aoki for typing and retyping the manuscript.

REFERENCES

Bromley, L. A., 1968, Heat capacity of sea water solutions: Jour. Chem. Eng. Data, v. 13, p. 60-62.

Bromley, L. A., Diamond, A. S., Salami, E., and Wilkins, D. G., 1970, Heat capacities and enthalpies of sea salt solutions to 200°: Jour. Chem. Eng. Data, v. 15, p. 246-253.

Burnham, C. W., Holloway, J. R., and Davis, N. F., 1969, Thermodynamic properties of water to 1000°C and 10,000 bars: Geol. Soc. America Spec. Paper 132, 96 p.

Davies, C. W., 1938, The extent of dissociation of salts in water. VIII. An equation for the mean ionic activity coefficient of an electrolyte in water, and a revision of the dissociation constants of some sulfates: Chem. Soc. (London) Jour., p. 2093-2098.

Debye, P., and Hückel, E., 1923, The theory of electrolytes. I. Lowering of freezing point and related phenomena: Zeitschr. Physik, v. 24, p. 185-206.

Dorsey, N. E., 1940, Properties of ordinary water-substance: New York, N.Y. Reinhold Publishing Corp., 673 p.

Franck, E. U., 1956, Hochverdichteter Wasserdampf II. Ionendissoziation von KCl in H_2O bis 750°C: Zeitschr. Phys. Chemie, v. 8, p. 107-126.

Gardner, W. L., Mitchell, R. E., and Cobble, J. W., 1969, Thermodynamic properties of high-temperature aqueous solutions. XI. Calorimetric determination of the standard partial molal heat capacity and entropy of sodium chloride solutions from 100 to 200°: Jour. Phys. Chemistry, v. 73, p. 2025-2032.

Guggenheim, E. A., 1935, Specific thermodynamic properties of aqueous solutions of strong electrolytes: Philos. Mag., v. 19, p. 588-643.

Güntelberg, E., 1926, Untersuchungen über loneninteraktion: Zeitschr. Phys. Chemie, v. 123, p. 199-247.

Hamer, W. J., 1968, Theoretical mean activity coefficients of strong electrolytes in aqueous solutions from 0 to 100°C: U.S. Natl. Bur. Standards, NSRDS-NBS 24, 271 p.

Hamer, W. J., and Wu, Y. C., 1972, Osmotic coefficients and mean activity coefficients of uni-univalent electrolytes in water at 25°C: Jour. Phys. and Chem. Ref. Data, v. 1, p. 1047-1099.

Harned, H. S., and Owen, B. B., 1958, The physical chemistry of electrolyte solutions, 3d ed.: New York, Reinhold, 803 p.

Heger, K., ms, 1969, Die statische Dielektrizitätskonstante von Wasser und methylalkohol im überkritischer Temperatur und Druckbereich: Ph.D. dissert., Univ. Karlsruhe, Karlsruhe, West Germany.

Helgeson, H. C., 1967a, Thermodynamic of complex formation in aqueous solution at elevated temperatures: Jour. Phys. Chemistry, v. 71, p. 3121-3136.

———— 1967b, Solution chemistry and metamorphism, *in* P. H. Abelson, ed., Researches in geochemistry, v. 2: New York, John Wiley & Sons, Inc., p. 362-404.

———— 1969, Thermodynamics of hydrothermal systems at elevated temperatures and pressures: Am. Jour. Sci., v. 267, p. 729-804.

Helgeson, H. C., and James, W. R., 1968, Activity coefficients in concentrated electrolyte solutions at elevated temperatures [abs]: Am. Chem. Soc., 155th Natl. Mtg., San Francisco, April 1968, Abs., p. 5-130.

Helgeson, H. C., and Kirkham, D. H., 1974a, Theoretical prediction of the thermodynamic behavior of aqueous electrolytes at high pressures and temperatures. I. Summary of the thermodynamic/electrostatic properties of the solvent: Am. Jour. Sci., v. 274, p. 1089-1198.

———— 1975a, Theoretical prediction of the thermodynamic behavior of aqueous electrolytes at high pressures and temperatures. III. Equation of state for aqueous species at infinite dilution: Am. Jour. Sci., v. 275.

———— 1975b, Theoretical prediction of the thermodynamic behavior of aqueous electrolytes at high pressures and temperatures. IV. Calculation of partial molal properties to 600°C and five kilobars: Am. Jour. Sci., v. 275.

Hensel, F., and Franck, E. U., 1964, Die elektrische Leitfähigkeit wassriger Salzlösungen bis zu 130° und 8000 bar: Zeitschr. Naturforsch., v. 19a, p. 127-132.

Keenan, J. H., Keyes, F. G., Hill, P. G., and Moore, J. G., 1969, Steam tables: New York, John Wiley & Sons, Inc., 162 p.

Kell, G. S., and Whalley, E., 1965, The PVT properties of water. I. Liquid water in the temperature range 0° to 150°C and at pressures up to 1 kb: Royal Soc. London Philos. Trans. Ser. A, Math. and Phys. Sci., v. 258, p. 565-617.

Kirkwood, J. G., 1939, The dielectric polarization of polar liquids: Jour. Chem. Physics, v. 7, p. 911-919.

Lewis, G. N., and Randall, M., 1961, Thermodynamics, 2d ed., revised by K. S. Pitzer and L. Brewer: New York, McGraw-Hill, 723 p.

Lietzke, M. H., and Stoughton, R. W., 1962, The calculation of activity coefficients from osmotic coefficient data: Jour. Phys. Chemistry, v. 66, p. 508-509.

Malmberg, C. G., and Maryott, A. A., 1956, Dielectric constant of water from 0° to 100°: Natl. Bur. Standards Research Jour., no. 2641, v. 56, p. 1-8.

Marshall, W. L., and Slusher, R., 1968, Aqueous systems at high temperature. Solubility to 200° of calcium sulfate and its hydrates in sea water and saline water concentrates, and temperature-concentration limits: Jour. Chem. Eng. Data, v. 13, p. 83-93.

Masson, D. O., 1929, Solute molecular volumes in relation to solvation and ionization: Philos. Mag., v. 8, p. 218-235.

Oshry, H. I., ms, 1949, The dielectric constant of saturated water from the boiling point to the critical point: Ph.D. dissert., Univ. Pittsburgh, Pittsburgh, Penn.

Oster, G., and Kirkwood, J. G., 1943, The influence of hindered molecular rotation on the dielectric constants of water, alcohols, and other polar liquids: Jour. Chem. Physics, v. 11, p. 175-178.

Owen, B., Miller, R. C., Milner, C. E., and Cogan, H. L., 1961, The dielectric constant of water as a function of temperature and pressure: Jour. Phys. Chemistry, v. 65, p. 2065-2070.

Quist, A. S., and Marshall, W. L., 1966, Electrical conductances of aqueous solutions at high temperatures and pressures. III. The conductances of potassium bisulfate solutions from 0 to 700° and at pressures to 4000 bars: Jour. Phys. Chemistry, v. 70, p. 3714-3725.

———— 1968a, Electrical conductances of aqueous sodium chloride solutions from 0 to 800° and at pressures to 4000 bars: Jour. Phys. Chemistry, v. 72, p. 684-703.

———— 1968b, Electrical conductances of aqueous hydrogen bromide solutions from 0 to 800° and at pressures to 4000 bars: Jour. Phys. Chemistry, v. 72, p. 1545-1552.

———— 1968c, Electrical conductances of aqueous sodium bromide solutions from 0 to 800° and at pressures to 4000 bars: Jour. Phys. Chemistry, v. 72, p. 2100-2105.

———— 1968d, Ionization equilibria in ammonia-water solutions to 700° and to 4000 bars of pressure: Jour. Phys. Chemistry, v. 72, p. 3122-3128.

———— 1969, The electrical conductances of some alkali metal halides in aqueous solutions from 0 to 800° and at pressures to 4000 bars: Jour. Phys. Chemistry, v. 73, p. 978-985.

Redlich, O., and Meyer, D., 1964, The molal volumes of electrolytes: Chem. Rev., v. 64, p. 221-227.

Robinson, R. A., and Stokes, R. H., 1959, Electrolyte solutions, 2d ed.: London, Butterworths, 559 p.

Scatchard, G., 1936, Concentrated solutions of strong electrolytes: Chem. Rev., v. 19, p. 309-327.

Sen, U., and Cobble, J. W., 1974, A unified approach to the theory of electrolytes in water: Am. Chem. Soc. Jour. (in press).